

**Soil Moisture Remote Sensing using GPS-Interferometric Reflectometry**

by

**Clara Chew**

B.A., Dartmouth College, 2009

A thesis submitted to the Faculty of the Graduate School  
of the University of Colorado in partial fulfillment  
of the requirements for the degree of  
Doctor of Philosophy  
Department of Geological Sciences

2015

This thesis entitled:

Soil Moisture Remote Sensing using Global Positioning System-Interferometric Reflectometry

Written by Clara C. Chew

Has been approved for the Department of Geological Sciences by:

---

Eric Small

---

Kristine Larson

---

Shemin Ge

---

Greg Tucker

---

Valery Zavorotny

Date: \_\_\_\_\_

The final copy of this thesis has been examined by the signatories, and we find that both the content and the form meet acceptable presentation standards of scholarly work in the above mentioned discipline.

Clara C. Chew

Soil moisture remote sensing using Global Positioning System-Interferometric Reflectometry

Thesis directed by Prof. Eric Small

Ground-reflected Global Positioning System (GPS) signals can be used opportunistically to infer changes in land-surface characteristics surrounding a GPS monument. GPS satellites transmit at L-band, and at microwave frequencies the permittivity of the ground surface changes primarily due to its moisture content. Temporal changes in ground-reflected GPS signals are thus indicative of temporal changes in the moisture content surrounding a GPS antenna.

The interference pattern of the direct and reflected GPS signal for a single satellite track is recorded in signal-to-noise ratio (SNR) data. Alternating constructive and destructive interference as the satellite passes over the antenna results in a noisy oscillating wave at low satellite elevation angles, from which the phase, amplitude, and frequency (or reflector height) can be calculated.

Here, an electrodynamic model that simulates SNR data is validated against field observations. The model is then used to show that temporal changes in these SNR metrics may be used to estimate changes in surface soil moisture in the top 5 cm of the soil column. Results show that changes in SNR phase are best correlated with changes in soil moisture, with an approximately linear slope. Surface roughness decreases the sensitivity of SNR phase to soil moisture, though the effect is not significant for small roughness values (<5 cm).

Modeling experiments show that all three SNR metrics are affected by changes in the permittivity and height of a vegetation canopy. SNR amplitude is the best indicator of changes in vegetation. An increase in either canopy permittivity or height will cause a corresponding decrease in SNR phase. Seasonal changes in vegetation must be removed if soil moisture is to be estimated using phase data.

An algorithm is presented that uses modeled relationships between canopy parameters and SNR metrics to remove seasonal vegetation effects from the phase time series, from which soil moisture time series may be estimated. Results indicate that this algorithm can successfully estimate surface soil moisture with an RMSE of  $0.05 \text{ cm}^3 \text{ cm}^{-3}$  or lower for many of the antennas that comprise the Plate Boundary Observatory (PBO) network.

## **Acknowledgements**

Five years ago, Eric Small made the strange decision to allow me to work in the GPS reflections group. I often look back to this time of my life and wonder just what possessed him to give me such an opportunity, and I have to chalk it up to serendipity. I am incredibly thankful to him for making my graduate school experience not only fruitful, but even enjoyable. He has always done his best to keep me thinking about the big picture, which has kept me from falling too deeply into numerous rabbit holes.

Along with Eric, Kristine Larson has also been an incredible advisor. Her dedication to GPS and work ethic is inspiring, and I can only hope a little rub of this has rubbed off on me. Her attention to detail is responsible for much of the success of the GPS reflections project, and I am very lucky to have been able to call her my mentor.

I am also indebted to Valery Zavorotny, without whom this entire thesis would not have been possible. His expertise in electromagnetic scattering is unparalleled, and I am certain he could have done all the work that I did in a tenth of the time. Even so, he patiently answered all of my questions, and always with a grin.

Next, I would like to thank Greg Tucker and Shemin Ge for serving on my committee. They have both been very encouraging during my time here, and seeing them excel at their own research has motivated me to work harder at mine.

I am very thankful for the opportunities I have had to work with current and past collaborators and colleagues—John Braun, Andria Bilich, Felipe Nievinski, Sarah Evans, Peter Shellito, Karen Boniface, James McCreight, John Pratt, Evan Pugh, Tevis Blom, Shahen Huda, Maria Rocco, and Cheney Shreve. Thank you for the support you have given, insightful conversations we have had, and the fieldwork we have shared.

This research would not have been possible without the support of funding from the University of Colorado, NASA, and NSF.

## Table of Contents

Acknowledgements.....	iv
List of Figures.....	viii
List of Tables.....	xii
Chapter 1: Introduction.....	1
Chapter 2: Background.....	3
2.1 Soil moisture measurement.....	3
2.2 Soil moisture variability.....	6
2.3 The Plate Boundary Observatory Network.....	7
2.4 Remote sensing using GPS reflected signals.....	8
2.5 GPS-Interferometric Reflectometry.....	9
2.6 Signal-to-Noise Ratio Data.....	12
2.6.1 SNR Equation and metrics.....	12
2.6.2 Temporal changes in SNR metrics.....	15
Chapter 3: Ground truth experiments and data.....	18
3.1 Description of measurement techniques.....	18
3.1.1 In situ soil moisture data.....	18
3.1.2 Vegetation surveys.....	21
3.2 Data Summary.....	21
3.2.1 Soil Moisture Data.....	21
3.2.2 Vegetation Data.....	24
Chapter 4: Forward modeling of SNR data in relation to soil moisture and vegetation.....	27
4.1 Model architecture.....	28
4.1.1 Reflection coefficient calculations.....	28
4.1.2 Permittivity profile generation: Soil.....	30
4.1.3 Permittivity profile generation: Vegetation.....	31
4.1.4 Note on the plane-stratified model for a vegetation canopy.....	35
4.1.5 Calculation of direct and indirect power.....	36
4.2 Model validation.....	38
4.2.1 Validation Set-Up: Field Observations and Model Input.....	38
4.2.2 Comparison of Simulated and Observed SNR Data.....	40
4.2.3 Comparison of Simulated SNR and Observed Metrics.....	43
4.3 Bare Soil Modeling.....	46

4.3.1	Soil moisture profiles .....	46
4.3.2	Modeled SNR interferograms .....	48
4.3.3	The effect of soil moisture on SNR metrics.....	50
4.4	Vegetation-soil model.....	55
4.4.1	First case: random combinations of vegetation parameters .....	57
4.4.2	Second case: Assuming relationships between canopy parameters .....	66
4.4.3	Third case: When specific vegetation parameters are correlated with one another .....	69
4.4.4	Effects of underlying soil moisture changes .....	71
4.4.5	Problems with the constant-frequency SNR equation .....	76
4.4.6	Conclusions.....	77
Chapter 5:	Correcting for vegetation effects on SNR data .....	79
5.1	Extent of vegetation effects in observed data .....	79
5.2	Development of the vegetation filter .....	80
5.2.1	SNR model simulations .....	81
5.2.2	Relationships between SNR metrics .....	82
5.3	Processing observed SNR metrics .....	83
5.4	Estimating phase change due to vegetation .....	84
5.5	Justification for the current filter .....	87
5.5.1	Concurrent inverse estimation of soil moisture and vegetation .....	87
5.5.2	The use of a more complex characteristic SNR equation .....	91
5.6	Limitations of the vegetation filter.....	93
Chapter 6:	Soil Moisture Estimations using GPS-IR.....	97
6.1	Empirical data issues.....	97
6.1.1	Persistent amplitude anomalies .....	97
6.1.2	Reflector height considerations.....	101
6.2	Soil moisture retrieval algorithm .....	115
6.3	Validation of soil moisture retrievals.....	127
6.4	Effect of changing model parameters .....	129
6.4.1	Sensitivity to changing the <i>a priori</i> reflector height .....	131
6.4.2	Sensitivity to changes in the smoothing method.....	133
Chapter 7:	Error Quantification .....	135
7.1	Errors for bare soil .....	135
7.1.1	Imperfect knowledge of <i>a priori</i> reflector height .....	135

7.1.2 Vertical gradients in SMC profiles .....	137
7.1.3 Differences in antenna height .....	139
7.1.4 Differences in soil texture .....	140
7.1.5 Changes in soil temperature .....	141
7.1.6 Changes in receiver temperature .....	142
7.1.7 Surface roughness .....	143
7.2 Errors for vegetated environments .....	146
7.2.1 Imperfect knowledge of antenna height .....	146
Chapter 8: Future Work .....	150
8.1 Improvements in model simulations for the vegetation filter .....	150
8.2 Improvements in quality control of observations .....	153
Chapter 9: Conclusions .....	156
Bibliography .....	158

## List of Figures

Figure 1: Locations of selected PBO GPS sites that are currently being used to estimate soil moisture.

Figure 2: Geometry of a multipath signal.

Figure 3: Plan view diagrams for the GPS station okl3.

Figure 4: Examples of SNR interferograms.

Figure 5: Examples of SNR metric time series.

Figure 6: Distributions of *in situ* soil moisture at the validation sites.

Figure 7: Relationships between vegetation field measurements.

Figure 8: Vegetation-soil model schematic.

Figure 9: Validation of the model with observed SNR interferograms.

Figure 10: Comparison between observed and modeled SNR metrics at the alfalfa field.

Figure 11: Validation of the soil-vegetation model against observed SNR metrics.

Figure 12: Modeled relationships between SNR metrics and soil moisture, for a bare soil.

Figure 13: Model simulations and observed data from a wheat field.

Figure 14: Modeled interferograms for a bare soil.

Figure 15: Modeled normalized amplitude and soil moisture, and modeled change in effective reflector height, for a bare soil.

Figure 16: Observed vegetation data and SNR metrics for a GPS station in Oklahoma.

Figure 17: Modeled relationships between dry biomass and SNR metrics.

Figure 18: Modeled relationships between vegetation wet weight and SNR metrics.

Figure 19: Modeled relationships between canopy height and SNR metrics.

Figure 20: Modeled relationships between vegetation true density and SNR metrics.

Figure 21: Relationships between modeled canopy permittivity, height, and SNR metrics.

Figure 22: Examples of observed changes in Lomb-Scargle Periodograms throughout the growing season.

Figure 23: Vegetation field data comparison between a desert steppe and alfalfa site.

Figure 24: Modeled relationships between vegetation wet weight and SNR metrics, for typical vegetation present at the desert steppe and alfalfa sites.

Figure 25: Modeled relationships between vegetation wet weight and SNR metrics, when vegetation true density is pinned to water content.

Figure 26: Sensitivity of SNR metrics to changes in soil moisture underlying modeled vegetation canopies.

Figure 27: Characterization of the misfit between interferograms and their associated metrics.

Figure 28: The fraction of PBO H<sub>2</sub>O data that is likely affected by vegetation.

Figure 29: Distributions of vegetation parameters used in the vegetation filter.

Figure 30: Relationships between SNR metrics and phase, given changes in modeled vegetation canopies.

Figure 31: Relationships between multiple SNR metrics and phase, given changes in modeled vegetation canopies.

Figure 32: SNR metrics for multiple satellite tracks at a GPS site in Oklahoma.

Figure 33: Estimated versus observed canopy height at the alfalfa site, bcgr.

Figure 35: Depiction of how the vegetation filter would change, given soil moisture change.

Figure 34: Modeled reflection coefficients for example vegetation canopies.

Figure 36: Modeled interferograms and SNR metrics for a theoretical, isotropic antenna.

Figure 37: Examples of observed amplitude anomalies.

Figure 38: Amplitude time series for one satellite track at a GPS site in Oklahoma.

Figure 39: Depiction of the tolerance limits for determining systemic amplitude problems.

Figure 40: Time series of normalized LSP amplitude data for several satellite tracks and the tolerance limits.

Figure 41: Time series of effective reflector height for one satellite track at the desert steppe site p041.

Figure 42: Time series of estimated soil moisture at site p041, before and after a flooding event.

Figure 43: Estimated and *in situ* soil moisture data from p041 at the beginning of 2012.

Figure 44: The effect of using an incorrect *a priori* reflector height on phase and amplitude.

Figure 45: Time series of effective reflector heights at p041, and phase time series before and after reflector height correction.

Figure 46: Comparison of estimated soil moisture time series at p041, with and without a reflector height correction.

Figure 47: Modeled relationships between canopy height and effective reflector height.

Figure 48: Examples of the current *a priori* reflector heights versus the median value of the effective reflector height.

Figure 49: Effects of changing the *a priori* reflector height on soil moisture retrievals.

Figure 50: Digital elevation model and ground tracks at the GPS site okl3.

Figure 51: Histogram of the number of satellite tracks used at PBO H<sub>2</sub>O stations and an example of the track number increasing at a site over time.

Figure 53: Soil moisture retrieval algorithm flowchart.

Figure 52: Soil moisture retrievals and *in situ* data from a desert steppe site mfle.

Figure 54: Soil moisture retrievals with and without using the vegetation filter at GPS site okl3.

Figure 55: A soil pit in Oklahoma and measurements from three different types of *in situ* soil moisture probes.

Figure 56: Validation plot showing GPS versus *in situ* soil moisture estimations.

Figure 57: Examples of how changing the *a priori* height at ames changes results from the vegetation filter.

Figure 58: Examples of how the choice of smoothing parameters affects the outcome of the vegetation filter.

Figure 59: Modeled errors in soil moisture retrievals from *a priori* reflector height errors.

Figure 60: Errors introduced from vertical gradients in soil moisture profiles.

Figure 61: Errors introduced from using data from antennas of different heights.

Figure 62: Differences in the relationship between soil moisture and phase for different soil textures.

Figure 63: Effect of ground temperature on phase and amplitude.

Figure 64: Observed effects of temperature on SNR metrics.

Figure 65: The effect of surface roughness on the relationships between soil moisture and SNR metrics.

Figure 66: The RMS error between surface roughness and subsequent soil moisture estimations.

Figure 67: Errors in estimated phase change due to vegetation, if the *a priori* reflector height is over- or under-estimated.

Figure 68: Phase observations and predictions using two versions of the vegetation filter at p042.

Figure 69: Estimated soil moisture time series for masw using two versions of the vegetation filter.

Figure 70: Time series of track-by-track soil moisture retrievals and *in situ* data at okl3.

### **List of Tables**

Table 1: Historical and current satellite missions with observations of soil moisture.

Table 2: Summary of theta probe and volumetric soil moisture surveys.

Table 3: GPS stations, antenna heights, and vegetation information.

Table 4: Mean Cross-Correlation Coefficients

Table 5: Slopes and  $r^2$  values for linear regressions of soil moisture and phase.

Table 6: Parameters used in the soil-vegetation model

Table 7: Description of parameters used in the soil moisture algorithm.

## Chapter 1: Introduction

Soil moisture has long been recognized as an important hydrologic variable, as it determines the relative partitioning between the turbulent sensible and latent heat fluxes [1], [2]. Soil moisture anomalies are likely to initiate positive feedback mechanisms due to the thermal inertia of soil moisture relative to precipitation anomalies [1]. It has been shown that in areas that lie in the transition zone between wet and dry climates, such as the Great Plains in the United States, the Sahel, and parts of India, soil moisture and precipitation are strongly coupled. In these areas, persistent soil moisture anomalies are likely to influence precipitation [3]. Better initialization of soil moisture will lead to better predictive skill in numerical weather forecasts and global climate models [3].

Currently, there is a paucity of soil moisture observations at all spatial and temporal scales that would be needed to initialize models or validate soil moisture products. In particular, there are few methods of soil moisture measurement or estimation that yield data on the field scale ( $\sim 1000 \text{ m}^2$ ). Direct soil moisture measurement using either soil gravimetry or electromagnetic probes yield measurements for small volumes of soil ( $< 1 \text{ m}^3$ ) [4], and remotely sensed products from satellites have resolutions of many square kilometers [5]. Methods that do exist for field-scale soil moisture measurement, such as instruments mounted on truck booms or flown on aircraft, are usually used in field campaigns and not for long-term data collection.

In recent years, Global Positioning System (GPS) multipath signals have been used opportunistically to infer land surface characteristics, such as snow depth, soil moisture, and changes in vegetation. GPS antennas and receivers are well suited for land surface remote sensing because the GPS satellite transmit frequency is L-band (microwave frequency) with

wavelengths of ~19 (L1) or 24.4 (L2) cm. Microwave remote sensing of land surface properties has been studied for over 20 years [6]–[8]. For microwave frequencies, the permittivity or dielectric constant of a medium is highly dependent on its water content [9]. For example, the dielectric constant of water is around 80, compared to a dielectric constant of 3.5 for dry soils. The permittivity of a material determines the extent to which an electromagnetic wave will reflect off of the material, with higher permittivity materials resulting in a greater reflection [10].

As a result, the ground-reflected GPS signal will be altered by the amount of moisture contained near the ground surface. The receiving antenna can record temporal changes in the ground-reflected signal, which correlate with changes in properties such as soil moisture, snow, vegetation, surface roughness, and surface temperature.

Here, I will present results pertaining to the development of a methodology for soil moisture remote sensing using commercial GPS antennas and receivers. This work has included adapting and validating an electrodynamic model that simulates the response of GPS ground reflections to changes in soil moisture and vegetation canopy parameters. There is also a field component to this research, with several years of observations made at several GPS stations that also have concurrent soil moisture and/or vegetation observations. Using the electrodynamic model as well as observations, I have created a soil moisture retrieval algorithm that can be used at GPS stations with choke ring antennas, located in areas with variable vegetation cover.

## Chapter 2: Background

### 2.1 Soil moisture measurement

Soil moisture in this document will always refer to volumetric soil moisture, which is the volume of water in a soil divided by the total volume of the soil. Soil moisture content will be abbreviated as SMC and will have units of  $\text{cm}^3 \text{cm}^{-3}$ .

SMC varies between residual and saturated values. The residual moisture content of a soil is always greater than zero due to the adsorption of a certain amount of water molecules to soil grains. The residual moisture content is controlled by its soil texture, and soils with higher clay contents will tend to have higher residual moisture contents. Typically, residual moisture contents vary between  $0.02 \text{ cm}^3 \text{ cm}^{-3}$  and  $0.075 \text{ cm}^3 \text{ cm}^{-3}$  [11]. The saturated moisture content for a soil is equal to its porosity, or the amount of void space within the soil. Thus, a soil with a porosity of 0.4 will also have a maximum SMC of  $0.4 \text{ cm}^3 \text{ cm}^{-3}$ .

Soil moisture is measured with both *in situ* and remote sensing methods. The two most popular methods of *in situ* soil moisture monitoring include gravimetric/volumetric sampling and the use of electromagnetic probes (time domain reflectometry (TDR), frequency domain reflectometry (FDR), etc.). Volumetric sampling for volumetric water content determination involves removing a known volume of soil and drying it to determine the mass of water lost. If the density of water is assumed to be  $1000 \text{ kg m}^{-3}$ , then the volume of water present in the original volume of soil can be determined. Gravimetric sampling is similar to volumetric sampling, except that the technique does not require a known volume—numbers are scaled by bulk density values. Gravimetric and volumetric surveys are time consuming, site destructive, and are usually only conducted during field campaigns. They are also unreliable where soils are rocky.

There are a variety of different kinds of electromagnetic probes, which yield instantaneous estimations of soil moisture. Some probes may be emplaced in the ground for a long period of time, or they may be used in short field campaigns to get point estimates of soil moisture. TDR probes work by measuring the time it takes for an electromagnetic wave to travel between probe rods in the soil and relating the impedance to soil moisture content [12]. FDR probes are constructed similarly to TDR probes, but they measure the change in the frequency of the transmitted signal, which is affected by the ground's permittivity/moisture content. Electromagnetic probes should be calibrated to the specific soil type for most accurate results. Both gravimetric/volumetric and electromagnetic methods estimate soil moisture for a small volume of soil ( $<1 \text{ m}^3$ ) [12].

Two remote sensing methods exist for soil moisture—the use of radar or radiometers. Radar remote sensing, also called active remote sensing, involves using an antenna to transmit signals towards the soil surface of a specified frequency, and changes in the reflected signal are measured by the receiving antenna. If the receiving antenna is the same as the transmitting antenna, it is deemed monostatic radar, and if the receiving antenna is different than the transmitting antenna, it is deemed bistatic radar. By and large the most popular method of active radar remote sensing is using monostatic radar measurements.

Soil moisture remote sensing is typically done using either a monostatic radar or radiometer. A monostatic radar system measures how transmitted electromagnetic waves are attenuated by changes in soil moisture (or vegetation). Transmitted waves are reflected back to the same transmitting antenna, and a backscatter coefficient is calculated, with higher backscatter usually correlated with higher moisture contents [6], [13]. Monostatic radar for soil moisture measurement, like GPS-IR, most commonly uses microwave frequencies. Radiometers differ

from radars in that they passively collect naturally-emitted microwave radiation from the soil. They are able to estimate changes in moisture content due to the fact that thermal emission of microwave radiation from soil is highly dependent on its moisture content [14].

Both monostatic radars and radiometers may be mounted on towers or truck booms [15], flown on airplanes [16]–[18], or be mounted on satellites or spacecraft [19]. Those that are mounted on towers or truck booms can give soil moisture estimates on the field scale, or tens to hundreds of square meters, while those on airplanes and satellites have successively larger sensing areas. These measurements tend to be conducted during field campaigns and do not tend to yield long-term records. The exception to this would be instruments on satellites, such as the Soil Moisture and Ocean Salinity (SMOS) or the recently-launched Soil Moisture Active Passive (SMAP) satellites, which give estimates of soil moisture approximately every three days [5]. The sensing area of spaceborne radars or radiometers is on the order of many square kilometers or more. Table 1 summarizes past and present satellite missions that have resulted in soil moisture estimations.

Table 1: Historical and current satellite missions with observations of soil moisture

Satellite	Radar/Radiometer	Sensing Area	Available Data
ASCAT	Radar	25 x 25 km	2007-present
NSCAT	Radar	50 x 50 km	1996-1997
AMSR-E	Radiometer	6 x 4 up to 75 x 43 km	2002-2011
ERS 1-2	Radar	30 x 30 m	1991-2011
SSM/I	Radiometer	70 x 45 km	1987-present
SMMR	Radiometer	25 x 25 km	1978-1987

SMOS	Radiometer	35 x 35 km	2009-present
SMAP	Radar, Radiometer	3 x 3 km	2015 - ?

---

## 2.2 Soil moisture variability

As described in the previous section, different methods of soil moisture measurement yield data representative of different spatial scales. Large differences in results regarding spatial variability exist due to the use of widely different sampling schemes, spacing between samples, number of samples, and measurement errors [20]. In general, soil moisture variability depends on a number of factors, such as vegetation, topography, season, and soil texture [21]. The relative importance of each factor will change depending on the moisture content [21]. For example, the role of vegetation in moisture regulation is relatively more important when the soil is dry, and the role of topography is relatively more important when the soil is wet [21].

Soil moisture variance is also related to the mean moisture content of the field, though studies have found contrasting trends. For example, in [22] it was found that the standard deviation of soil moisture was greatest at intermediate moisture contents and lower when the sampling area was either very dry or very wet. However, [23] found that soil moisture variability tends to decrease linearly with increasing moisture content. [24] observed that soil moisture variability is greater upslope than downslope immediately after a rainstorm, but this variability decreases as the soil dries.

Given the complicating factors just described, it is difficult to say with any certainty a typical value of soil moisture variability for the spatial scale that I will be working with—the field scale. [22] reported standard deviations of moisture contents between 0.025 and 0.04 cm<sup>3</sup> cm<sup>-3</sup>, for a 10 ha maize field with low relief. [21] reported standard deviations between 0.01 and

0.049 cm<sup>3</sup> cm<sup>-3</sup>, for transects approximately 300 m long. [24] reported deviations upwards of 0.06 cm<sup>3</sup> cm<sup>-3</sup> for a 200 m long transect, though these data were taken on a hillslope. Thus, when comparing our GPS soil moisture estimations against *in situ* observations, as will be done in Chapter 8, it will be important to keep in mind that the natural spatial variability of soil moisture will fluctuate through time and be inherently different for sites located in areas of differing vegetation and soil classes.

### **2.3 The Plate Boundary Observatory Network**

The PBO network is an installation of over 1000 geodetic-quality GPS antennas, the majority of which are located in either the western United States or Alaska (Figure 1). The antennas are maintained by UNAVCO via support from NSF. Nearly all of them are choke-ring antennas covered by a radome and are between 1-2.5 m in height (Figure 2b). A choke-ring antenna is designed such that the patch antenna is surrounded by several concentric rings, which are put there to suppress GPS ground reflections, or multipath signals. The radome is a hemispherical dome placed on top of the antenna such that the antenna will not be damaged due to weather or other events. Each antenna has between 1-5 monument legs, which are drilled directly into underlying bedrock, sometimes over 20 m into the ground. Antennas and monuments are designed to record movement due to plate tectonics using predominantly Trimble NetRS receivers.

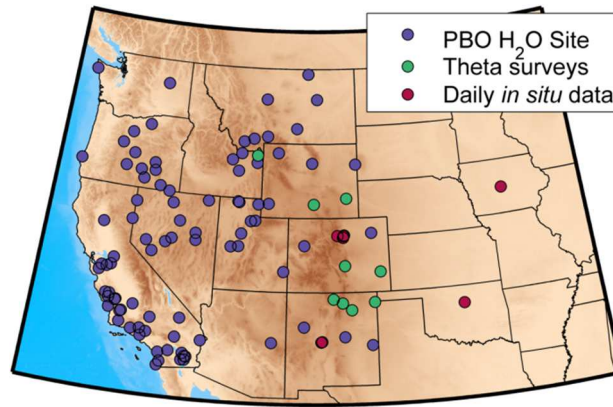


Figure 1: Locations of selected PBO GPS sites that are currently being used to estimate soil moisture (purple), sites that are part of the PBO network that have *in situ* soil moisture data from theta probe surveys (green), and sites that have *in situ* soil moisture probes installed at the site (red). The majority of the sites in red are not PBO sites but have the same types of antennas and receivers as those in the PBO network. There are about a half dozen additional PBO soil moisture sites in the Caribbean that are not shown here.

## 2.4 Remote sensing using GPS reflected signals

Using ground-reflected signals from navigation satellites to remotely sense environmental variables was first proposed in [25] to determine surface wind velocity over the ocean. Subsequent studies primarily pursued the potential of Global Navigation Satellite Systems (GNSS) ground reflections to estimate sea surface wind speed [26]–[28], act as an ocean altimeter [29], [30], or estimate sea ice thickness [31]. More recent studies have explored the ability of GNSS ground reflections to estimate land surface parameters, including snow depth [32]–[34], soil moisture [35], and vegetation phenology [36]–[38].

The above studies focused primarily on using specially-designed GPS or GNSS receivers to infer changes in environmental parameters. However, a subset of studies conducted recently have also shown success in using geodetic-quality GPS antennas in conjunction with commercial receivers to estimate the same environmental variables: snow depth [39], [40], changes in vegetation [41]–[43], and soil moisture [44], [45]. This technique, known as GPS-Interferometric Reflectometry (GPS-IR), relates temporal changes in signal-to-noise ratio (SNR) interferograms

to changes in environmental parameters surrounding a GPS antenna for an area which scales with the monument height [46].

## 2.5 GPS-Interferometric Reflectometry

The constellation of GPS transmitting satellites (up to 32 in number) sends out earth-bound signals indiscriminately, with receiving antennas passively intercepting incoming signals. Part of the incoming signal will travel directly from the GPS satellite to the receiving antenna (called the direct signal), and part of the signal will reflect off of the ground of nearby surfaces before being intercepted by the antenna (indirect, ground-reflected, or multipath signal).

The ground-reflected signal represents a source of noise that geodesists attempt to suppress. Figure 2a shows that the indirect, or multipath, signal tends to pierce the antenna at low angles—this is why the choke-rings are in place, to suppress this signal to the greatest extent possible. The gain pattern of the antenna is also designed such that the antenna itself tries to suppress information coming in from these angles. This causes the indirect signal to be small in magnitude compared to the direct signal, the pierce-point of which is at higher elevation angles.

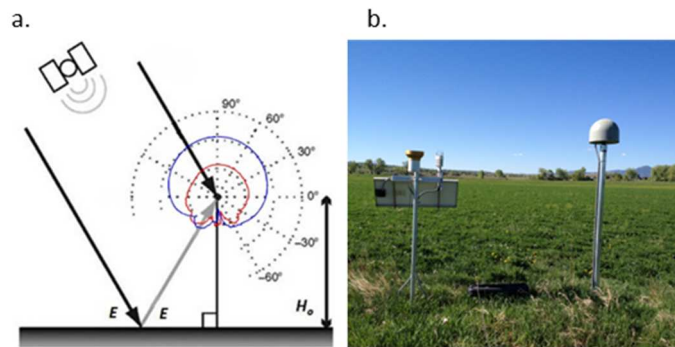


Figure 2: a. Geometry of a multipath signal, for antenna height ( $H_o$ ) and satellite elevation angle ( $E$ ). Bold black lines represent the direct signal transmitted from the satellite. The gray line is the reflected signal from the ground. The antenna's phase center is shown as the small dot. The blue line/outer ring (higher gain) represents the RHCP gain of the antenna. The red line/inner ring (lower gain) represents the LHCP gain of the antenna. At  $0^\circ$ , the RHCP and LHCP gains are approximately  $-38$  dB and  $-50$  dB, respectively. At  $90^\circ$ , the RHCP and LHCP gains are

approximately -20 dB and -40 dB, respectively. b. Photo of a GPS antenna located in an alfalfa field near Boulder, Colorado.

GPS receivers record information about the amount of noise in the environment in signal-to-noise ratio (SNR) interferograms. These data are satellite track specific, such that each track on a given day has its own SNR data time series. SNR data are recorded as a function of time, which is also a function of the elevation angle of the satellite with respect to the horizon (90 degrees defined as zenith). A GPS satellite will rise above the horizon, sending out signals, eventually will pass overhead or nearly so (with respect to the antenna) and then eventually set. Most satellites rise and set over different azimuths with respect to the antenna (Figure 3a). Here, SNR data resulting from different satellite tracks will be referred to by the pseudo-random number sequence (PRN) of the satellite as well as the quadrant that the ground-reflections come from. Thus, if PRN 7 is rising in quadrant 4, the SNR data resulting from this pass will be labeled as PRN 7 Q 4.

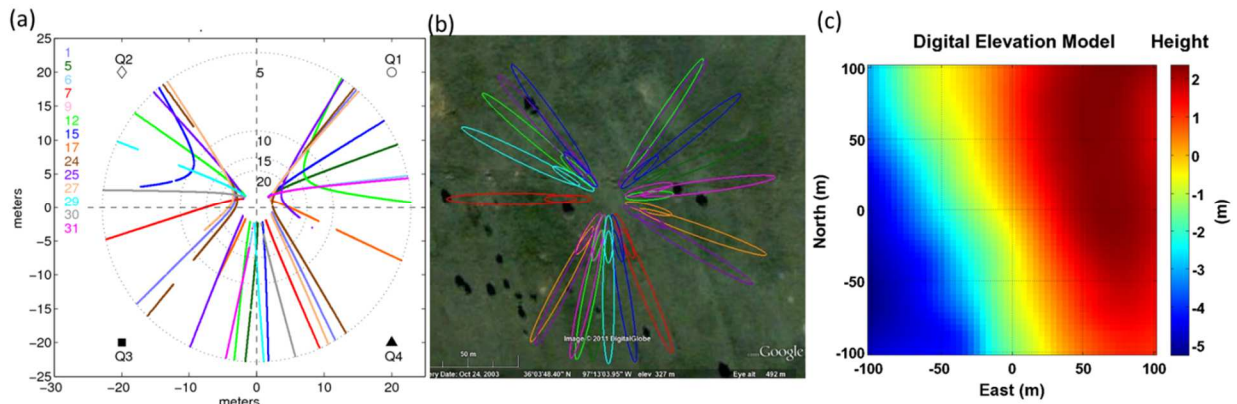


Figure 3: Plan view diagrams for the GPS station OKL3. The GPS antenna is in the situated at the center of each diagram. (a) Reflection point diagram, which shows path traces for selected satellites. Gaps in traces indicate problems with data from trees or other obstructions. Concentric circles show distances illuminated by the first Fresnel zone at that elevation angle. (b) Fresnel zones for selected satellite tracks, which show the total area illuminated by the first Fresnel zone for each track at 5 degrees (large ellipse). (c) Digital elevation model for the GPS site.

At low satellite elevation angles, both the direct and indirect signals are greatly suppressed, so the SNR is relatively low (Figure 4a). At these angles, the indirect signal interferes with the direct signal. The frequency of the oscillating interference pattern is primarily a function of the difference in path lengths. As the satellite rises overhead, the relative proportion of the direct signal received increases due to the antenna's gain pattern, which increases the SNR and decreases the effect of the oscillation pattern (Figure 4a). The time that it takes for a satellite to go from 5-30 degrees above the horizon is approximately one hour. Note that rarely is there SNR data for a satellite below 5 degrees, as the receiver is often hardwired to not accept data from such low angles.

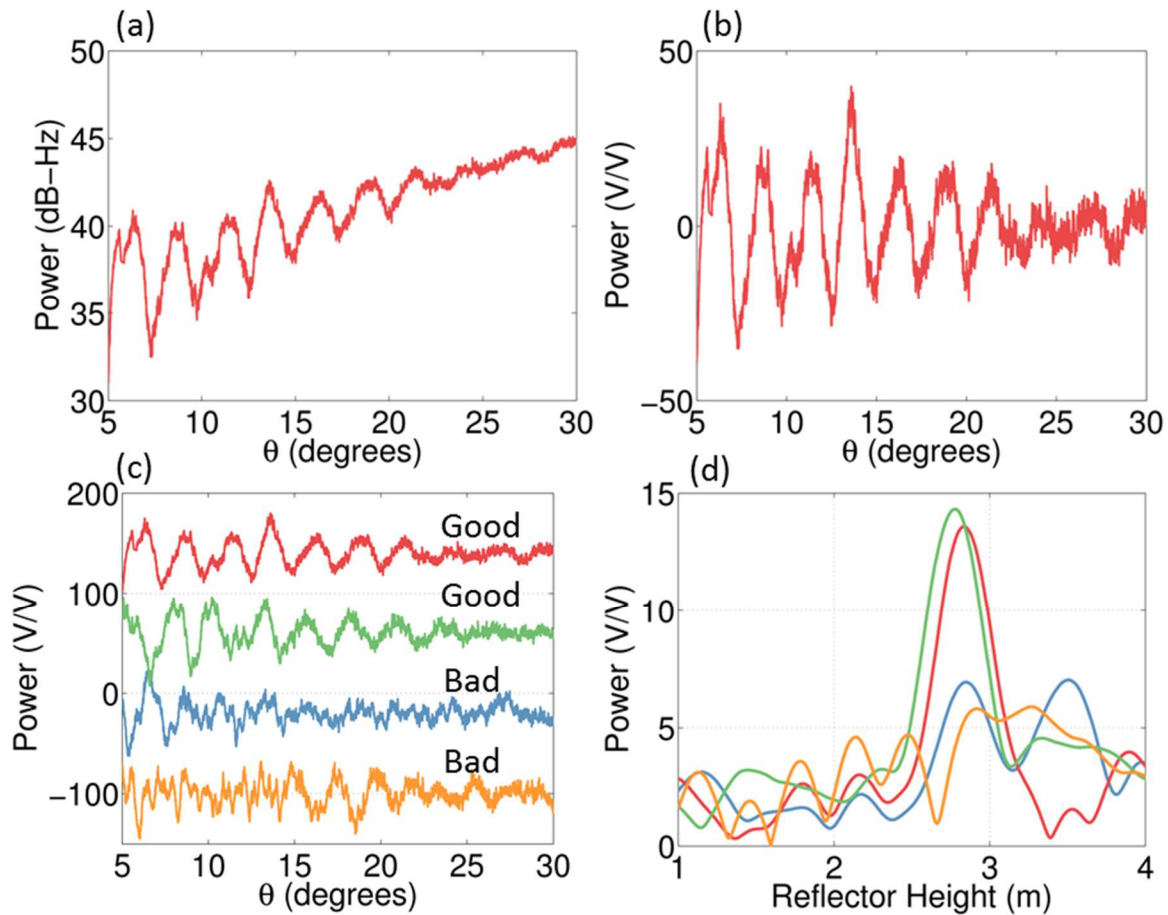


Figure 4: (a) SNR interferogram from PRN 7, quadrant 4. Data are for DOY 120 in 2012 at the Oklahoma GPS station (OKL3). (b) Same SNR data as in (a), but converted to a linear scale and

detrended with a low-order polynomial. (c) Detrended SNR interferograms from four different satellite tracks for DOY 120 in 2012 at the Oklahoma GPS station (OKL3). Interferograms are vertically offset for clarity. (d) Lomb-Scargle Periodograms for the interferograms in (c).

## 2.6 Signal-to-Noise Ratio Data

### 2.6.1 SNR Equation and metrics

The interference between the direct and reflected GPS signals is recorded in SNR interferograms. For a typical geodetic-quality GPS antenna's gain pattern, this interference is greatest at satellite elevation angles smaller than 30 degrees, as shown in Figure 4a.

The influence of the direct signal is seen in a large arcing trend in the SNR interferogram in Figure 4a. In order to remove this influence and only see the interference pattern, the SNR interferogram is converted to a linear scale (volt/volt) (1) and then detrended with a low-order polynomial, estimated for each satellite track on each day (Figure 4b).

$$SNR_{V/V} = 10^{SNR_{dB-Hz}/20} \quad (1)$$

Where:  $SNR_{dB-Hz}$  are the raw data, and  $SNR_{V/V}$  are the data transformed to a linear, volt/volt, scale. Hereafter, the  $V/V$  subscript is dropped for clarity.

The resulting, detrended data are shown in Figure 4b. Note that the interferogram itself is quite noisy. This noise comes from irregularities in the environment and instrument noise. Each satellite track will have its own interferogram for each day, examples of which are shown in Figure 4c. The amplitude of the interferogram is partly determined by the transmit power of the satellite. Newer satellites have higher transmit powers and thus higher amplitudes, relative to interferograms for older satellites. Other factors that affect interferograms that are not the result of changes in the environment include the length of the cable between the antenna and the receiver and the internal temperature of the receiver.

The amplitude of the interferogram decreases as elevation angle increases—this is primarily due to the gain pattern of the antenna. However, changes in soil moisture and vegetation surrounding the antenna will also lead to elevation-angle dependent amplitude changes, as will be shown in later chapters.

Detrended SNR data have previously been modeled using the following equation [47]:

$$SNR = A \cos\left(\frac{4\pi H_0}{\lambda} \sin E + \phi\right) \quad (2)$$

Where:  $H_0$  is the height of the antenna,  $E$  is the elevation angle of the satellite,  $A$  is a constant amplitude,  $\lambda$  is the GPS wavelength, and  $\phi$  is a phase shift. This expression assumes that the SNR data have a constant frequency ( $\frac{4\pi H_0}{\lambda}$ ). The observations in Figure 4c show that  $A$  is not constant but depends upon elevation angle.  $A$  and  $\phi$  are found from the SNR data using least-squares estimation, with  $H_0$  set to the best approximation of the height of the antenna.

Eq. (2) forms the foundation for remote sensing of soil moisture using GPS-IR. The parameters in (2),  $A$  and  $\phi$ , are two of four metrics that have been investigated with regards to their utility in inferring changes in surface soil moisture. The simplification of  $A$  and  $\phi$  being independent of elevation angle, when at least  $A$  certainly is not independent, do make certain aspects of soil moisture estimation not straightforward, as will be shown later. However, because complications from topography, tilted surfaces, and slight differences in antenna gain patterns exist in real data, it will be shown that implementing a more complicated parameterization of  $A$  with elevation angle would not be practical.

Although  $A$  and  $\phi$  are calculated under the assumption that  $H_0$  is a known constant, for observed data,  $H_0$  must be derived empirically and varies between satellite tracks due to changes

in the microtopography surrounding an antenna.  $H_0$ , or the ‘*a priori* reflector height’ is estimated using a Lomb-Scargle Periodogram (LSP), which is a method of spectral analysis that is akin to a Fourier transform, except that it can process the unevenly-sampled SNR data recorded by the GPS receiver. The LSP returns the spectral amplitude of a range of frequencies in the interferogram, and the dominant/peak frequency is converted to an effective reflector height,  $H_{eff}$ , using the following relationship [48]:

$$H_{eff} = \frac{1}{2} f_m \lambda \quad (3)$$

Where  $f_m$  is the peak frequency of the LSP. The power of the dominant frequency will be referred to as  $A_{LSP}$ . In cases where  $H_{eff}$  and  $H_0$  are identical or nearly so,  $A_{LSP}$  and  $A$  will be equal or nearly so. Examples of LSPs are shown in Figure 4d. Note that two of the satellite tracks from Figure 4c do not have distinguishable, dominant frequencies relative to noise, as shown by the LSPs in Figure 4d (orange and blue lines). Calculated phase and amplitude for these two tracks will not be as reliable as phase and amplitude calculated from the other two satellite tracks, shown in red and green.

In order to estimate  $H_0$ , the median of a relatively long time series of  $H_{eff}$  values are used. What constitutes a long enough time series varies depending on the site conditions, though in general the longer the time series, the better. However, one needs to ensure that the data are not being chosen during times of year when there is likely to be snow or significant vegetation present.

Together,  $A$ ,  $\phi$ ,  $H_{eff}$ , and  $A_{LSP}$  constitute the four ‘SNR metrics’ that will be investigated with regards to their sensitivities to changes in land surface characteristics.

## 2.6.2 Temporal changes in SNR metrics

Observed time series of the four SNR metrics each undergo data processing before they may be compared to time series of SNR metrics from different satellite tracks. The absolute magnitudes of both  $A$  and  $A_{LSP}$  are primarily controlled by the transmit power of the particular GPS satellite—newer satellites have higher transmit powers. The time series in Figure 5 show time series for both  $A$  and  $A_{LSP}$  from two satellite tracks. All of the time series exhibit similar seasonal fluctuations throughout the year; however, both  $A$  and  $A_{LSP}$  for PRN 5 are consistently higher than for PRN 12, indicating a higher transmit power for PRN 5.

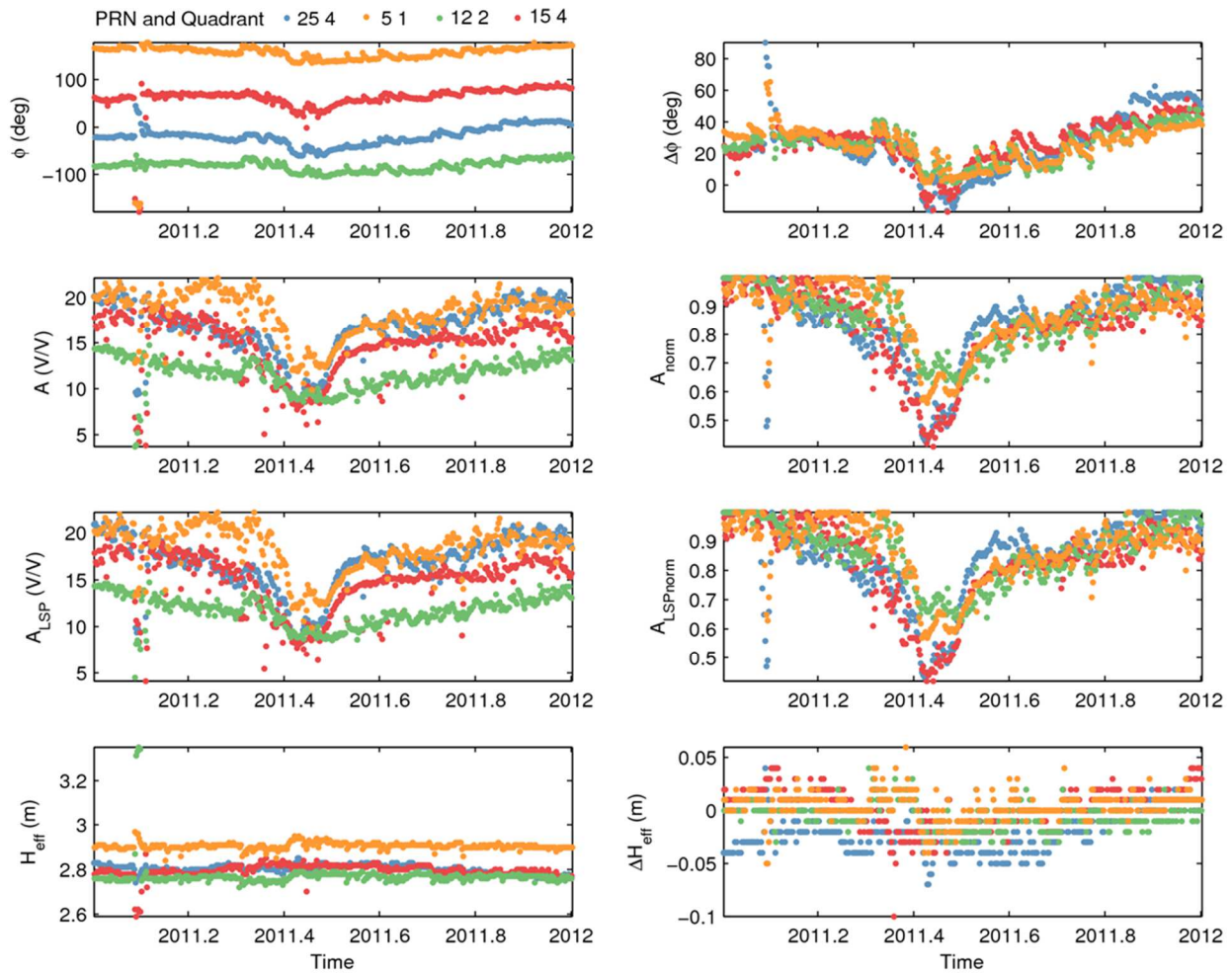


Figure 5: (left column) Raw SNR metric time series for four satellite tracks at the GPS station OKL3. There is significant noise present in all four time series around 2011.1, indicating a snow

event. (*right column*) The corresponding zeroed, normalized, or differenced metric time series. The snow signature has not been removed from these time series.

In order to compare relative changes in the  $A$  and  $A_{LSP}$  time series across satellite tracks and GPS sites, each time series is normalized with respect to the mean of the top 20% of the data in each time series:

$$A_{LSPnorm} = A_{LSP} / \overline{A_{LSP20\%}} \quad (4)$$

$$A_{norm} = A / \overline{A_{20\%}} \quad (5)$$

Where:  $\overline{A_{20\%}}$  and  $\overline{A_{LSP20\%}}$  are the mean of the top 20% of data from each time series.  $A_{norm}$  and  $A_{LSPnorm}$  are thus unitless measures of relative change in each satellite track's amplitude time series (see Figure 5 for examples of the conversion).

Similarly, the absolute magnitude of  $H_{eff}$  varies between satellite tracks due to differences in microtopography surrounding the antenna. In order to see relative changes in  $H_{eff}$ , the  $H_{eff}$  time series is subtracted from the estimated antenna height, yielding  $\Delta H_{eff}$ .

$$\Delta H_{eff} = H_0 - H_{eff} \quad (5)$$

Example time series of the conversion between  $H_{eff}$  and  $\Delta H_{eff}$  are shown in Figure 5.

Phase, calculated under the assumption that antenna height is equal to  $H_0$ , is also characterized as having a satellite-track specific 'baseline' value, as shown in Figure 5. Figure 5 shows that each  $\phi$  time series exhibits similar seasonal and higher frequency fluctuations, despite the different baseline values. The baseline phase value for each satellite track is determined by many factors, such as tilting of the ground surface and errors in  $H_0$  estimation. When the baseline values are subtracted from each track's time series, as in Figure 5, data are more easily

comparable to one another. For empirical data, the following equation is used to ‘zero’ each phase time series.

$$\Delta\phi = \Delta\phi_{obs} - \bar{\phi}_{30\%} \quad (10)$$

Where  $\bar{\phi}_{30\%}$  is the mean of the lowest 30% of observed phase values for a specific year. Phase data tend to be zeroed on a per-year basis, whereas amplitude normalization and effective reflector height differencing tend to use the entire time series. The reason for this will be described in Chapter 6.2.

All further analyses will show results in terms of  $\Delta\phi$ ,  $\Delta H_{eff}$ ,  $A_{norm}$ , and  $A_{LSPnorm}$ .

## Chapter 3: Ground truth experiments and data

In order to investigate the sensitivity of GPS-IR to changes in soil moisture and vegetation in field settings, dozens of vegetation surveys were conducted, and several years' worth of *in situ* soil moisture data were collected, either using permanently-installed probes or from surveys with a theta probe. This section summarizes the field data. The data were used for validating the electrodynamic soil and vegetation model described in Chapter 4 as well as validating soil moisture retrievals using GPS-IR described in Chapter 6.

### 3.1 Description of measurement techniques

#### 3.1.1 In situ soil moisture data

##### 3.1.1.1 Time domain reflectometry probes

Fig. 1 from Chapter 2.2 shows a map of GPS sites that either have permanently-installed soil moisture probes (red points) or have at least one soil moisture survey (green points). The majority of the sites with permanently-installed probes are not part of the PBO network, with the exception of p041 in north-western Colorado, though most of these sites are part of the PBO H<sub>2</sub>O network. Most stations have been providing 30-minute soil moisture data for approximately the past five years. Time-domain reflectometry probes at these sites are Campbell Scientific 616 moisture probes. The typical installation at the GPS sites is as follows: 3 or more probes are connected to a data logger powered near the GPS receiver. Each probe has at least a 40 ft. long cable connecting the data logger to the probe itself, which means probes may be installed up to 40 feet away from the GPS antenna. The probes tend to be installed south of the antenna and at least 10 or more feet away from one another, in order to record spatial heterogeneities in soil moisture. The first 3-5 probes are buried at a depth of only 2.5 cm. This depth actually gives a

vertical-average of the soil moisture between 0-5 cm. If there are more probes available at the site, they are buried at 7.5 cm, which gives the average soil moisture between 5-10 cm. At a few sites, there are also probes buried at 20 cm, and in rare cases, 40 cm.

Time-domain reflectometry probes, like the CS 616s, emit an electromagnetic pulse that travels down the length of the rod and is reflected back to its source. The velocity of the pulse depends on the dielectric permittivity of the surrounding medium (in this case, soil). The higher the moisture content of the soil, the higher the permittivity, and the slower the signal velocity [49]. The probes record the time it takes between the emitted pulse and the subsequent received reflection, and if the length of the probe is known, travel velocity may be calculated. The velocity of the reflected signal is related to the moisture content, using the factory-calibrated relationships. Factory calibrations may not be representative of true field conditions if the conductivity of the soil is unusually high, if the soil is compacted, or if the soil has a high clay content. In these situations, more accurate results would be achieved using a field-specific calibration. We have used the factory calibration (quadratic fit) at all of our field sites since there is a good correlation between our probe data and data from volumetric samples.

Variations in ground temperature are a significant source of error in soil moisture estimations using the CS616 probes that we account for at all of the sites. A standard temperature correction is used before conversion to soil moisture, using Campbell Scientific temperature probes (thermistors) buried at either 2.5 cm or 7.5 cm depth. In cases where there are probes buried at 20 or 40 cm, these data are not corrected for temperature effects.

### **3.1.1.2 Theta probe surveys**

We have conducted several theta probe surveys at select GPS sites, which yield estimates of soil moisture content over the top 6 cm of the soil column. Many of these sites are PBO stations, and some sites have data from both CS616 and theta probe surveys. The theta probe we use is the ML3, manufactured by Delta-T Devices. The theta probe also emits an electromagnetic pulse into the soil and measures the resulting voltage, relating the voltage to the refractive index of the soil, which is close to the square root of the permittivity [50]. The ML3 probe provides factory calibrations to relate the recorded voltage to the moisture content of mineral and organic soils. We use the factory calibration for the organic soil to produce our soil moisture estimates. These data are not corrected for temperature.

Theta probe surveys consist of several point measurements within 35 m of a GPS antenna, usually on the order of 20-30 measurements, which are then averaged.

### **3.1.1.3 Gravimetric soil moisture surveys**

Gravimetric soil moisture surveys have also been conducted at selected GPS stations. Gravimetric soil moisture sampling is one of the only ways to directly measure soil moisture. Gravimetric sampling involves inserting a column (usually metal) with a known volume vertically into the soil and removing all of the soil contained within the column. The soil is weighed, dried at 100 degrees Celsius for 24 hours, and then weighed again. This method may provide a measurement of volumetric moisture content, assuming the density of water is 1000 kg m<sup>-3</sup>.

### **3.1.2 Vegetation surveys**

At GPS sites with vegetation field data, vegetation samples are generally collected regularly throughout the growing season, though some sites only have a few surveys. An individual vegetation sampling survey consists of collecting seven vegetation samples, at random azimuths and distances (between 7-35 m), around an antenna. At each sampling location, a 30 x 30 cm or 50 x 50 cm grid is tossed on the ground, and vegetation canopy height is measured. The measured canopy height is meant to represent the 90<sup>th</sup> percentile height. For some very heterogeneous environments, the height measurement may not be representative of the vegetation that is actually within the sampling grid. All of the vegetation within the grid is then cut and weighed. The cut vegetation is then dried for 48 hours at 50 degrees Celsius and weighed again, to measure how much water was in each sample. The dried vegetation is referred to as the dry biomass. Once the data from the seven samples are averaged, we have estimates of the mean canopy height, water content, and dry biomass on each day that samples were collected. This vegetation collection does not modify site characteristics to any noticeable degree, given the relatively larger sensing area of each antenna. For example, 15 sampling days during a growing season would disturb only 10 m<sup>2</sup> of vegetation, about 1% of the sensing area within the GPS footprint.

## **3.2 Data Summary**

### **3.2.1 Soil Moisture Data**

Figure 6 shows the distributions of 30-minute soil moisture using data from the CS616 probes for each GPS station that has data. Data are grouped by rough site location; for example the three wheat/oat sites are labeled “Wheat,” and the sites in Oklahoma are labeled

“Rangeland.” Note that most of the soil moisture distributions are not Gaussian, which means using statistics like the mean or median will be slightly misleading.

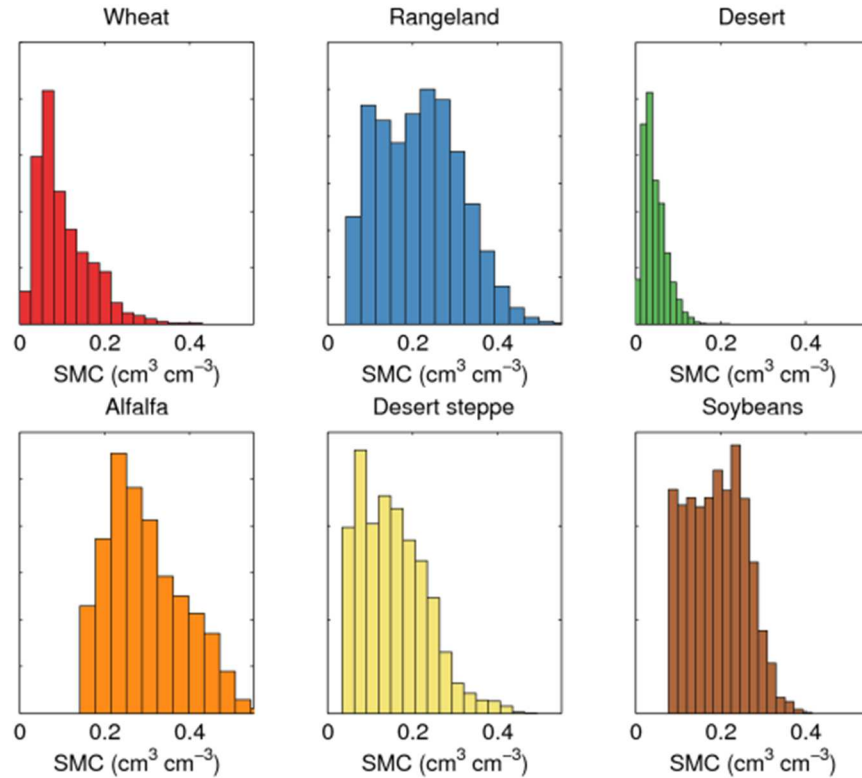


Figure 6: Distributions of 30-minute soil moisture content for the GPS stations with CS 616 probes. Data are from probes buried at 2.5 cm depth.

Table 2 indicates how many theta probe and gravimetric soil moisture surveys exist at official and provisional PBO H<sub>2</sub>O sites. More surveys have been conducted at other sites that are not sites used for soil moisture estimation.

Table 2: Summary of theta probe and volumetric soil moisture surveys conducted at GPS stations. The horizontal line indicates that split between our validation sites and PBO sites.

Site	Years	Total # of theta survey points	Total # of gravimetric survey points
OKL2	2011-2012	33	0
OKL3	2011-2012	33	0

OKL4	2011-2012	32	0
P041	2014	25	4
bcgr	2011-2014	38	15
Oats	2012	14	3
ames	2012	1	2
Bcw2	2011	5	8
P036	2013-2014	5	1
P070	2013-2014	5	1
P040	2013-2014	5	1
P037	2013-2014	5	1
P039	2013-2014	5	1
P123	2014	3	0
P035	2014	2	0
P038	2014	2	0
P032	2013	2	2
P042	2013	2	2
P360	2013	1	1
P048	2011	0	1
P049	2011	0	1
P050	2011	0	1
P053	2011	0	1
P103	2011	0	1
P678	2011	0	1
P679	2011	0	1
P684	2011	0	1

P719	2011	0	1
P722	2011	0	1

### 3.2.2 Vegetation Data

Table 3: GPS stations, antenna heights, and vegetation information shows, for many of the stations for which we have vegetation field data, the range of wet weight ( $M_f$ ), dry biomass ( $M_d$ ), and canopy height ( $H_{veg}$ ) measurements. The sites vary significantly from one another, depending on the vegetation type. For example, the vegetation at the alfalfa site can contain more than three times the amount of water as the vegetation at the rangeland sites. Figure 7 shows vegetation data from field surveys in the form of how different vegetation parameters vary with one another. In this figure, GPS stations have been grouped into different classes, which depend on either the location of the GPS antenna or the vegetation type. Each point in Figure 7 is the average of each vegetation field survey. Figure 7a shows how vegetation biomass and canopy height vary with one another, depending on the vegetation group. Plotting biomass on the x-axis is not meant to imply that biomass determines canopy height. The outliers in the agricultural group (red points) are bcgr 2013 (alfalfa field) data, which differ from the other data due to heavy rains that caused the canopy to fall over and made measurement difficult. There tends to be a good relationship between biomass and canopy height within vegetation groups. Figure 7b shows the relationship between canopy height and water content. There is more scatter in this relationship than between biomass and height, especially for the agricultural sites. Figure 7c shows the relationship between canopy biomass and water content. There is a good relationship between 2010-2012 agricultural data, but no clear relationships for the other vegetation groups.

The relevance of Figure 7 will be described in Chapter 4.4. For now, the important thing to keep in mind is that there is a large amount of variability in the relationships between vegetation parameters, even within the same vegetation class. These relationships change throughout a growing season and between growing seasons. General conclusions about the vegetation characteristics at a site could be made based on class (i.e. “At grasslands, it is unlikely the water content will exceed  $1 \text{ kg m}^{-2}$ ”), but conclusions with any more detail would be difficult to draw.

Table 3: GPS stations, antenna heights, and vegetation information

Station	$H_0$ (m)	Years	# of surveys	Range of Data			$\epsilon' + \epsilon''$
				$M_f$ ( $\text{kg m}^{-2}$ )	$H_{veg}$ (cm)	$M_d$ ( $\text{kg m}^{-2}$ )	
Desert Steppe A	1.96 +/-0.03	2011	21	0.16-0.71	8-47	0.1-0.35	1.03+0.009i
Desert Steppe B	2.83 +/-0.03	2012-2013	39	0.08-.32	3-31	0.03-0.24	1.015+0.005i
Rangeland C	2.72 +/-0.06	2011-2012	29	0.29-1.02	5-38	0.19-0.65	1.03+0.011i
Rangeland D	2.82 +/- 0.03	2011-2012	30	0.33-1.55	3-49	0.20-1.01	1.035+0.011i
Rangeland E	3 +/- 0.05	2011-2012	30	0.36-1.44	8-32	0.23-0.98	1.04+0.017i
Alfalfa	2.69 +/- 0.15	2011-2013	56	0.11-4.95	5-80	0.06-2.59	1.06+0.013i
Soybean	2.96 +/- 0.09	2012	5	0.04-2.57	9-90	0.01-0.78	1.04+0.004i

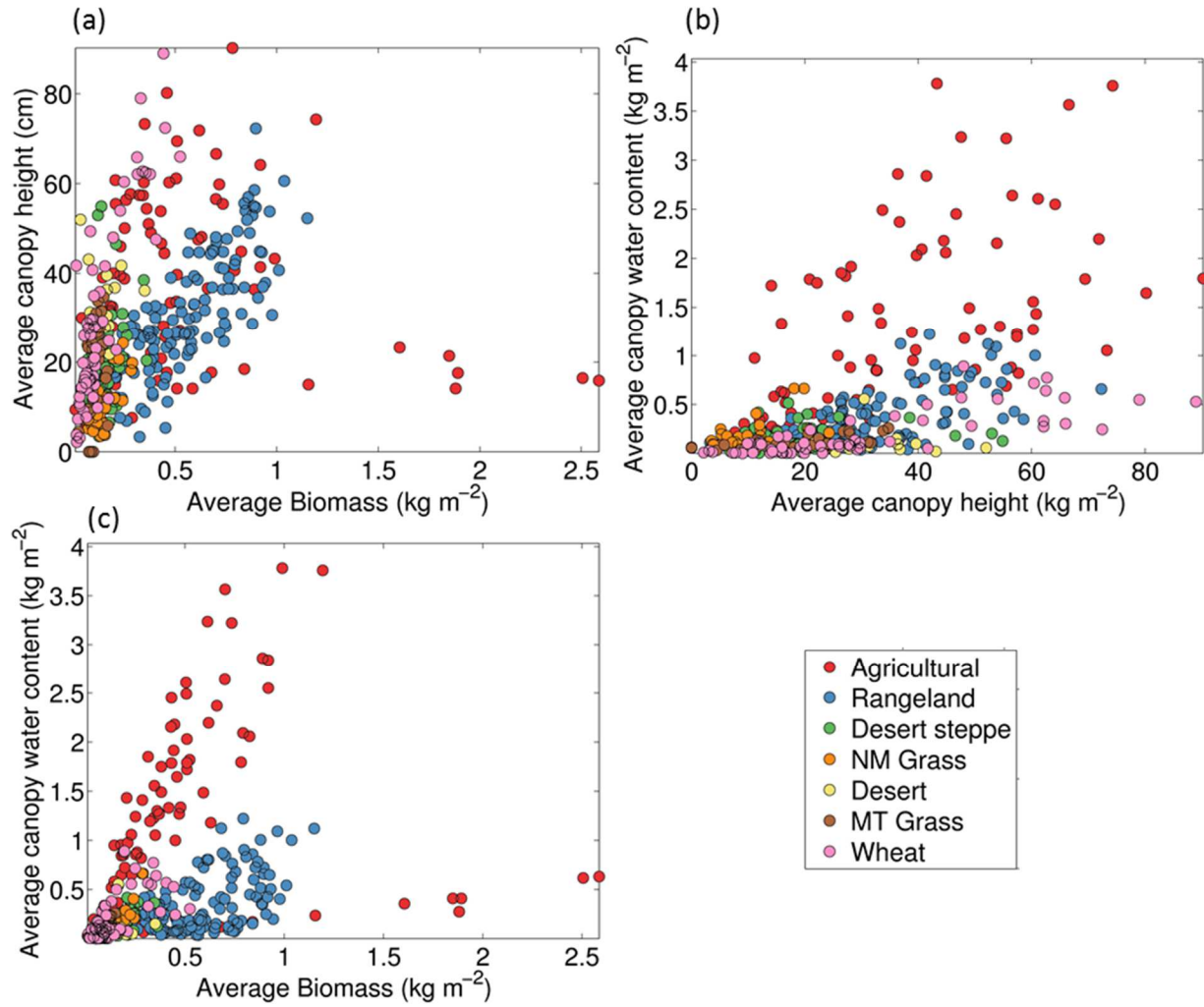


Figure 7: GPS stations with vegetation surveys have been grouped into several classes: agricultural (bcgr, ames), rangeland (Oklahoma), desert steppe (low3, p041, mflc), New Mexico grass (p070, p123, p035, p036, p037, p038, p039, p040), desert (shr1, grs2), Montana grass (p719, p046, p048), and wheat (bcwh, bcw2, oats). Each panel shows vegetative field relationships for each of the classes. (a) biomass versus canopy height (best  $r^2$  was for the Rangeland sites, 0.52) (b) canopy height versus water content (best  $r^2$  was for the NM Grass sites, 0.83) (c) biomass versus water content (best  $r^2$  was for the agricultural sites, 0.46).

## **Chapter 4: Forward modeling of SNR data in relation to soil moisture and vegetation**

In this chapter, I describe an electrodynamic model that simulates how SNR interferograms (and their resulting metrics) are affected by changing the moisture content of the soil as well as changing vegetation canopy parameters. Data from the previous chapter will be used to validate this model. Modeling interferograms is useful because observed SNR metric time series from different satellite tracks, even at the same site, show large differences, as in Figure 5. There are many complicating factors that exist in observed data that cannot always be adequately quantified or identified (temperature effects, spatial heterogeneities, azimuthal differences in gain pattern, etc.). Modeling is the only way to remove these effects and only look at contributions of soil moisture and vegetation parameters to changes in SNR data.

This chapter is organized as follows. First, the model architecture is described. I cannot take credit for the majority of the model development; the heavy lifting in model design was all accomplished by Valery Zavorotny of NOAA. However, in order to better understand the contribution that I made to the model (addition of a vegetation canopy), it is necessary to describe the model from the ground up. The model is then validated, using observed SNR data, vegetation field data, and *in situ* soil moisture data for comparison. Next, how soil moisture content affects SNR metrics for a bare soil is quantified. A simple relationship is derived for estimating soil moisture using SNR metrics. Following this, the effect of adding a vegetation canopy on SNR metrics is explored, assuming that the moisture content of the soil does not change. The most important canopy parameters are identified, and the influence of interactions between parameters on metrics is explored. Finally, the effect of changing the underlying soil moisture content, with variable overlying vegetation, on SNR metrics is investigated.

## 4.1 Model architecture

The theoretical basis for the relationships between SNR metrics and soil and vegetation parameters is derived from a 1-D, electrodynamic, single-scattering, forward model. The foundation for the model was developed in [51]. The model simulates SNR interferograms, from which metrics may be calculated, given antenna, soil, and vegetation canopy information as input parameters. The model assumes that the topography surrounding the antenna is perfectly smooth, though some experiments with adding surface roughness have been done. A large part of this project was adapting the model foundation, which was developed for bare soil simulations, to include the effects of a vegetation canopy.

### 4.1.1 Reflection coefficient calculations

The core component of the model is the numerical calculation of reflection coefficients for a GPS signal reflecting from a surface. The procedure for calculating the coefficients is presented in [10]. For a vertically layered medium with arbitrary dielectric constants assigned to each layer, the model calculates the horizontal and vertical polarization reflection coefficients for the signal reflecting out of each layer, taking into consideration absorption within each layer. The soil layers in the model are very thin—fractions of a millimeter, so the model is basically calculating reflection coefficients for a continuous profile. Calculation of coefficients is outlined in the following equations:

$$\varepsilon_m = \varepsilon'_m + i\varepsilon''_m \quad (3)$$

$$R_{Ht} = \frac{\sqrt{\varepsilon_{m+1} - \varepsilon_M \sin^2 \theta} - \sqrt{\varepsilon_m - \varepsilon_M \sin^2 \theta}}{\sqrt{\varepsilon_{m+1} - \varepsilon_M \sin^2 \theta} + \sqrt{\varepsilon_m - \varepsilon_M \sin^2 \theta}} \quad (4)$$

$$R_{Vt} = \frac{\varepsilon_m \sqrt{\varepsilon_{m+1} - \varepsilon_M \sin^2 \theta} - \varepsilon_{m+1} \sqrt{\varepsilon_m - \varepsilon_M \sin^2 \theta}}{\varepsilon_m \sqrt{\varepsilon_{m+1} - \varepsilon_M \sin^2 \theta} + \varepsilon_{m+1} \sqrt{\varepsilon_m - \varepsilon_M \sin^2 \theta}} \quad (5)$$

$$\psi = 2k_w dz \sqrt{\varepsilon_m - \varepsilon_M \sin^2 \theta} \quad (6)$$

$$q = e^{i\psi} \quad (7)$$

$$R_{Hb,m+1} = \frac{R_{Ht} + R_{Hb,m}q}{1 + R_{Ht}R_{Hb,m}q} \quad (8)$$

$$R_{Vb,m+1} = \frac{R_{Vt} + R_{Vb,m}q}{1 + R_{Vt}R_{Vb,m}q} \quad (9)$$

Where  $\varepsilon_m$ ,  $\varepsilon_{m+1}$ , and  $\varepsilon_M$  are the complex permittivities of layer  $m$ , layer  $m+1$  above layer  $m$ , and the top or surface layer, respectively.  $\theta$  is the angle of incidence.  $R_{Ht}$  and  $R_{Vt}$  are the horizontal and vertical reflection coefficients, respectively, for the boundary interface between layers  $m$  and  $m+1$ .  $dz$  is the height of layer  $m$ , and  $k_w$  is the wave number, equal to  $2\pi/\lambda$  ( $\lambda$  is the wavelength of the GPS signal).  $q$  represents the amount of absorption in layer  $m+1$ .  $R_{Hb,m+1}$  and  $R_{Vb,m+1}$  are the horizontal and vertical reflection coefficients after absorption in layer  $m+1$ , which upon iteration for the next layer become  $R_{Ht}$  and  $R_{Vt}$ .

Once the effective reflection coefficients have been calculated for the entire layered medium, they are converted into reflection coefficients at left- and right-handed circular polarization ( $R_{LC}$  and  $R_{RC}$ ), using the following relationships:

$$R_{LC} = 0.5(R_{Vb} - R_{Hb}) \quad (10)$$

$$R_{RC} = 0.5(R_{Hb} + R_{Vb}) \quad (11)$$

The model calculates reflection coefficients for a range of satellite elevation angles ( $\theta$ ), from 5-30 degrees in increments that are usually 0.002 degrees. However, a larger angle spacing

does not significantly affect conclusions for how resulting SNR interferograms vary with environmental input parameters.

#### **4.1.2 Permittivity profile generation: Soil**

For GPS-IR, the layered medium of interest is a soil with an overlying vegetation canopy. As stated previously, the permittivity of a soil at microwave frequencies is predominantly dependent on its moisture content, though there is a second-order dependence on soil texture, or the relative amounts of sand, silt, and clay within the soil. The relationships between soil texture, moisture content, and permittivity at microwave frequencies is fairly well studied. This model uses relationships found in [9], [52] which presents complex permittivity measurements using semi-empirical relationships for 1.4 GHz (L-band), five soil textures ranging from a sandy loam to a silty clay, and a wide range of moisture contents.

The soil component of the model requires user-specified volumetric soil moisture estimates at variable depths in the soil column and as well as a soil texture. The depths at which soil moisture is specified is up to the user, though the model does not currently consider moisture contents below 20 cm depth. Specified moisture contents are allowed to vary between 0.01 and 0.5  $\text{cm}^3 \text{cm}^{-3}$ . The model discretizes, interpolates, and extrapolates as necessary the input moisture contents using a cubic spline to create a vertical soil moisture profile with soil layers that are generally 0.1 mm thick, though this parameter may be specified. The vertical soil moisture profile is then converted to a vertical complex permittivity profile, using the specified soil texture and semi-empirical relationships found in [9] in a lookup table.

### **4.1.3 Permittivity profile generation: Vegetation**

A vertical permittivity profile of the overlying vegetation canopy, if there is one present, must also be calculated. Although the model is able to accommodate the addition of vegetation layers (analogous to the soil layers), here I assume the vegetation canopy is comprised of only one layer, the reason for which is discussed below. The permittivity of vegetation material has been the subject of many studies [53]–[56]; however, empirical measurements are more difficult to make than for soil, and other properties than water content (i.e. volume fraction of vegetation within the canopy) affect the overall permittivity of the vegetation canopy. A lookup table of permittivity estimates is not possible here. Most empirical measurements of vegetation permittivity focus on vegetation that is already mostly dried, so there are not many published data on the range of permittivities possible for a specific vegetation type. In addition, the permittivity of the vegetation material itself will be quite different from the effective permittivity of the canopy, which itself is a mixture of vegetation material and air. Few studies exist that directly attempt to measure the permittivity of a vegetation canopy, and those that do note that the volume fraction of vegetation within the canopy is an important factor [56]. The volume fraction of vegetation within the canopy will be highly dependent on vegetation type and will vary depending on the point in the growth cycle.

Due to the complexities described above, it is most common to use a model to estimate vegetation permittivity. The vegetation permittivity model that is used here was developed in [55]. This model was validated using data from corn leaves and only calculates the permittivity of the vegetation material, not of a canopy, which would include contributions from both vegetation and air. It requires user-specified input parameters of signal frequency, vegetation

salinity [‰], dry biomass [ $\text{kg m}^{-2}$ ], and the fresh biomass (wet weight of vegetation material) [ $\text{kg m}^{-2}$ ].

$$M_g = \frac{M_f - M_d}{M_f} \quad (12)$$

$$\sigma = 0.16S - 0.0013S^2 \quad (13)$$

$$\varepsilon_r = 1.7 - 0.74M_g + 6.16M_g^2 \quad (14)$$

$$v_{fw} = M_g(0.55M_g - 0.076) \quad (15)$$

$$v_b = \frac{4.64M_g^2}{1+7.36M_g^2} \quad (16)$$

$$\varepsilon_{veg} = \varepsilon_r + v_{fw} \left[ 4.9 + \frac{75.0}{1+if/18} - i \frac{18\sigma}{f} \right] + v_b \left[ 2.9 + \frac{55.0}{1+(if/0.18)^{0.5}} \right] \quad (17)$$

Where:  $M_f$  is fresh biomass,  $M_d$  is dry biomass,  $M_g$  is gravimetric moisture content,  $S$  is vegetation salinity,  $\sigma$  is the ionic conductivity [ $\text{Siemens m}^{-1}$ ],  $\varepsilon_r$  is the dielectric of the non-dispersive residual component of the vegetation,  $v_{fw}$  is the volume fraction of free water within the vegetation,  $v_b$  is the volume fraction of bound water,  $f$  is the signal frequency, and  $\varepsilon_{veg}$  is the complex permittivity of the vegetation material. Ideally,  $\varepsilon_r$  would be independent of moisture content, which is a limitation of the model. However, its overall contribution to the resulting permittivity estimate is relatively small. Because there are no vegetation salinity data for our PBO sites,  $S$  has been assumed to be a constant 8.5‰, which was the value found in [55] to show best agreement with their validation data.

Once the permittivity of vegetation material has been determined, the permittivity of the canopy is calculated. The model assumes that the only constituents in the canopy are vegetation and air, or:

$$v_{total} = v_{air} + v_{veg} \quad (18)$$

The volume fraction of vegetation within the canopy,  $v_{veg}$ , is determined to be:

$$v_{veg} = \frac{M_f}{H_{veg} \times \rho_{veg}} \quad (19)$$

Where:  $H_{veg}$  is the height of the canopy, and  $\rho_{veg}$  is the true density of vegetation material [ $\text{kg m}^{-3}$ ]. Eq. 19 simply calculates how ‘spread-out’ the water and bulk vegetation material is in the canopy.  $\rho_{veg}$  is expected to vary with vegetation type and moisture content, and its relationship with moisture content can be somewhat unintuitive. For example, if one assumed that the volume of vegetation material stays the same regardless of moisture content, the addition of water would increase  $\rho_{veg}$  to a maximum value of  $1000 \text{ kg m}^{-3}$ , if gravimetric moisture content were 100%. However, in reality it can be assumed that when vegetation water content decreases, the volume will shrink an amount proportional to that of the lost water [55] and vice versa. The exact relationship will depend on plant type and even within specific plant geometric components. For example, the dependence of true density with moisture content of plant seeds has been shown to be a parabolic function of moisture content for some seed types [57]. Unfortunately, there is a dearth of published data for a wide range of moisture content and natural plant types (most studies address fruits and seeds).  $\rho_{veg}$  is an important parameter for determining effective canopy permittivity. In model validation, discussed in a later section, we assumed  $\rho_{veg}$  to be directly proportional to water content, which assumes volume changes to be

negligible, and found good agreement with observations. In the vegetation filter, which is also discussed in a later section, we no longer assume this relationship to ensure the filter can be applied to vegetation types that do not have such a relationship with water content and  $\rho_{veg}$ .

Once the volume fractions of air and vegetation have been determined, the Complex Refractive Index mixture equation [58] is used to calculate the resulting permittivity of the canopy:

$$\epsilon_{canopy}^{1/2} = v_{veg}\epsilon_{veg}^{1/2} + v_{air}\epsilon_{air}^{1/2} \quad (20)$$

The permittivity of air has no dispersive component and is:

$$\epsilon_{air} = 1.0 + i0.0 \quad (21)$$

In general in the model, the permittivity of the plant canopy is assumed to be constant with height, though some vegetation types with definitive layers could be modeled, if one knew how the moisture content varied with different plant constituent parts. A schematic of the combined permittivity profiles of soil and vegetation is shown in Figure 8.

The effective permittivity of the canopy is often very close to that of air, which is expected, given that most plant canopies are comprised mostly of air [53]. As will be shown, modeled values of permittivity agree well with published values using time domain reflectometry to measure canopy permittivity, which are also very close to the permittivity of air [56].

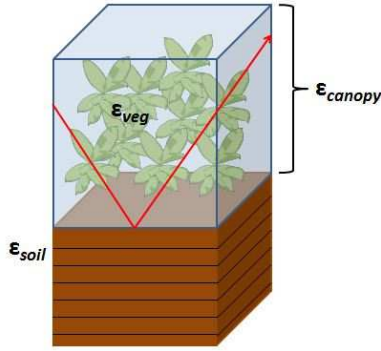


Figure 8: Schematic of the combined soil moisture and vegetation permittivity profiles.

#### 4.1.4 Note on the plane-stratified model for a vegetation canopy

The model I have presented here is a plane-stratified model—many studies have used plane-stratified models to simulate emission from vegetation canopies at microwave frequencies (e.g. [59], [60]). This is in contrast to a geometrical modeling approach, in which each component of the plant canopy, such as stalks and leaves, is modeled by their geometrical shapes (e.g. [15], [61]). Geometrical modeling is used because, at microwave frequencies, a canopy layer is often considered inhomogeneous and anisotropic [54]. Geometric effects are most important when the components of the canopy, i.e. stalks, leaves, or branches, are the same size or larger than the wavelength of the signal. Because the wavelength of the GPS L-band signal is  $\sim 24$  cm, which is much longer than X- or C-bands ( $\sim 3$  and 5 cm, respectively), we use a plane-stratified model that does not consider internal canopy geometry. Geometric models, which would take into account the relative distribution and orientation of stalks of leaves, are commonly used in radar remote sensing and would likely lead to better agreement with observations. We decided on a plane-stratified approach due to its ability to use only commonly-measured field parameters as input, with no additional information needed about individual plant components. For natural, non-forested environments, geometric components of

the canopy tend to be smaller than the wavelength of the L-band signal. The model might not accurately simulate vegetation types that have geometric components of greater than 24 cm.

Assuming that structural geometric effects are negligible means that coherence losses of the reflected wave due to volume scattering within the plant canopy due to geometric effects are neglected. However, the model can take into account multiple reflections between one-dimensional layers within the medium, if they are specified, which does allow for modeling the resulting coherence loss from permittivity changes.

#### **4.1.5 Calculation of direct and indirect power**

The permittivity profiles for soil and the optional vegetation layer are used in the reflection coefficient calculations, described in Section 4.1.1. After reflection coefficients are calculated, they must be combined with the antenna gain pattern to calculate direct and indirect power, from which an SNR interferogram may be simulated. A more detailed explanation of this part of the model is found in [51]. Complex signal amplitudes, both reflected (*ref*) and direct (*dir*) for both circular polarization components (*R* for right-handed and *L* for left-handed) are calculated. Because the direct signal is only right-handed circularly polarized, the left-handed component of this term is zero. The gain pattern, *G*, is specified by the user for both right- and left-handed polarizations, at all elevations (assumed to be azimuthally symmetrical). The gain pattern used in the model is for a choke ring antenna, whose radiation pattern was measured in an anechoic chamber.

An additional phase shift term (unrelated to  $\phi$  calculated from the SNR interferogram) must be included in the reflected powers to account for the extra path delay from the direct and reflected signal. This geometric phase delay is a function of the *a priori* reflector height,  $H_0$ .

When there is significant vegetation or snow present, the height of either the vegetation canopy or snow layer has to be subtracted first. Equations for complex signal amplitudes and geometric phase shifts are summarized below.

$$\Phi = 2k_w H_0 \cos \theta \quad (22)$$

$$u_{Rdir} = G_{Rdir} \quad (23) \quad u_{Rref} = G_{Rref} \times R_{RC} \times e^{i\pi\Phi} \quad (24)$$

$$u_{Ldir} = 0 \quad (25) \quad u_{Lref} = G_{Lref} \times R_{LC} \times e^{i\pi\Phi} \quad (26)$$

$$u_R = u_{Rref} + u_{Rdir} \quad (27) \quad u_L = u_{Lref} + u_{Ldir} \quad (28)$$

$$u_{dir} = u_{Ldir} + u_{Rdir} \quad (29) \quad u_{ref} = u_{Lref} + u_{Rref} \quad (30)$$

The incoherent power received is:

$$P_I = |u_{up}|^2 + |u_{dn}|^2 \quad (31)$$

The coherent power received is:

$$P_C = |u_R + u_L|^2 \quad (32)$$

Although observed SNR interferograms must be detrended with a low-order polynomial to remove the effect of the direct signal, because both coherent and incoherent power are known in the model, the incoherent power can simply be subtracted from the coherent power to produce the detrended interferogram. The interferogram is multiplied by  $10^5$  in order for the amplitude to be the correct magnitude.

$$SNR = P_C - P_I \quad (33)$$

## 4.2 Model validation

In this section, the soil and vegetation model is validated using SNR observations and *in situ* measurements of soil moisture and vegetation field data. The purpose of model validation is to evaluate whether the model can successfully simulate SNR data observed in the field. First, the modeled and observed SNR curves are compared, calculating how the correlation between modeled and observed data varies with vegetation water content. Here, we test the assumption that the vegetation canopy can be characterized as one bulk layer by also testing a gradually-varying canopy top. Then, whether or not the model can reproduce observed SNR metrics and how they vary with vegetation parameters is evaluated.

### 4.2.1 Validation Set-Up: Field Observations and Model Input

The validation data comprise observed SNR data from GPS antennas located in different vegetative environments. Antennas are surrounded by a managed alfalfa field (BCGR), a cultivated soybean field (AMES), a grazed rangeland (OKL2, OKL3, OKL4), and a desert steppe (p041). The GPS systems at these sites have identical hardware (Trimble NetRS receivers and Choke-Ring antennas with a radome), though the height of each antenna varies slightly. Some of the field sites have multiple antennas operating concurrently and/or located closely to one another; this information is summarized in Table 3.

Each of the sites is also instrumented with Campbell Scientific 616 soil moisture probes (at least five probes at 2.5 cm depth, five at 7.5 cm, and two at 20 cm). The soil moisture probes each record data every 30 minutes, though here the data are averaged from the probes to get one daily value at each depth. Vegetation samples were collected regularly throughout the growing season (see Table 3 for vegetation statistics). The samples were collected using the procedure as described in Chapter 3. Data from vegetation samples collected during each survey were

averaged, such that we have estimates of the mean canopy height, water content, and dry biomass on each day that samples were collected.

The vegetation field observations and soil moisture observations for each day are averaged and are used as the inputs to the soil-vegetation model. Thus, each sampling day has one corresponding modeled SNR curve generated using the mean vegetation and soil moisture data collected on that day.

Because observed SNR data from different satellite tracks are characteristically different, I compare the model simulations to observations from several satellite tracks. Observed SNR data from five satellite tracks are used for most sites, though only two and three tracks from Antennas D and E at the rangeland site are used, respectively. Tracks were selected such that none were influenced by trees or had significant topography (much greater than 5%). Phase, amplitude, and effective reflector height are computed from the SNR data from each satellite track.  $H_0$  for each satellite track was determined empirically. Amplitude was normalized for each site by dividing each daily-mean amplitude value by the maximum daily-mean amplitude observed at that site. Because the height of the GPS antenna is different for every site, we only looked at  $H_{eff}$  deviations from  $H_0$  ( $\Delta H_{eff}$ ).

Phase was zeroed with respect to the median phase value. For the four field sites, this occurs during times of the year when vegetation is either dormant or absent. We also zero our modeled phase values, though a slightly different approach had to be used. There are relatively few modeled phase values in our time series because the model is only run for days when vegetation was sampled. Therefore, we chose the zeroing value to be the value that corresponds to the lowest observed vegetation wet weight. After zeroing observed and modeled phase time

series, both are approximately zero when there is little to no vegetation and are less than zero when vegetation grows.

#### **4.2.2 Comparison of Simulated and Observed SNR Data**

The first goal of model validation is to evaluate whether modeled SNR data matches well with observed. Comparing SNR data requires that one curve is shifted to account for offsets introduced by the different baseline phase values of different satellite tracks. Because of this, we performed a cross-correlation on the modeled and observed SNR curves to determine the phase lag that would allow for the highest correlation ( $\gamma$ ) between the two curves. This shifting is done on a track-by-track basis. The modeled data are thus shifted to best match the observed data. This means that when we compare the shapes of modeled and observed SNR data, we are comparing their shape only and not how their respective phases change due to soil moisture or vegetation. The modeled and observed phase shifts are compared separately.

Two examples of observed and modeled SNR data from the soybean site are shown in Figure 9a,b. The observed SNR data are from one satellite track—different satellite tracks have slightly different SNR data. The modeled SNR curves for bare soil and vegetated conditions match the corresponding observed SNR curves. The model reproduces the reduction of amplitude resulting from the addition of vegetation. In addition, variations in amplitude with elevation angle that result from the presence of vegetation are also well simulated. The SNR data simulated using the gradual canopy top (meaning the permittivity was allowed to decrease to 1.0 over the top 10% of the canopy) does not match observations as well as the SNR data simulated with the homogeneous canopy, although the differences between the two are small compared to the changes associated with adding a vegetation canopy.

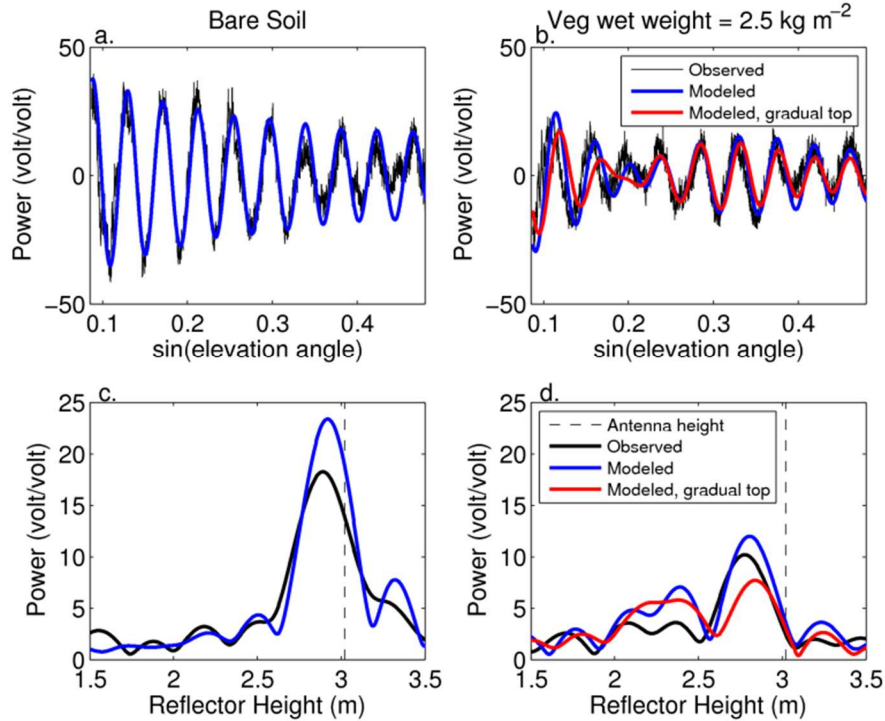


Figure 9: (a) Black line is SNR data from one satellite passing over the soybean site when ground was bare. Blue line is one modeled representation with a soil moisture of  $0.15 \text{ cm}^3 \text{ cm}^{-3}$ , using field inputs from the same day as the observed data. (b) Same as in a., except for when the vegetation was at its maximum extent (vegetation wet weight  $2.5 \text{ kg m}^{-2}$ ). The red line uses the same field inputs as the blue line, except also with a gradual canopy top that begins to thin out at 90% height. (c) Corresponding Lomb-Scargle periodograms for the curves in a. (d) Corresponding Lomb-Scargle periodograms for the curves in b.

The modeled and observed periodograms are similar (Figure 9c,d), although the match is not as close as for the SNR data. In particular, the maximum power of the periodogram is less in the observed data than modeled data, for both bare soil and vegetated conditions. This could be a result of colored noise in the observations, due to terrain effects in real environments, or differences in the modeled and observed satellite transmit power or antenna gain pattern.

In the bare soil example (Figure 9a),  $\gamma$  between the model simulation and observed SNR data is 0.87. For the example with vegetation,  $\gamma$  between the observed SNR data and the simulation with the abrupt canopy top is 0.81; between the observed SNR data and the

simulation with the gradual canopy top, 0.70. A  $\gamma$  value of 1 would indicate a perfect match; however, because observed data contains noise,  $\gamma$  will never be 1.

We computed  $\gamma$  between our modeled and observed SNR data at the four field sites. For each day that vegetation was sampled at our sites, we chose observed SNR data for up to five different satellite tracks and computed  $\gamma$  between the modeled SNR data and each satellite observation. We also computed  $\gamma$  between observed SNR data from the different satellite tracks. This means that we computed  $\gamma$  between the 1st satellite track and the 2nd,  $\gamma$  between the 1st satellite track and the 3rd,  $\gamma$  between the 2nd satellite track and the 3rd, and so on. Observed  $\gamma$  values are useful because they indicate the differences that may occur in observed data—due to azimuthal differences in vegetation or soil moisture, differences in the amount of noise in the observed data, or differences in satellite transmit powers. At all four field sites, the average  $\gamma$  value between the model and observations was higher than the  $\gamma$  value between concurrent observations (Table 4). This indicates that the variability between data from individual satellite tracks is greater than the differences between observations and the modeled data. From this analysis, we conclude that our model is able to successfully simulate observed SNR data, at least relative to the natural variability that exists in observed data.

Table 4: Mean Cross-Correlation Coefficients

Station	Mean $\gamma$ value	
	Model and Observations	Observations and concurrent observations
Desert Steppe	0.86	0.82
Rangeland	0.77	0.71
Alfalfa	0.72	0.65
Soybeans	0.72	0.65

#### 4.2.3 Comparison of Simulated SNR and Observed Metrics

The second goal of model validation is to evaluate whether modeled SNR metrics (phase, amplitude, effective reflector height) respond to changes in vegetation in the same way as observed SNR metrics. Example time series of observed and modeled SNR metrics for the alfalfa site from 2013 are shown in Figure 10. In a qualitative sense, the model is able to reproduce the fluctuations in SNR phase, amplitude, and effective reflector height observed at this site. Vegetation field data (Figure 10a) shows that the alfalfa was harvested three times during 2013. The relationship between vegetation wet weight and canopy height changed substantially after the 1<sup>st</sup> harvest. The observed SNR data (Figure 10b-d) mimic the three observed growth cycles. The magnitude of each metric decreases as the alfalfa grows. Then, each metric returns to approximately the original value after each harvest. The return to pre-harvest values is not instantaneous, as the alfalfa is first cut and then left in the field for a period of a few days to dry before it is collected. Simulated metrics, based only on the average measured vegetation and soil moisture parameters, show the same variations associated with growth and harvest. The magnitude of change is the same as determined from the observed SNR data. The

modeled SNR metric is always close to or falls within the mean +/- standard deviation of the observed metric.

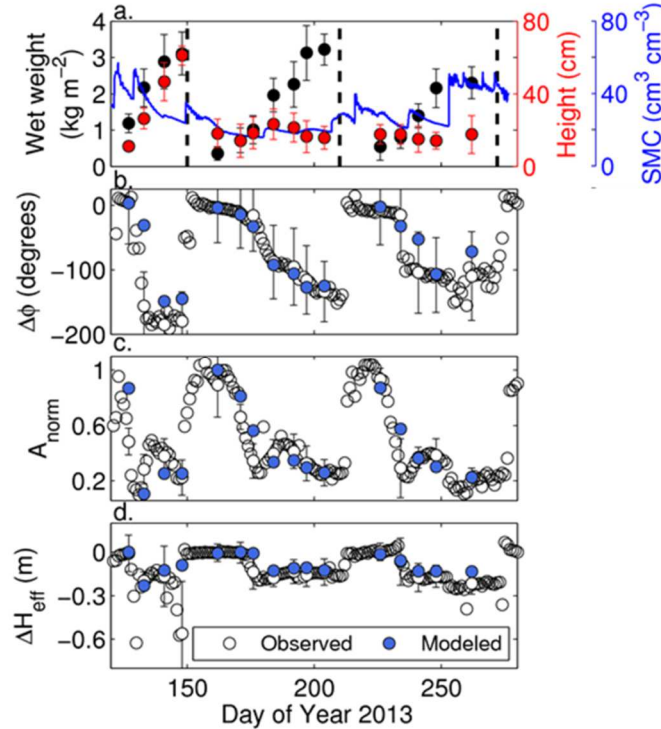


Figure 10: a. Field vegetation wet weight (black) and canopy height (red) for the alfalfa site in 2013. Error bars are the standard deviation of the seven collected field samples. Dashed lines indicate the approximate date of each harvest. b-d. Time series of GPS metrics, both modeled and observed, at the alfalfa field site in 2013. Open white circles are the average metric observed from five satellite tracks. Error bars are the standard deviations of the metrics on each day when vegetation was sampled. Error bars are not shown on every day for clarity. Blue circles are the modeled metric, using average vegetation and soil moisture field data as input.

Simulated and observed SNR metrics from all field sites in all years are now compared (Figure 11).  $A_{LSPnorm}$  of modeled data was not compared to observed data. However, if both modeled  $A_{norm}$  and  $\Delta H_{eff}$  are similar to the observed data, it would be expected for  $A_{LSPnorm}$  to also be similar. Modeled metrics were simulated using the average of measured vegetation parameters on each day and the average soil moisture value on the day during which vegetation was sampled. Observed metrics were calculated by averaging the SNR metrics from the five satellite tracks described previously. Simulated and observed  $A_{norm}$  are highly correlated across

the entire range of observed vegetation wet weight ( $0\text{-}5\text{ kg m}^{-2}$ ), with an  $r^2$  value of 0.79 and root-mean-square error (RMSE) of 0.12. The  $r^2$  value between modeled and observed values of  $\Delta\phi$  is also very high (0.84), and the RMSE is 20 degrees.  $\Delta H_{eff}$  has the lowest  $r^2$  of the three metrics, with a value of 0.62 and RMSE of 0.09 m. This is likely due to the fact that, when there is high vegetation, there are sometimes two very prominent reflector heights shown in the LSP, which compete to be the dominant frequency. Small adjustments in vegetation input would cause one reflector height to be slightly more powerful than the other, causing apparent jumps in  $\Delta H_{eff}$  time series.

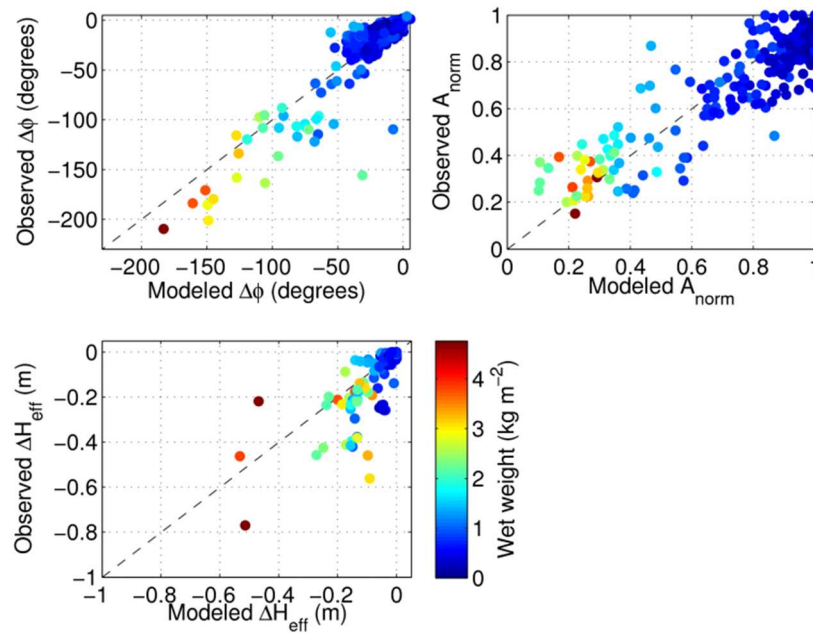


Figure 11: Observed versus modeled SNR metrics, which includes data from all four field sites. Points are colored by the observed vegetation wet weight, which was used as model input. Observed metrics are the average, for a given day, of the metrics calculated using five satellite tracks. Modeled metrics are created using the average vegetation field parameters collected on that day. There is the same number of points in each panel. Many of the points in the  $\Delta H_{eff}$  plot are clustered around zero.

## 4.3 Bare Soil Modeling

### 4.3.1 Soil moisture profiles

Now that the soil and vegetation model has been validated, relationships between soil and vegetation input parameters and SNR metrics are quantified. This section assumes that the environment surrounding a GPS antenna is devoid of vegetation. Here, contribution of only soil moisture change to subsequent changes in SNR metrics is quantified. For this analysis, soil moisture profiles that are constant with depth as well as ‘wetting’ or ‘drying’ profiles are simulated in the model. These profiles are depicted in Figure 12a. In these profiles, soil moisture was constant below 5 cm. The model was also run with soil profiles that had moisture variations with depth down to 10 cm, but no significant differences were found compared with results from the above profiles. It was thus deemed reasonable to keep soil moisture values constant below 5 cm depth. For profiles that vary with depth, the surface volumetric soil moisture value is denoted as  $SM_0$ , and the average volumetric soil moisture value for the top 5 cm of soil is denoted as  $SM_{0-5}$ .

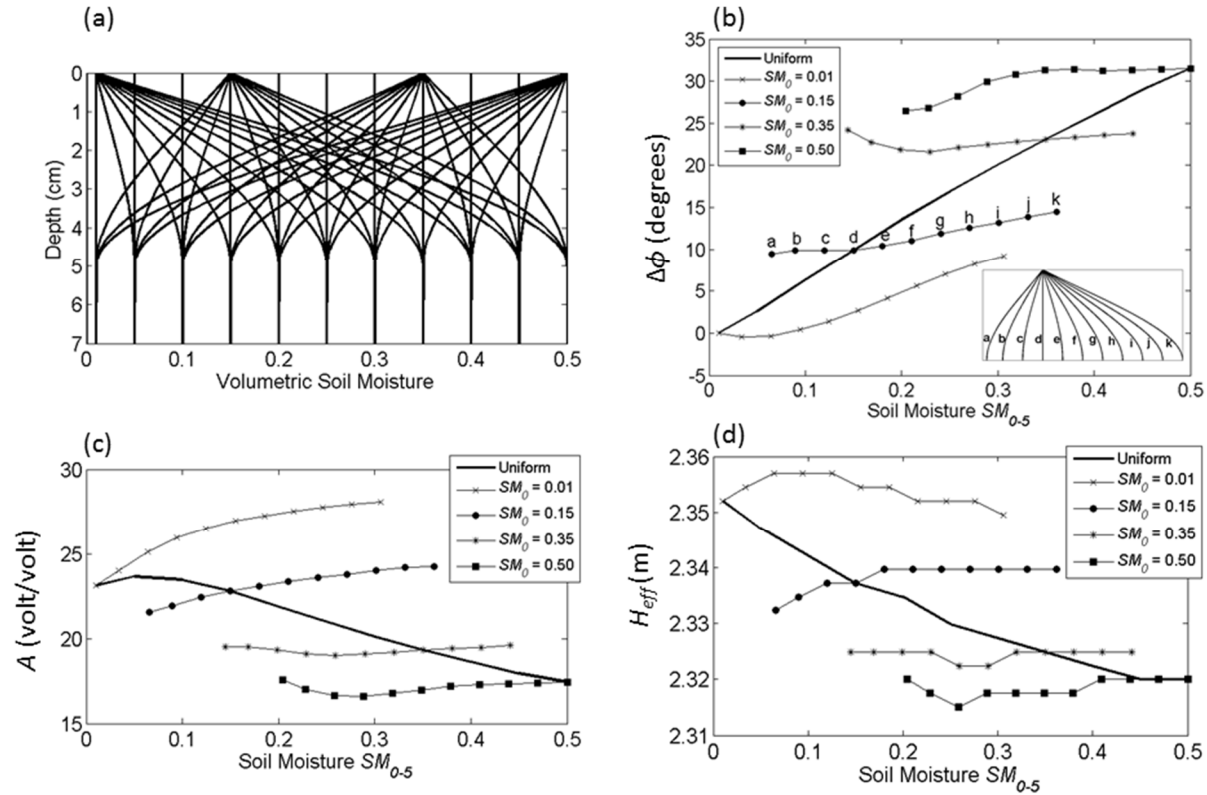


Figure 12: (a) Simulated soil moisture profiles. Only the top 7 cm of the profiles are shown, as soil moisture values were constant below 5 cm depth. (b) Relationship between  $\phi$  and soil moisture averaged over the top 5 cm,  $SM_{0-5}$ . The unmarked line indicates results for profiles in which soil moisture did not vary with depth. For these cases, the surface soil moisture is equal to  $SM_{0-5}$ . Other data (lines with symbols) are grouped by the value of soil moisture at the surface,  $SM_0$ . Within each group, each point corresponds to one profile in (a). The inset provides an example of one group of profiles with the same surface soil moisture ( $0.15 \text{ cm}^3 \text{ cm}^{-3}$ ), taken from (a). (c) Relationship between amplitude and soil moisture averaged over the top 5 cm,  $SM_{0-5}$ . The unmarked line indicates results for profiles in which soil moisture did not vary with depth. Other data (lines with symbols) are grouped by the value of soil moisture at the surface, as in (b). (d) Relationship between effective reflector height,  $H_{eff}$ , and volumetric soil moisture averaged over the top 5 cm,  $SM_{0-5}$ . The unmarked line indicates results for profiles in which soil moisture did not vary with depth. Other data (lines with symbols) are grouped by the value of soil moisture at the surface, as in (b).

In addition to the theoretical wetting, drying, and depth-invariant soil moisture profiles, *in situ* soil moisture data from the unirrigated agricultural wheat field (bcwh, see 3.1.1.1 and 3.2.2) were used to provide a representation of a set of realistic soil moisture profiles (Figure 13a). The data used to generate these profiles were collected using eleven Campbell Scientific 616 water content reflectometers: five were buried at a depth of 2.5 cm, five at 7.5 cm, and one

at 20 cm. Over 230 consecutive days of data were used to provide soil moisture profiles for the model.

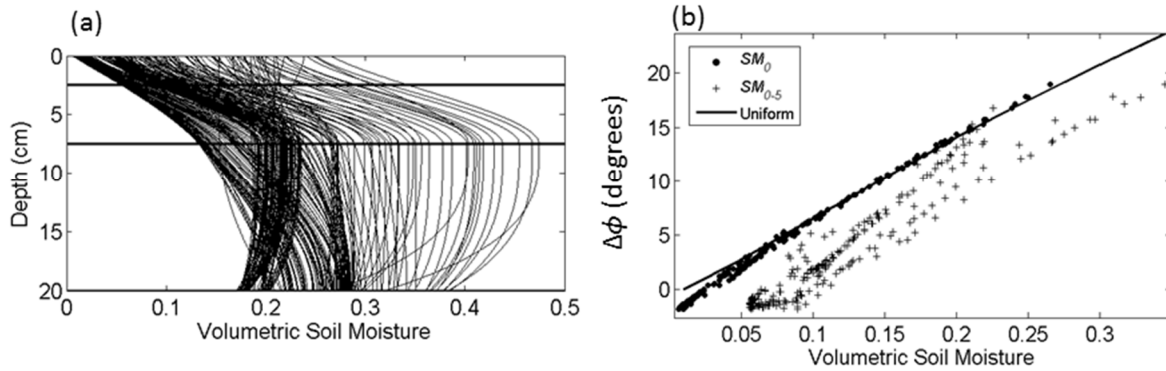


Figure 13: (a) Interpolated soil moisture profiles from the wheat field (BCWH), given three point measurements at 2.5, 7.5, and 20 cm (horizontal lines). (b) Relationship between  $\phi$  and soil moisture interpolated from field data. Solid dots correspond to surface soil moisture,  $SM_0$ , extrapolated from field measurements at 2.5 and 7.5 cm depths. The plus (+) signs correspond to soil moisture, averaged over the top 5 cm of the interpolated field profiles,  $SM_{0.5}$ . The solid line is the relationship between phase and soil moisture for profiles that do not vary with depth, as in Figure 12b.

Reflectometer data were used as point measurements of soil moisture at each installation depth. However, as discussed previously, the geometry of CS616 probes actually yields a measurement that integrates soil moisture over a depth of approximately 5 cm [29]. The factory calibration for the soil moisture probes was used, even though a calibration developed specifically for the soil at the site should yield more accurate volumetric soil moisture values.

### 4.3.2 Modeled SNR interferograms

Figure 14 shows two simulated interferograms where the only difference in input parameters was the specified soil moisture profile. The interferogram shown by the black solid line was produced using a depth-invariant soil moisture profile with a constant value of  $0.05 \text{ cm}^3 \text{ cm}^{-3}$ . The interferogram shown by the black dashed line was produced using a depth-invariant

profile with a constant value of  $0.45 \text{ cm}^3 \text{ cm}^{-3}$ . Changing the input antenna height,  $H_0$ , would change the number of oscillations in each interferogram.

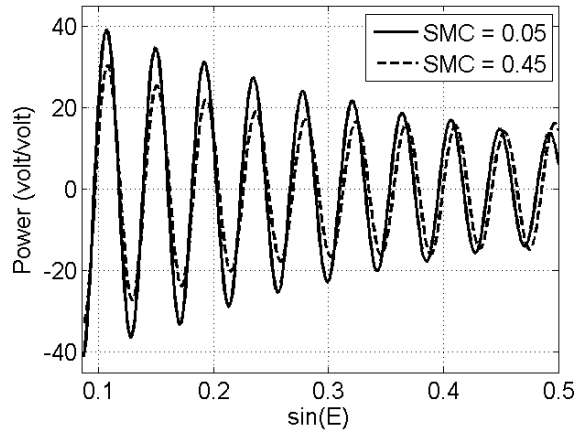


Figure 14: Two simulated interferograms, using either a constant soil moisture profile of  $0.05 \text{ cm}^3 \text{ cm}^{-3}$  or  $0.45 \text{ cm}^3 \text{ cm}^{-3}$  as input. All other input parameters were the same between simulations.

The interferogram simulated using the saturated soil moisture profile (dashed line) has a lower amplitude than the interferogram simulated using the dry soil moisture profile (solid line) except when  $\sin(\text{elevation angle})$  is greater than about 0.45. This is somewhat counterintuitive because a higher soil moisture content should result in greater reflection and thus a greater interference amplitude. However, reflection coefficients are both right- and left-handed circularly polarized. The proportions of right- and left-handed polarization in the reflected wave depends on soil moisture and the angle of incidence. Also, the gain pattern of the antenna accepts both right- and left-handed polarizations differently depending on satellite elevation angle. These complications make it difficult to predict SNR amplitude based solely on ground permittivity.

### 4.3.3 The effect of soil moisture on SNR metrics

#### 4.3.3.1 Relationship between phase and soil moisture

Given uniform soil moisture profiles,  $\phi$  exhibits a positive and nearly linear relationship with volumetric soil moisture (Figure 12b). Phase varies by 30 degrees over the range of dry to wet uniform soil moisture profiles that we tested. The slope of this relationship, or the sensitivity of  $\phi$  to uniform soil moisture, is  $65.1 \text{ deg cm}^3 \text{ cm}^{-3}$ . This means that a 20 degree change in  $\phi$  would correspond to a 0.31 change in volumetric soil moisture. This relationship is the same regardless of soil type and does not depend on the height of the antenna,  $H_0$  (Table 5).

Table 5: Slopes and  $r^2$  values for linear regressions of soil moisture and phase using different soil types for  $H_0 = 2.4 \text{ m}$ . Linear regressions assume soil moisture profiles do not vary with depth.

Soil Type	Slope ( $\text{deg cm}^3 \text{ cm}^{-3}$ )	$r^2$ value
Sandy Loam	65.8	0.996
Loam	65.1	0.997
Loam ( $H_o = 1\text{m}$ )	66.9	0.998
Loam ( $H_o = 3\text{m}$ )	65.7	0.997
Silt Loam I	65.0	0.997
Silt Loam II	66.1	0.998
Silty Clay	65.3	0.998

For soil moisture profiles that vary with depth,  $\phi$  does not vary consistently with  $SM_{0.5}$ . Figure 12b shows the relationship between  $SM_{0.5}$  and  $\phi$  for a variety of different soil moisture profiles, a subset of which are depicted in the inset. The subset of profiles, labeled a-k in the figure, all have the same surface volumetric soil moisture ( $0.15 \text{ cm}^3 \text{ cm}^{-3}$ ). However, the volumetric soil moisture beneath the surface may be lower (profiles a-c) or higher (e-k) than at the surface. As a result, these profiles have different values of  $SM_{0.5}$ . As can be seen in the figure, the relationship between  $SM_{0.5}$  and  $\phi$  for these profiles is not linear, and the slope is much smaller than that for uniform moisture profiles. This is true for the other groups of profiles that

have moisture variations over depth.  $\phi$  for these profiles appears to depend predominantly on the surface soil moisture value and not strongly on  $SM_{0.5}$ .

#### 4.3.3.2 Relationship between amplitude and soil moisture

For uniform soil moisture profiles, soil moisture and  $A$  have a linear, inverse relationship (Figure 12c). This relationship does not hold when the soil moisture is below 0.10. For these dry values,  $A$  does not respond significantly to soil moisture changes. Figure 15a should show how  $A_{norm}$  would vary with changes in surface soil moisture for a SMC profile that does not vary with depth.

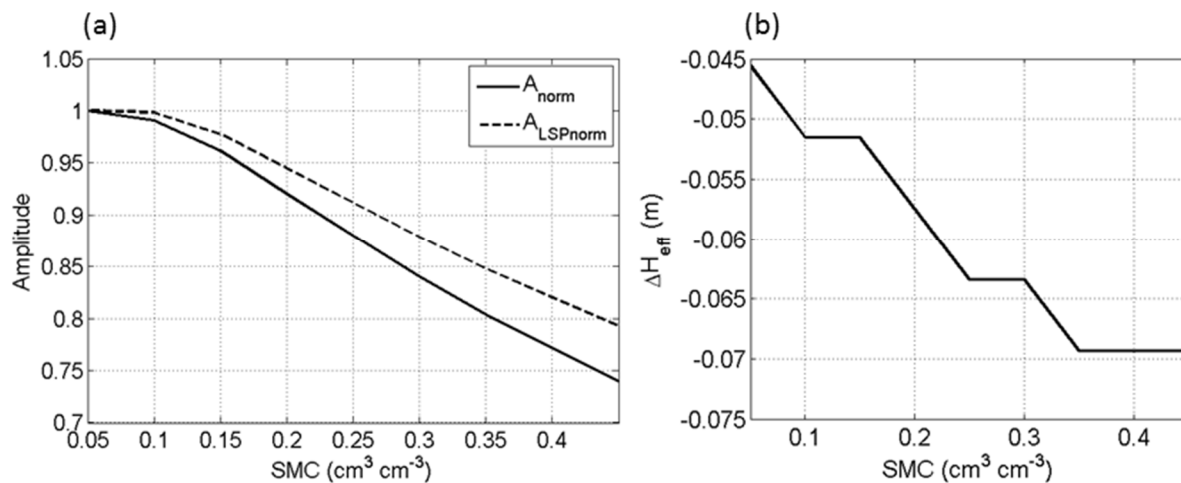


Figure 15: (a) Relationship between normalized amplitude (black) and normalized LSP amplitude (dashed) and soil moisture for a bare soil with an invariant vertical soil moisture profile. The normalized amplitude line is the same relationship as in Figure 12b. (b) Relationship between the deviation of reflector height from antenna height and soil moisture for a bare soil with an invariant vertical soil moisture profile. This relationship is the same as in Figure 12d except antenna height has been subtracted from effective reflector height.

For moisture profiles that vary with depth,  $SM_{0.5}$  and  $A$  are either positively related or unrelated, depending on the value of the surface soil moisture. This is in contrast to the linear, inverse relationship that exists between uniform moisture profiles and amplitude. For the non-uniform moisture profiles that have relatively wet  $SM_0$  values (asterisks or squares in Figure

12c),  $A$  does not vary with  $SM_{0.5}$ . For the profiles with lower  $SM_0$  (circles or 'x's in Figure 12c),  $A$  is positively related to  $SM_{0.5}$ . As is the case for  $\phi$ , it appears that amplitude also depends primarily on surface soil moisture, not  $SM_{0.5}$ .

Figure 15a shows the relationship between amplitude and soil moisture for a constant soil moisture profile for the more general case when amplitude is normalized with respect to its maximum value. This figure also shows the relationship between normalized LSP amplitude ( $A_{LSPnorm}$ ) and soil moisture for a constant soil moisture profile. Normalized LSP amplitude is not affected by soil moisture as much as normalized amplitude calculated using the constant frequency assumption, though the relationship does have the same general shape.

#### ***4.3.3.3 Relationship between effective reflector height and soil moisture***

For uniform moisture profiles, as the soil becomes wetter the height estimated from the Lomb-Scargle Periodogram ( $H_{eff}$ ) decreases (Figure 12d). The variation in  $H_{eff}$  is approximately 3.3 cm for the range of soil moisture values tested.

As with both  $\phi$  and  $A$ , once soil moisture profiles are allowed to vary with depth, the dependence of  $H_{eff}$  on  $SM_{0.5}$  is neither strong nor consistent. As is seen in Figure 12d,  $H_{eff}$  varies by  $< 1$  cm with  $SM_{0.5}$  for moisture profiles that vary with depth. Thus,  $H_{eff}$  appears to be primarily influenced by  $SM_0$ . The millimeter differences in  $H_{eff}$  that result from moisture variations at depth would be difficult to distinguish in field measurements. However, the cm-level changes between uniform wet and dry profiles should be observable, as previously shown by [14] and [15].

Figure 15b shows the same relationship as in Figure 12d for effective reflector height and soil moisture, for a constant soil moisture profile with depth, though here antenna height,  $H_0$ , has

been subtracted from  $H_{eff}$ , yielding  $\Delta H_{eff}$ . Because the ground surface is not a perfect reflector, there will be a frequency change upon reflection, resulting in the dominant frequency of the LSP being different from that of the height of the antenna. In soil moisture simulations, the effective reflector height is always lower than the actual input antenna height.

#### **4.3.3.4 Relationship between metrics and SMC from field data**

Here, results are presented for SNR data that were simulated using soil moisture profiles interpolated from field data.  $SM_0$  and  $\phi$  have a near-perfect correlation with an  $r^2$  value of 0.997 (Figure 13b) despite the wide range of soil moisture profiles tested. This indicates that  $\phi$  is highly dependent on changes in surface soil moisture. The correlation between  $\phi$  and  $SM_{0.5}$  is still excellent ( $r^2 = 0.91$ ) (Figure 13b). However, some of this correlation is the result of the covariance between  $SM_{0.5}$  and  $SM_0$  rather than the effects of soil moisture at depth on SNR. Soil moisture at 0 cm was extrapolated from the value measured at 2.5 cm using the gradient measured at depths of 2.5 and 7.5 cm. Thus, the predicted  $SM_0$  was always tightly coupled with this gradient. The covariance between  $SM_0$  and the soil moisture at deeper depths may not be as strong in the field. Nearly all of the interpolated profiles have dryer soil at the surface than at depth. Therefore, each  $\phi$ - $SM_{0.5}$  point plots to the right of the corresponding  $\phi$ - $SM_0$  point. This is consistent with results shown in Figure 12a (e.g., points e-k), for cases when the soil is drier at the surface than at depth.

$A$  and  $H_{eff}$  have similar correlations with the soil moisture profiles that were interpolated from field measurements. The  $r^2$  value for the correlation between  $A$  and  $SM_0$  is 0.81 and 0.63 for the correlation between  $A$  and  $SM_{0.5}$ . The smaller  $r^2$  (compared to that for  $\phi$  and soil moisture) is expected, given the complex relationship between  $A$  and soil moisture (Figure 12c). The  $r^2$  value for the correlation between  $H_{eff}$  and  $SM_0$  is 0.97; between  $H_{eff}$  and  $SM_{0.5}$ , it is 0.86.

#### 4.3.3.5 Note on signal penetration depth

It is well known that L-band signals penetrate further into soils that are dry than soils that are wet [31]. It is possible to calculate the effective penetration depth, which is usually defined as the depth at which the signal's power has been attenuated to  $1/e$  of its value at the soil surface [31]. For passive L-band remote sensing, this depth varies from 0.1-1 m, depending on whether the soil is wet or dry [31].

This definition of penetration depth, however, is not appropriate for defining the depth of soil that significantly affects SNR. The signal may penetrate to this depth in the soil. However, this does not mean that a significant portion of the signal returns back through the soil surface to the antenna. In addition, SNR depends not only upon the depth at which the wave was reflected but also on the dielectric properties of the soil. Other studies have also addressed this issue [31][32]. The term for the region of soil that affects the overall signal is sometimes referred to as the "moisture sensing depth" and is often taken to be one-tenth of a wavelength in the soil, which corresponds to less than 2 cm for L-band [31].

Figure 13b indicates that the surface soil moisture value (top ~1 mm) is the determining factor in  $\phi$ . This is to be expected, since low elevation angles have higher surface reflection coefficients than higher angles [28]. It appears that the observed correlations between  $\phi$  and soil moisture averaged over the top 5 cm of soil, like those shown in Figure 12b, result from a combination of (1) strong covariance between  $SM_0$  and soil moisture at 2.5 cm and (2) soil moisture at deeper depths affecting the overall signal. Although the relative contributions of these two factors were not quantitatively compared, results show that the correlation between  $SM_0$  and soil moisture at 2.5 cm is the driving factor in the correlation between the GPS interferogram metrics  $A$ ,  $H_{eff}$ , and  $\phi$  and  $SM_{0-5}$ .

#### 4.4 Vegetation-soil model

With the exception of deserts and plowed agricultural fields, there are few examples of environments that are completely devoid of all vegetation. In natural environments, there is almost always some amount of standing biomass, even in winter. It is thus important to quantify the contribution of vegetation to changes in SNR metrics.

Observed SNR metric time series show significant variations in all metrics during times of seasonal vegetation change (Figure 16). Figure 16 shows field vegetation and soil moisture data collected from a GPS station in Oklahoma (OKL3) along with SNR metric time series from that station. There are a few important things to note from this figure. One, the vegetation field data show that the site is spatially heterogeneous, indicated by the large error bars in some of the samples. Two, the vegetation field data do not show the same magnitude of change during the summers of 2011 and 2012 (The site was burned in the winter of 2012.). Three, the SNR data from different satellite tracks (indicated by the different colors in Figure 16) show wide ranges of responses in every metric. Four, there is significant seasonality in the amplitude and phase time series. Seasonality in the effective reflector height time series is not as apparent. And five, there are smaller frequency oscillations in the phase time series that correspond with rain events and subsequent dry downs.

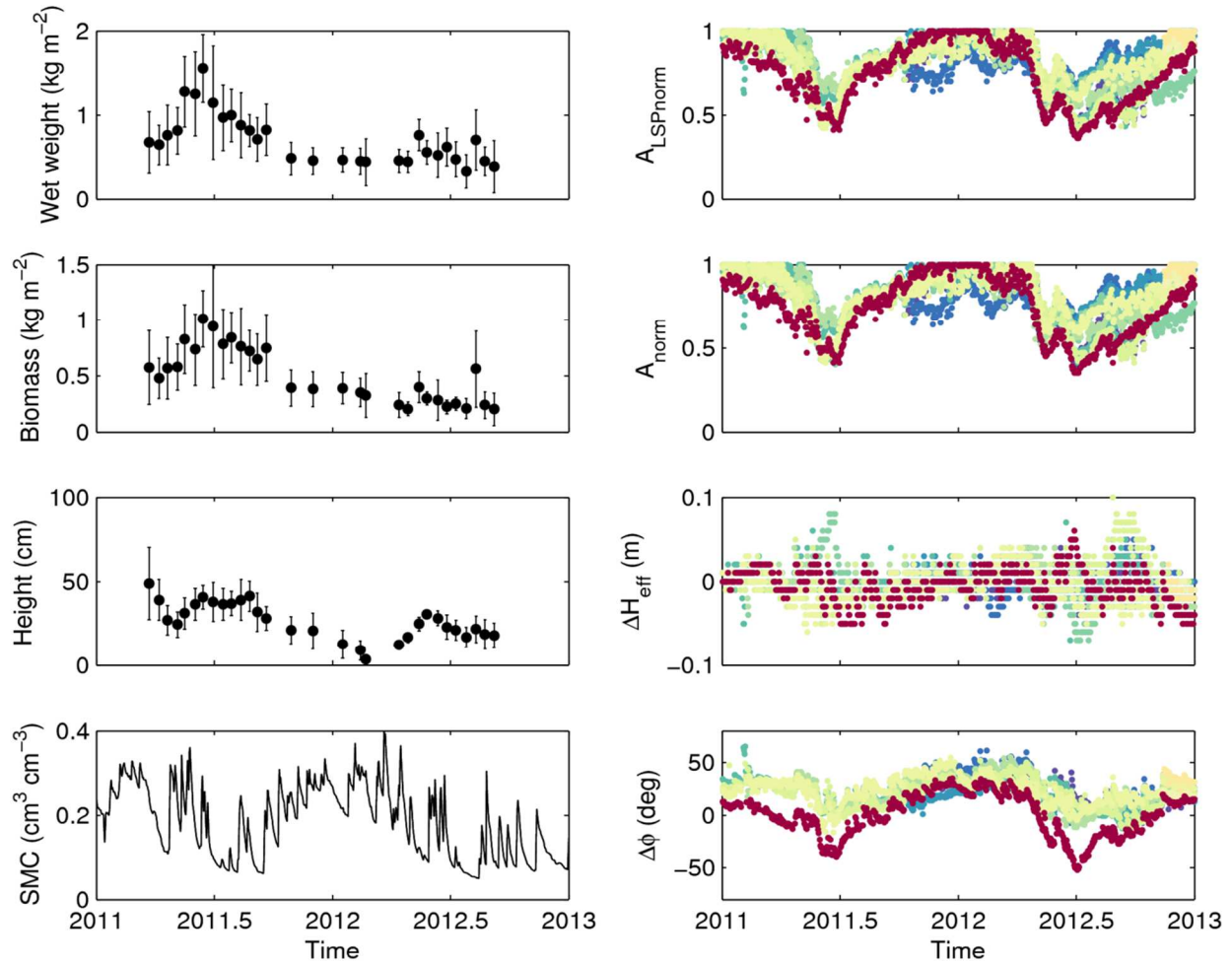


Figure 16: *In situ* vegetation and soil moisture data for a GPS station in Oklahoma (OKL3) and associated changes in SNR metrics for the same time interval. SNR metrics from different satellite tracks are indicated by different colors.

It is clear from Figure 16 that SNR metrics are affected by seasonal variations in land surface characteristics. The goal of this section is to identify and quantify the most important parameters controlling the seasonal changes in SNR metric time series using the soil-vegetation model. This section will also address how concurrent changes in soil moisture and overlying vegetation lead to complicated responses in SNR metrics.

The soil-vegetation model is able to reproduce the changes in the shape of SNR interferograms as well as changes in associated metrics due to changes in a vegetation canopy, as

shown in Figure 9. I will now address what vegetation and soil parameters are most important in affecting metrics.

I will start with the most general case, which is how random combinations of the vegetation parameters in Table 6 affect SNR metrics. I will then present how assigning relationships between vegetation parameters affects our results. In addition, the role of changing underlying soil moisture will be discussed.

Table 6: Parameters used in the soil-vegetation model

Parameter	Symbol/Abbreviation	Time-varying
<i>A priori</i> reflector height	$H_0$	No
Soil type	$n$	No
Soil moisture	SMC	Yes
Canopy height	$H_{veg}$	Yes
Fresh biomass	$M_f$	Yes
Dry biomass	$M_d$	Yes
Vegetation salinity	$S$	No
True density	$\rho_{veg}$	Yes

#### 4.4.1 First case: random combinations of vegetation parameters

Here, vegetation parameters, specifically  $M_f$ ,  $M_d$ ,  $H_{veg}$ , and  $\rho_{veg}$ , are varied randomly, and combinations of the random parameters are used as input to the model. Antenna height and vegetation salinity are held constant, and soil moisture is kept at  $0.15 \text{ cm}^3 \text{ cm}^{-3}$ . Some bounds are placed on parameters, such that  $M_f$  must be under  $3 \text{ kg m}^{-2}$ ,  $M_d$  is under  $1.5 \text{ kg m}^{-2}$ ,  $H_{veg}$  is under 80 cm, and  $\rho_{veg}$  is between 200-1500  $\text{kg m}^{-3}$ . Approximately 10,000 model simulations were run

with random combinations of these parameters, and SNR metrics were calculated.  $A_{norm}$ ,  $A_{LSPnorm}$ ,  $\Delta H_{eff}$ , and  $\Delta\phi$  were calculated using the bare soil case ( $SMC = 0.15 \text{ cm}^3 \text{ cm}^{-3}$ ) as a reference from which to normalize and zero metrics. In these simulations,  $\Delta H_{eff}$  is defined as the change in effective reflector height *with respect to its value during times when soil is essentially 'bare.'* Note that this is slightly different than how it would normally be defined in the model, when the *a priori* reflector height is perfectly known.

Figure 17-Figure 20 show the relationships between the vegetation parameters in the model and corresponding SNR metrics. Figure 17, which shows how metrics vary with the dry biomass of vegetation ( $M_d$ ), indicates very weak relationships with all metrics. An increase in dry biomass in general causes a decrease in  $A_{norm}$ ,  $A_{LSPnorm}$ , and  $\Delta\phi$ . Also, an increase in dry biomass causes  $H_{eff}$  to decrease with respect to its bare soil value, indicated by the positive values of  $\Delta H_{eff}$ . The small cloud of outliers in the  $\Delta H_{eff}$  plot is caused by a second, competing frequency in the LSP that will sometimes be the most powerful frequency. This is discussed in more detail below.

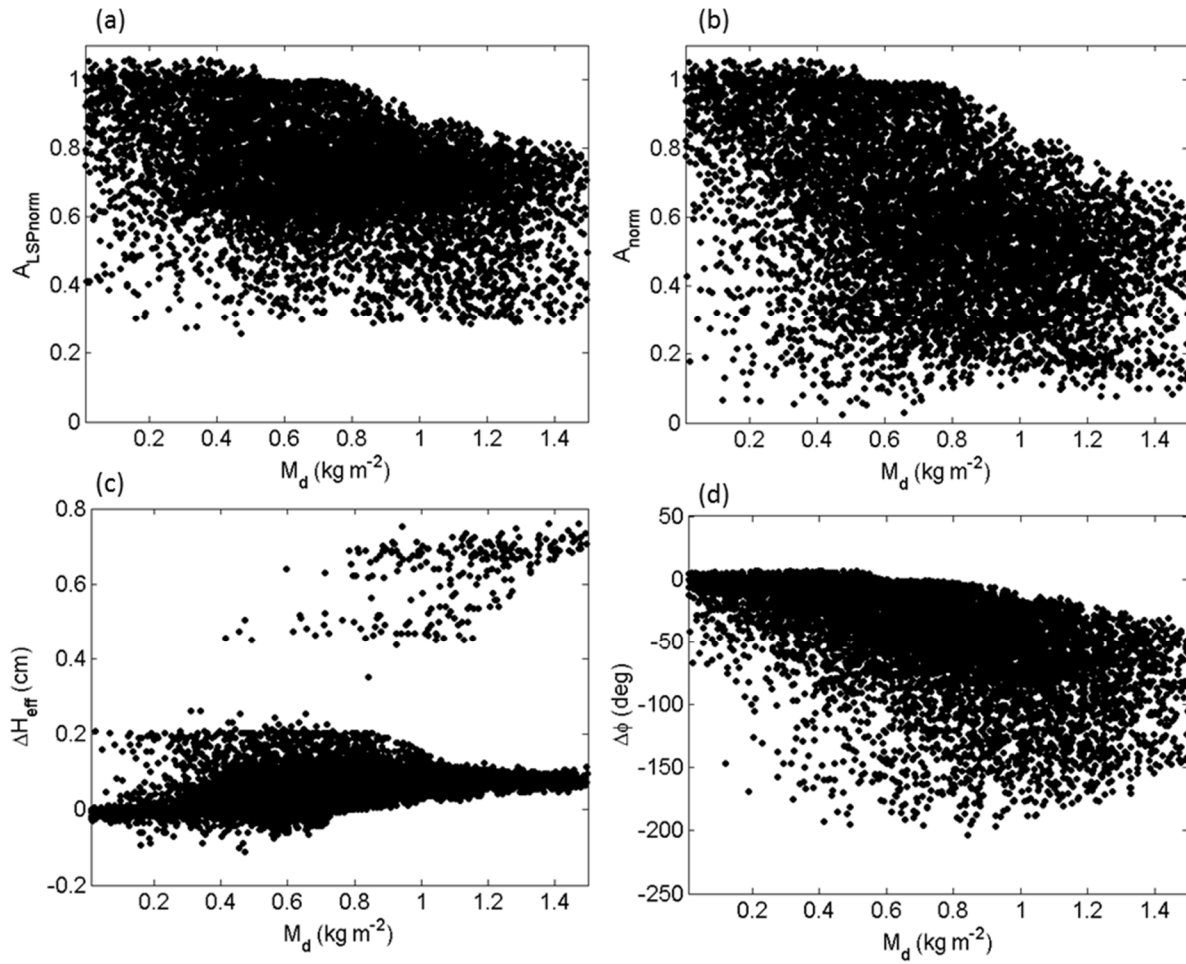


Figure 17: Modeled relationships between  $M_d$  (dry biomass/dry weight of vegetation) and SNR metrics, for an underlying soil moisture content of  $0.15 \text{ cm}^3 \text{ cm}^{-3}$ .

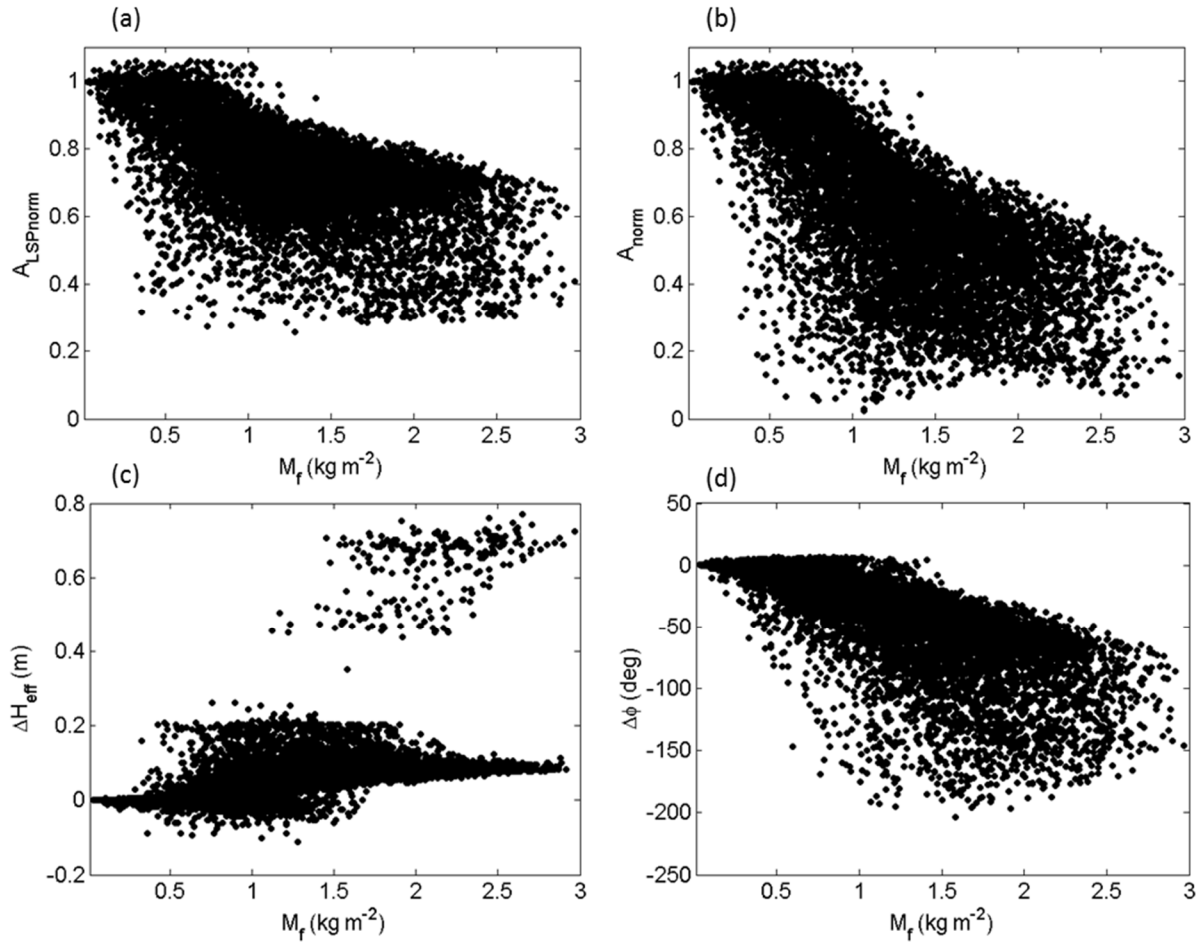


Figure 18: Modeled relationships between  $M_f$  (fresh biomass/wet weight of vegetation) and SNR metrics, for an underlying soil moisture content of  $0.15 \text{ cm}^3 \text{ cm}^{-3}$ .

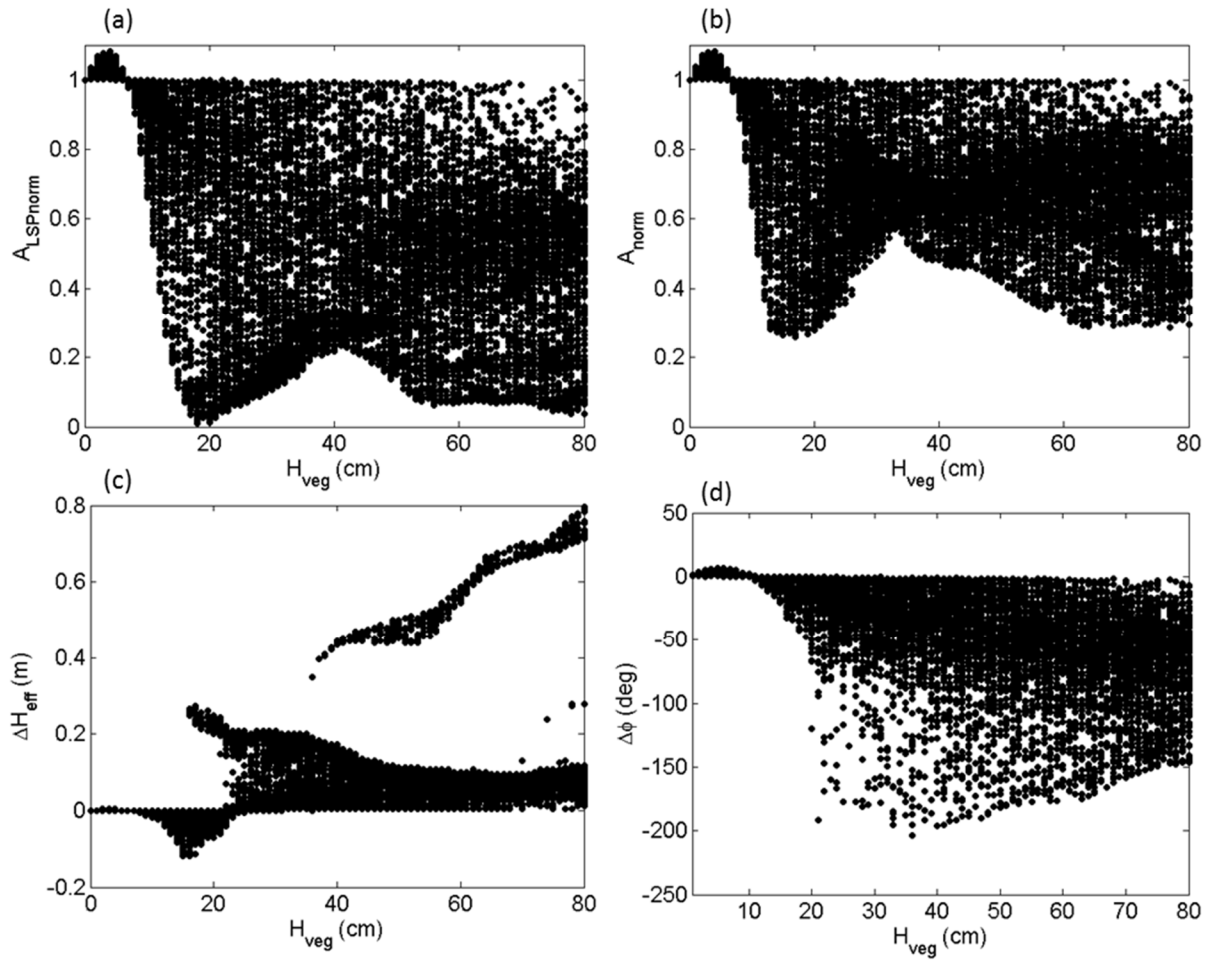


Figure 19: Modeled relationships between  $H_{veg}$  (height of vegetation canopy) and SNR metrics, for an underlying soil moisture content of  $0.15 \text{ cm}^3 \text{ cm}^{-3}$ .

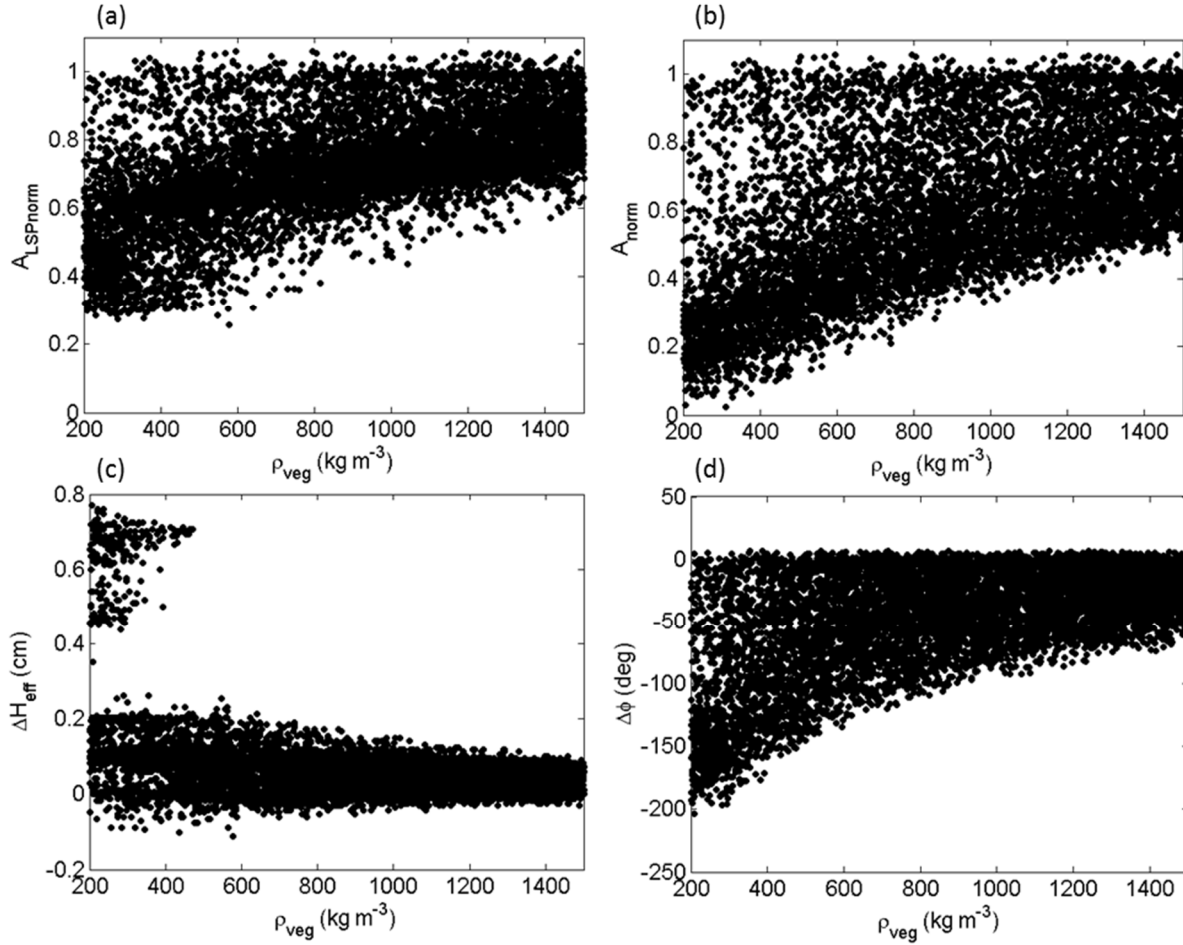


Figure 20: Modeled relationships between  $\rho_{veg}$  (true density of vegetation) and SNR metrics, for an underlying soil moisture content of  $0.15 \text{ cm}^3 \text{ cm}^{-3}$ .

Figure 18 shows the relationship between the wet weight/fresh biomass of vegetation ( $M_f$ ) and SNR metrics. Like  $M_d$ ,  $M_f$  also causes SNR metrics to decrease. The relationship between  $M_f$  and the amplitude metrics is clearer than that for  $M_d$ , though there is still significant scatter. There do not appear to be significant differences between the relationships of  $M_f$ ,  $M_d$  and  $\Delta\phi$ ,  $\Delta H_{eff}$ .

Changes in vegetation canopy height result in very different changes in SNR metrics than changes in fresh or dry biomass (Figure 19). Vegetation canopy growth from bare soil to 14 cm results in only very small changes in SNR metrics, relative to larger changes in vegetation

height. Beyond 14 cm, changes in canopy height could result in significant decreases in all SNR metrics, or result in no changes. This is a good indication that changes in SNR metrics are controlled by the interaction between multiple canopy parameters. When the canopy height is between 20 and 50 cm, SNR amplitude metrics could actually begin to increase again, depending on the value of other parameters, which will be explored below. In general, the relationship between changes in canopy height and  $\Delta H_{eff}$  are not 1:1, except for a small number of cases. This will also be discussed in more detail below.

Figure 20 shows how SNR metrics are affected by changes in the true density of vegetation. True density is weakly associated with amplitude and phase metrics, with an increase in true density resulting in increases in  $\Delta\phi$ ,  $A_{norm}$ , and  $A_{LSPnorm}$ . There is no obvious relationship between changes in true density and changes in  $\Delta H_{eff}$ .

Now that the relationships between changes in single vegetation parameters and SNR metrics has been presented, it is apparent that SNR metrics are affected by changes in not just one, but multiple, vegetation parameters. Combining vegetation parameters into a single parameter, the effective canopy permittivity, yields better relationships with SNR metrics, and the combination of canopy height and permittivity yields the best relationships. Presenting results in terms of canopy permittivity also makes sense because reflection coefficients are calculated using the permittivity value—not any individual vegetation parameter.

How  $A_{norm}$  is affected by changes in canopy permittivity and canopy height is shown in Figure 21a. For low values of canopy permittivity ( $<1.04$ ), an increase in canopy height will not affect  $A_{norm}$ . When canopy permittivity is higher than 1.04, an increase in canopy height will cause a general decrease in  $A_{norm}$ . Depending on the specific plant type, canopy height and

permittivity could be correlated at part or all of its growth cycle, which means an increase in either one would cause a decrease in  $A_{norm}$ .

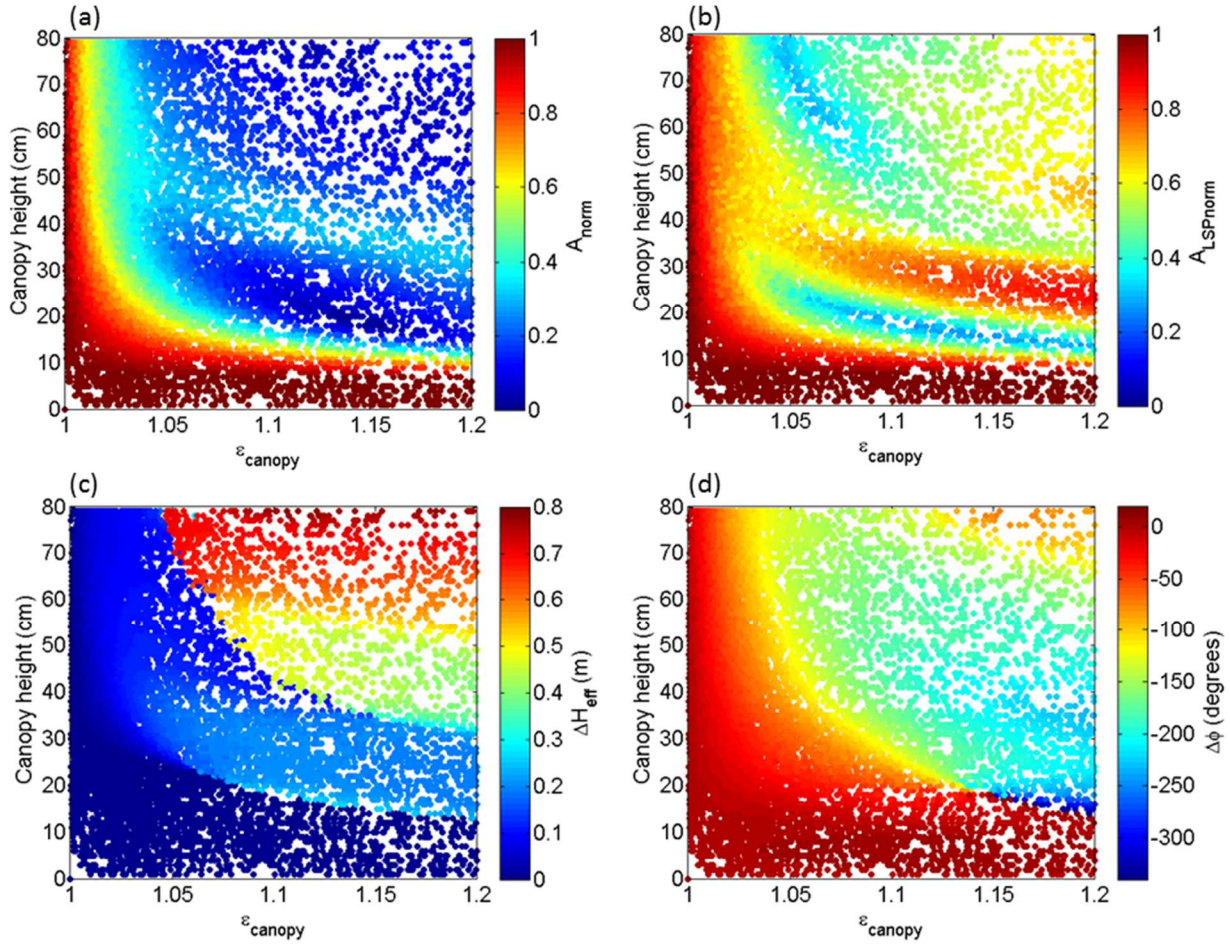


Figure 21: Relationships between canopy permittivity (real part), canopy height, and SNR metrics. Underlying soil moisture was kept at  $0.15 \text{ cm}^3 \text{ cm}^{-3}$ .

Figure 21b shows the relationship between  $A_{LSPnorm}$ , canopy height, and permittivity.  $A_{LSPnorm}$  is affected by canopy height and permittivity somewhat similarly as  $A_{norm}$ , with some notable exceptions. For low values of canopy permittivity or low values of canopy height, both  $A_{LSPnorm}$  and  $A_{norm}$  respond similarly. However, for some combinations of canopy height and permittivity,  $A_{LSPnorm}$  may increase substantially for a period of time (again, depending on the particular plant's growth strategy). This increase is likely due to the growth of a second dominant

frequency in the LSP, which ‘takes over’ the dominant frequency. The second frequency, which will be related to the height of the vegetation for the majority of these cases, can either be completely separate from the dominant frequency resulting from the reflection off of the soil, or the two frequencies may be combined into one, broader frequency peak. Growth of vegetation will cause the reflection coming from the vegetation layer to become stronger, which will increase the amplitude of the SNR interferogram, at least for a short while. Examples of situations when there could be two competing frequencies in the SNR interferogram are shown in Figure 22. The LSPs are derived from the modeled SNR interferograms for the alfalfa field. Note that when there are two competing frequencies, the dominant frequency may ‘jump’ back and forth between the two for small increases in vegetation water content (magenta lines).

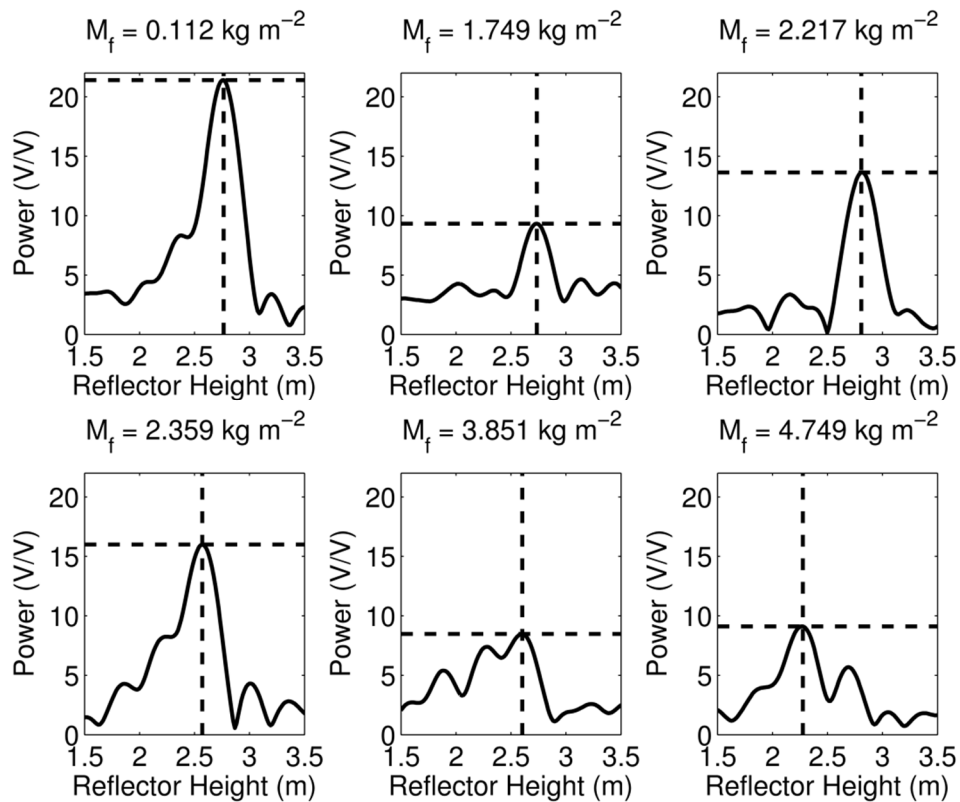


Figure 22: Lomb-Scargle Periodograms (black curves) from observed SNR interferograms at the alfalfa site, bcgr. Dashed black lines are the dominant frequency ( $H_{eff}$ ) and its power ( $A_{LSP}$ ) for each LSP.

How  $\Delta H_{eff}$  is affected by canopy permittivity and height is presented in Figure 21c. For a large portion of the permittivity/canopy height parameter space,  $\Delta H_{eff}$  does not change more than 20 cm. For very tall canopies with high permittivities,  $\Delta H_{eff}$  is strongly correlated with canopy height, with second-order effects from changes in permittivity.

Figure 21d shows how height and permittivity affect  $\Delta\phi$ . Changes in  $\Delta\phi$  are generally restricted to less than 200 degrees for the canopies simulated here. The small region with changes larger than 360 (dark blue) resulted from inadequate phase zeroing. In almost all cases, phase will decrease due to a combination of permittivity and height increases, unlike  $A_{LSPnorm}$ .

#### **4.4.2 Second case: Assuming relationships between canopy parameters**

As mentioned above, SNR metrics will respond differently to plants with different growth strategies. To illustrate differences, I will present examples using vegetation field data from mfle and bcgr (the desert steppe and alfalfa sites). For these examples, I derived general empirical relationships between vegetation canopy parameters for each site and used these relationships in model simulations.

Empirically derived relationships are shown in Figure 23. Figure 23a shows how, at each site, biomass varies with water content. Each data point is the average from one field survey. The vegetation at the desert steppe site does not vary as much as the vegetation at the alfalfa site. The vegetation at the desert steppe site is also much drier, as indicated by the smaller slope between biomass and water content. The linear regressions for each site are shown by the dashed lines—this relationship is strong for both sites. Figure 23b shows how canopy height varies with biomass. Relationships are not as strong, though linear regressions are still shown.

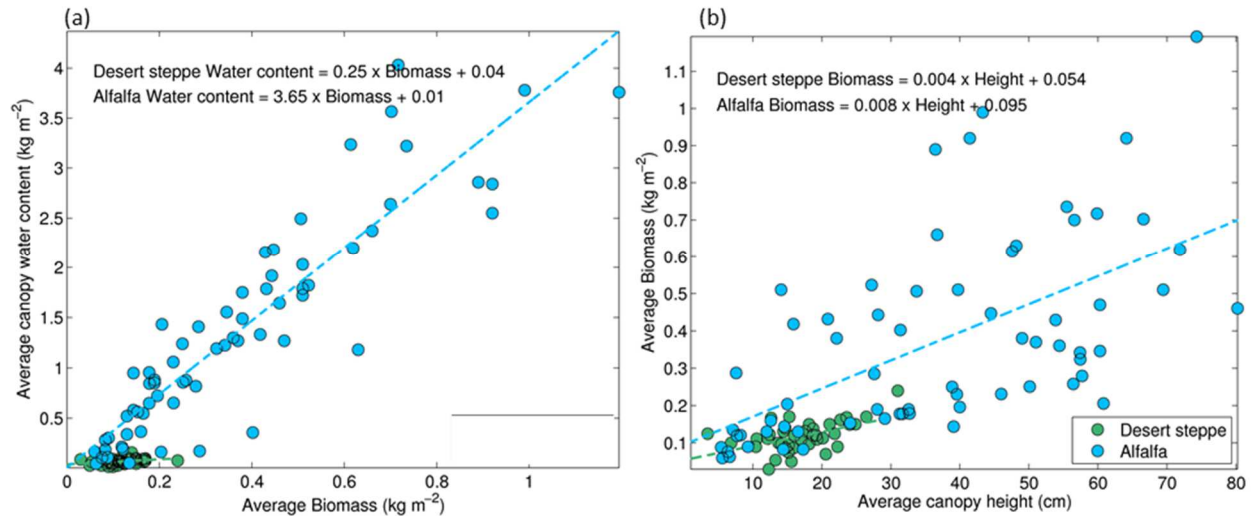


Figure 23: (a) Average biomass at the desert steppe (mfle, green circles) and alfalfa (bcgr, blue circles) sites versus the average canopy water content. The best fit linear regressions for each sites are dashed lines. (b) Average canopy height versus average biomass for the two sites, with best-fit linear regressions shown by the dashed lines.

Model simulations were created using results of the linear regressions for these variables. Because there were no field measurements of true density, it was assumed to vary proportionally with water content, with no bulk density component, such that a sample that was 100% water would have a true density of  $1000 \text{ kg m}^{-3}$ , and a sample that was 0% water would have a true density of  $0 \text{ kg m}^{-3}$ . This assumes that the dry component of vegetation is negligible and that there is no volume change in vegetation with changes in water content—neither assumption is valid. However, because the purpose of this experiment is to show some theoretical examples of how different plant growth strategies could affect SNR metrics, it is not instructive to try to derive a more realistic relationship. As before, underlying soil moisture was kept at  $0.15 \text{ cm}^3 \text{ cm}^{-3}$ . Results are presented in terms of changes in vegetation water content. However, because water content for these simulations is correlated with changes in other vegetation parameters, analogous relationships with SNR metrics would be found if using different parameters for plotting purposes.

Figure 24 shows how changes in vegetation water content for the scenarios described above affect SNR metrics. One can think of this as theoretical changes in SNR metrics throughout the growing season for the two different vegetation types. Figure 24a indicates that both the desert steppe and alfalfa sites would see a slight increase in  $A_{norm}$  at the beginning of the growing season, followed by sharp decreases. The decrease in  $A_{norm}$  would be more significant at the beginning of the desert steppe's growth cycle relative to alfalfa, but much shorter lived.

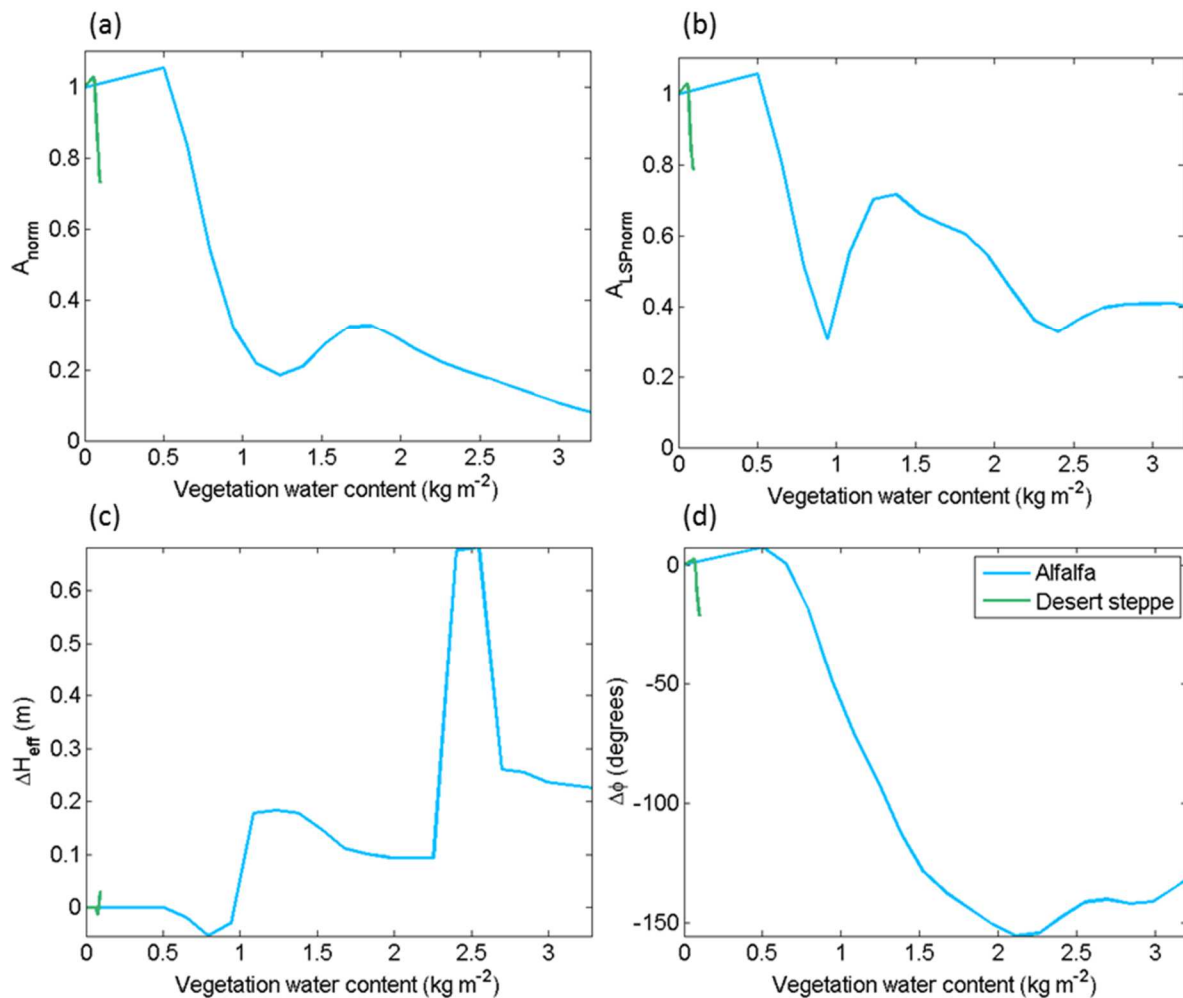


Figure 24: (a) Modeled decreases in  $A_{norm}$  at the desert steppe (green) and alfalfa (blue) sites as vegetation water content increases. (b) Modeled effect of vegetation water content on  $A_{LSPnorm}$  at the desert steppe and alfalfa sites. (c) Modeled effect of vegetation water content on  $\Delta H_{eff}$  at the desert steppe and alfalfa sites. (d) Modeled effect of vegetation water content on  $\Delta\phi$  at the desert steppe and alfalfa sites.

Figure 24b, which shows how  $A_{LSPnorm}$  varies with vegetation water content, indicates that for the desert steppe site,  $A_{LSPnorm}$  and  $A_{norm}$  are virtually the same. At the alfalfa site, however, there is an increase and subsequent decrease in  $A_{LSPnorm}$  from 1.5-2.5 kg m<sup>-2</sup>, which is much larger than the effect seen in  $A_{norm}$ .

There is hardly any change in  $\Delta H_{eff}$  at the desert steppe site (Figure 24c). Conversely, there are large step changes in  $\Delta H_{eff}$  as vegetation water content increases at the alfalfa site. These step changes are also indicated in Figure 21c as well. These step changes are caused by two or more frequencies in the SNR interferogram that compete to be the dominant frequency.

The effect of increasing vegetation water content on  $\Delta\phi$  is shown in Figure 24d. The effect is very similar to both  $A_{norm}$  and  $A_{LSPnorm}$ —the desert steppe site shows a faster decrease of phase for low increases in water content than the alfalfa site.  $\Delta\phi$  does show a small increase at 2 kg m<sup>-2</sup> at the alfalfa site, though there is no intermittent increase/decrease effect as in the amplitude data.

#### **4.4.3 Third case: When specific vegetation parameters are correlated with one another**

The example above shows very specific cases for when the relationships between all vegetation parameters are linear and known. However, in real field settings these relationships are never known with 100% certainty, as indicated by the significant scatter in Figure 23. In addition, most PBO sites have little to no vegetation data. Even sites that do have data will be expected to vary substantially from year to year. Thus, although the above example is instructive for showing how different the response of metrics to vegetation may be at two different sites, it cannot be used practically. A slightly less specific example, though still more specific than when vegetation parameters are completely unknown, is now presented.

For these simulations, vegetation wet weight ( $M_f$ ) was allowed to vary between 0-4 kg m<sup>-2</sup>, canopy height ( $H_{veg}$ ) between 1-100 cm, and vegetation percent water content (from which one can infer dry biomass) between 10-90%. Parameter sets which resulted in permittivities higher than 1.1 were excluded from the final analysis. The primary difference between these simulations and the completely random simulations described previously is in the treatment of vegetation true density,  $\rho_{veg}$ , which now is set to be directly proportional to its water content, as in the desert steppe/alfalfa simulations above. Here, underlying soil moisture was 0.05 cm<sup>3</sup> cm<sup>-3</sup> in our ‘dry’ library. An identical library of vegetation model simulations for ‘wet’ conditions was also created, in which soil moisture was 0.4 cm<sup>3</sup> cm<sup>-3</sup>. This allowed investigation of how changing soil moisture beneath a vegetation canopy will affect SNR metrics.  $A_{LSPnorm}$  was not calculated for these model simulations, as they were completed before this metric was recognized as being potentially valuable in vegetation estimation.

Figure 25 shows how changes in vegetation wet weight ( $M_f$ ) affects SNR metrics for these simulations. Each model simulation is colored by its canopy height. Notably in Fig. 34a (bottom), it appears that even at high values of vegetation wet weight, differences in canopy height can significantly change  $\Delta\phi$ . Canopy height does not change the relationship between wet weight and  $A_{norm}$  as drastically, as shown in Figure 25b (bottom). There are similar step changes in  $\Delta H_{eff}$  (Figure 24c) as in the simulations modeling the alfalfa field.

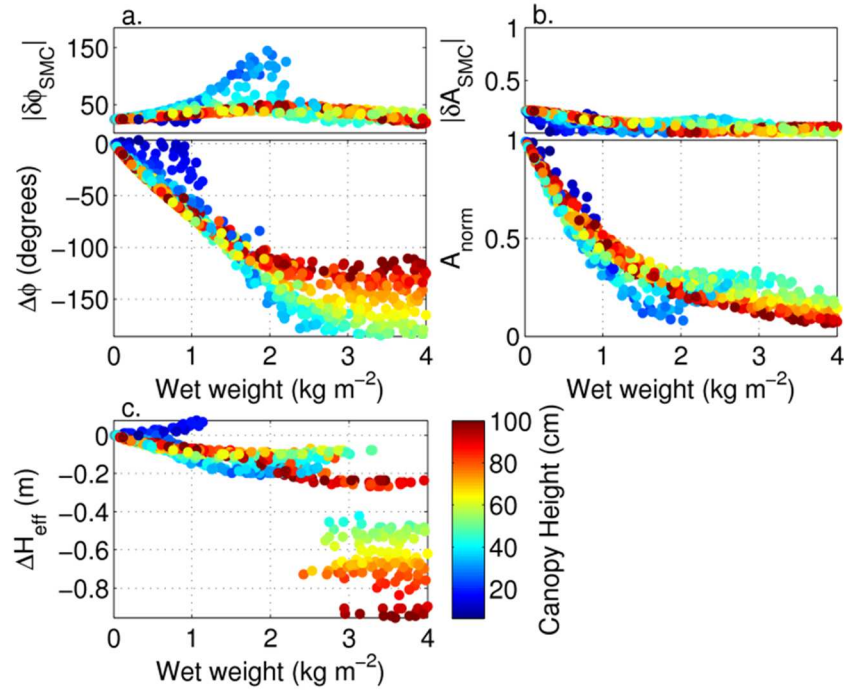


Figure 25: Model SNR metrics using random combinations of vegetation parameters and a dry (0.05) soil moisture profile as input. Metrics are plotted against modeled vegetation wet weight and colored by modeled canopy height. a. (*top*) The absolute magnitude of phase change if a wet (0.40) soil moisture profile were used as input. The range of the box is the same as the range in the box below. The subscript SMC is used to denote that the phase change is from soil moisture only. (*bottom*) The relationship between phase and vegetation wet weight for random model simulations with the dry soil moisture profile. b. (*top*) The absolute magnitude of normalized amplitude change if a wet (0.40) soil moisture profile were used as input. The range of the box is the same as the range in the box below. The subscript SMC is used to denote that the amplitude change is from soil moisture only. (*bottom*) The relationship between normalized amplitude and vegetation wet weight for random model simulations with the dry soil moisture profile. c. The relationship between change in effective reflector height and vegetation wet weight for random model simulations with the dry soil moisture profile.

#### 4.4.4 Effects of underlying soil moisture changes

The above three scenarios describe how vegetation affects SNR metrics, and section 4.3 showed how fluctuations in soil moisture for a bare surface changed SNR metrics. This section describes how concurrent changes in both soil moisture and vegetation obfuscate much of what was stated above (but don't worry, you didn't completely waste your time by reading the previous two sections!). Temporal changes in each SNR metric are some combination of changes of that metric from soil moisture and changes from vegetation. The simplest of combinations

would be if the total change of a metric were a linear combination of the two contributors, i.e. total phase change is the summation of the phase change due to vegetation and the phase change due to soil moisture.

We will now investigate whether or not this is the case, first by showing how changing soil moisture would affect conclusions drawn from the third scenario described in the previous section. Figure 25 (a-b, top) indicates the change in phase or normalized amplitude if soil moisture changes from  $0.05 \text{ cm}^3 \text{ cm}^{-3}$  to  $0.4 \text{ cm}^3 \text{ cm}^{-3}$ , for a given overlying vegetation canopy. Here, I have plotted the absolute value of the change and scaled each box to the range of their respective boxes below. I did not include the analogous panel for effective reflector height because changes exceeded  $\pm 0.1 \text{ m}$ , or 10% of the range, in only a handful of cases. Figure 25 (b, top) shows that the influence of soil moisture on  $A_{norm}$  is relatively small compared to the influence of vegetation on this metric. The figure also shows that the influence of soil moisture on normalized amplitude is relatively constant, compared to the  $A_{norm}$  changes expected from vegetation.

If one were only worried about estimating vegetation changes using SNR metrics, using  $A_{norm}$  as a proxy for vegetation change would have relatively small uncertainties introduced from soil moisture variations. Figure 25 (a, top) shows that the case for  $\Delta\phi$  is different. The change in phase due to soil moisture is approximately one third of that caused by vegetation for most of the canopies tested. However, for short and dense canopies,  $\Delta\phi$  from soil moisture is roughly equal to that from vegetation. This suggests that a large phase change could be due to either a change in soil moisture or in vegetation, or concurrent changes in both.

The model simulates changes in both phase and amplitude from soil moisture across the range of canopies tested here. Intuitively, one would expect a decrease in sensitivity to soil moisture for denser vegetation canopies. This general effect is simulated by the model: the influence of soil moisture on phase does generally diminish as permittivity increases. However, the simulated vegetation canopy does not completely obscure soil moisture effects until the canopy permittivity exceeds  $\sim 2.0$  (not shown). The canopies tested here are primarily composed of air, so the permittivity is almost always between 1.01 and 1.10. These permittivity values are consistent with published values [56]. For these permittivity values, the vegetation canopy does not completely obscure the underlying soil.

We now return to the original case of not having any *a priori* knowledge of vegetation at the site. How does a change in soil moisture change our conclusions drawn from Figure 21? The same combinations of randomized vegetation parameters as above were used to create additional simulations, except the parameters were each paired with an underlying soil moisture of  $0.05 \text{ cm}^3 \text{ cm}^{-3}$  and  $0.45 \text{ cm}^3 \text{ cm}^{-3}$ . SNR metrics were recalculated. Then, for each modeled vegetation canopy, the difference between metrics was calculated for the case when soil moisture was  $0.45 \text{ cm}^3 \text{ cm}^{-3}$  and the case when soil moisture was  $0.05 \text{ cm}^3 \text{ cm}^{-3}$ .

In other words, this experiment essentially shows how the slope between phase and soil moisture will change as overlying vegetation changes. The sensitivity of phase to soil moisture for the bare soil case was approximately 25 degrees, for typical ranges of possible moisture contents. Figure 26d shows how the sensitivity of phase to soil moisture changes depending on the vegetation canopy. For example, a change in soil moisture of  $0.4 \text{ cm}^3 \text{ cm}^{-3}$  would result in a phase change of approximately 25 degrees for a canopy with permittivity of 1.05 and height of 10 cm. However, the same soil moisture change would result in a greater than 50 degree phase

change if the permittivity were 1.1 and the height were 30 cm. Again, this is not intuitive. Shouldn't phase sensitivity to soil moisture decrease when either the height or permittivity of the canopy increases?

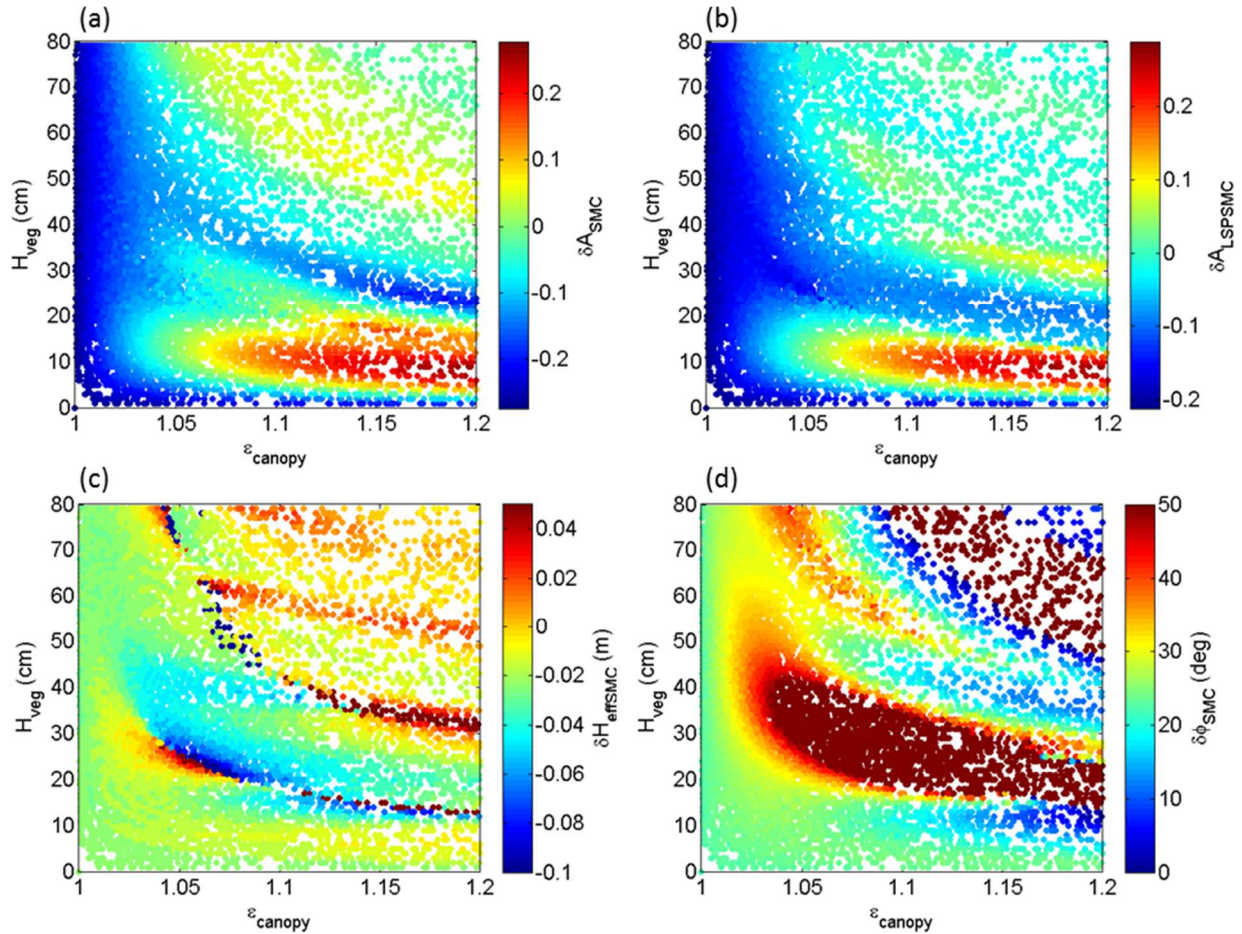


Figure 26: Model simulations showing the relationship between vegetation canopy permittivity ( $\epsilon_{\text{canopy}}$ ), the height of the vegetation ( $H_{\text{veg}}$ ), and how much (a) amplitude (b) LSP amplitude (c) effective reflector height and (d) phase would respond to a change in soil moisture from  $0.05 \text{ cm}^3 \text{ cm}^{-3}$  to  $0.45 \text{ cm}^3 \text{ cm}^{-3}$  for the given vegetation canopy parameters. The amplitude metrics were normalized with respect to the bare soil values at  $0.15 \text{ cm}^3 \text{ cm}^{-3}$  moisture content.

The difference between the frequency/*a priori* reflector height ( $H_0$ ) used to estimate phase and amplitude and the actual frequency(cies)/effective reflector height(s) ( $H_{\text{eff}}$ ) of the SNR data is largely, though not totally, responsible for the apparent increase in the response of phase to soil moisture for some vegetation canopies, which is seen in Figure 26d. When the

discrepancy between  $H_0$  and  $H_{eff}$  becomes large, the frequency that is used in least-squares estimation of phase and amplitude is no longer characteristic of the actual data, and errors will be introduced in their estimation. The apparent large response of phase to soil moisture changes for these dense canopies is more reflective of the errors introduced by the frequency discrepancies in least-squares estimation than in an actual phase response. However, assuming all other things equal, these types of responses of phase to soil moisture should also be apparent in observed data. Though, additional noise and other complexities found in real data could preclude this effect.

Figure 26a-c show the sensitivity changes of other metrics to changes in soil moisture. Figure 26a, which shows how  $A_{norm}$  responds to soil moisture beneath vegetation canopies, is subject to the same errors as phase, in terms of inappropriate frequency assignment in least-squares estimation. Figure 26b, which shows how  $A_{LSPnorm}$  responds to soil moisture changes, is also subject to analogous errors due to multiple strong ground- and canopy-reflections, though mostly once the reflection coming from the canopy layer is strong enough to compete with the reflection coming from the soil layer. Both amplitude metrics indicate that the amplitude value may either decrease or increase from its bare soil value, depending on the vegetation canopy.

Figure 26c indicates that  $\Delta H_{eff}$  does not behave in the same way as the phase and amplitude metrics do. There is not as apparent oscillatory behavior in its sensitivity to soil moisture fluctuations. Large jumps in sensitivity are probably caused by the presence of a second, competing frequency in the SNR data. For the most part, sensitivity of  $\Delta H_{eff}$  to soil moisture fluctuations is between 0-2 cm.

#### 4.4.5 Problems with the constant-frequency SNR equation

As briefly discussed earlier, SNR metrics are calculated under the assumption that the SNR interferogram is comprised of a singular amplitude, phase, and frequency. Just looking at an interferogram, it is apparent that at least the amplitude of the interferogram is not constant with elevation angle. This is mostly due to the effect of the antenna's gain pattern of the ground-reflected signal. As Figure 9 shows, amplitude at different elevation angles increases or decreases depending on the vegetation canopy. The LSPs shown in Figure 22 indicate that there are situations in which there are multiple frequencies in the interferograms.

I have shown that SNR metrics are affected in nonlinear, complex ways due to concurrent changes in soil moisture and vegetation. Part of these complicated interactions is due to the fact that the SNR metrics themselves do not always describe the interferogram adequately. Using least-squares with the constant-frequency characterization of (2) can be fraught with problems when the actual data have non-constant amplitude and potentially multiple frequencies. What I will show now is how the characteristic equation of SNR data (2) will sometimes mischaracterize the actual data, particularly when there is high vegetation present.

One can visualize the mischaracterization of SNR data by plugging the estimated  $A$  and  $\phi$  values back into (2) and assuming that the frequency is a function of  $H_0$ , the *a priori* reflector height. Figure 27 shows how the SNR metrics from the model simulations in Figure 25 actually characterize their respective interferograms. Here, model simulations have been plotted with respect to their wet weight/ $M_f$  values, though they could have been plotted against another parameter. I chose to quantify how well each modeled interferogram can be recreated using the estimated SNR metrics from (2) alone using  $r^2$ . In other words, I computed the  $r^2$  value between each interferogram and the interferogram that results from plugging in the SNR metrics into (2).

What we see is that as wet weight increases, the  $r^2$  value decreases non-linearly and significantly. This confirms the suspicion that vegetation growth causes an increase in the mischaracterization of the actual interferogram, due to the fact that the constant-frequency assumption in (2) is no longer appropriate.

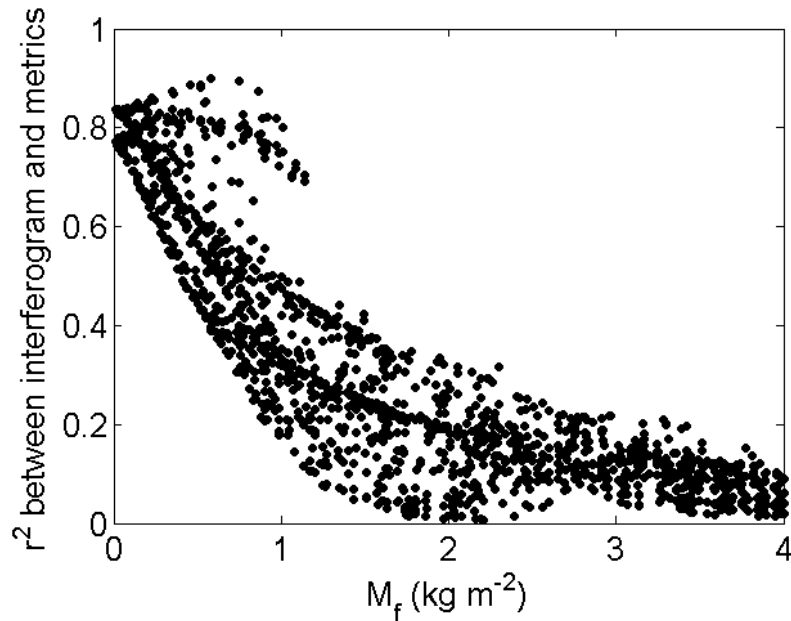


Figure 27: Results from random model simulations using the soil-vegetation model. The fresh mass/wet weight of the model simulation is plotted against the  $r^2$  value between the simulated interferogram, and the interferogram that would result if its estimated phase and amplitude were used in Eq. (2).

It is apparent that assuming the dominant frequency of the SNR data is equal to the *a priori* reflector height can oftentimes result in the mischaracterization of SNR data. The way SNR data are characterized with the current SNR metrics is obviously a problem, though the way this problem is addressed is discussed in later sections.

#### 4.4.6 Conclusions

In summary, this chapter has explored the theoretical effects of both soil moisture and vegetation canopy parameters on SNR interferograms and metrics. The model was first validated

using field observations from four field sites. Next, the way in which SNR metrics would be changed due to bare soil moisture fluctuations was quantified, and it was decided that SNR phase would be the best predictor of changes in soil moisture content. Following this, the effect of varying vegetation parameters on SNR metrics was explored, without varying soil moisture. It was shown that canopy height and effective permittivity drive changes in SNR metrics. When soil moisture and vegetation both vary, it was shown that the sensitivity of SNR metrics to changes in underlying soil moisture is nonlinear with unexpected behavior. Some of this effect is due to the errors in SNR metric calculation resulting from forcing interferograms to fit with the basic model in (2).

Before moving on to the next chapter, however, I want to briefly revisit the question stated by (34): Is the total phase change a linear combination of the phase change due to soil moisture and the phase change in vegetation? Unfortunately, I do not think the relationship can be simplified in such a way. I have spent a lot of energy finding out how the sensitivity of phase changes for underlying soil moisture, depending on the vegetation canopy. However, this question could be posed in reverse: How does the sensitivity of phase (or whatever SNR metric you like) change for the vegetation canopy, depending on the underlying soil moisture? Trying to answer these two questions independently of one another has led to many circular arguments. Regardless, in future chapters, I will assume that the linear combination assumption is ‘true enough’ for the analysis of real data. At least for the sites I examine here, the linear combination assumption does not appear to significantly detract from our ability to estimate soil moisture.

## Chapter 5: Correcting for vegetation effects on SNR data

This chapter addresses how the vegetation effect on SNR data is mitigated using simulations generated from the soil and vegetation model described in Chapter 4.

### 5.1 Extent of vegetation effects in observed data

At a number of Plate Boundary Observatory (PBO) network GPS sites, the SNR data are affected by both soil moisture change and seasonal vegetation growth cycles. One way that we have estimated the extent of vegetation effects on SNR data is by looking at smoothed and normalized SNR amplitude ( $A_{norm}$ ) time series. [62] showed that  $A_{norm}$  is the SNR metric that is affected predominantly by changes in vegetation, and to a lesser extent by soil moisture. We use the amplitude time series as a proxy for changes in vegetation.

Figure 28 shows a histogram of  $A_{norm}$  values for all satellites tracks at all PBO H<sub>2</sub>O sites. The dashed line shows an approximate cutoff where one can be reasonably certain that there are significant changes in vegetation at the GPS site ( $A_{norm} = 0.78$ ). The cutoff is an approximation of how much  $A_{norm}$  would be expected to decrease when soil moisture content (SMC) increases from residual to saturated values (Figure 15), though this cutoff would change for soil types that could have larger or smaller SMC ranges. Figure 28 indicates that at least 20% of the data are affected by vegetation. This is a minimum estimate, as higher  $A_{norm}$  values may still indicate vegetation changes, depending on soil moisture changes.

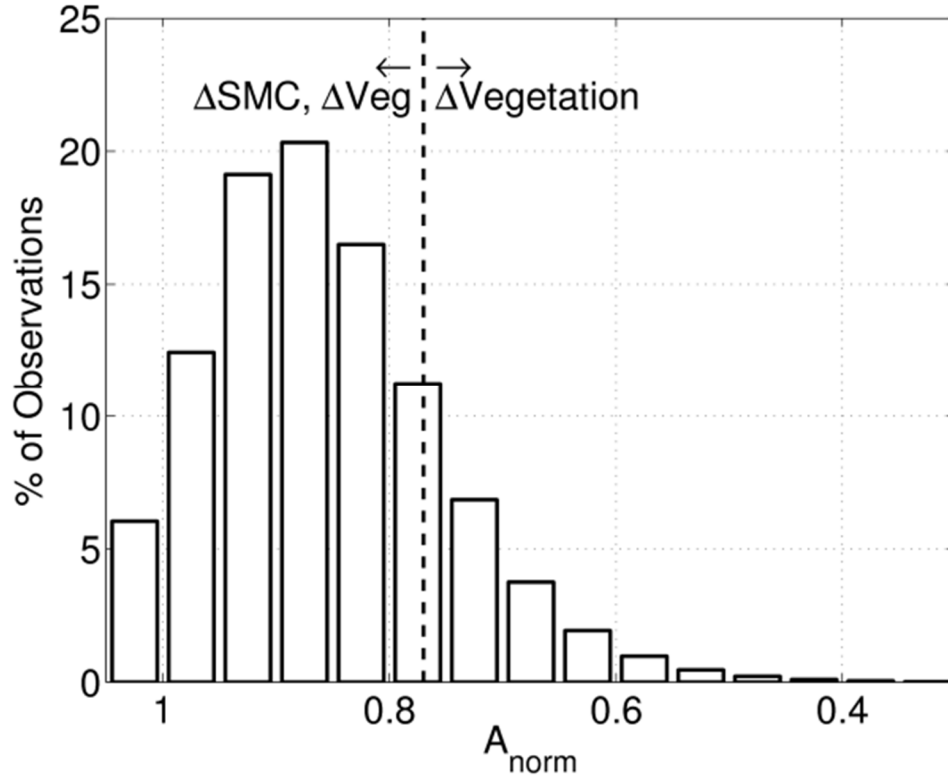


Figure 28: Histogram showing the percentage of PBO H<sub>2</sub>O data that fall into normalized amplitude bins. The dashed line indicates the point at which observations are significantly affected by vegetation.

### 5.2 Development of the vegetation filter

As stated previously, an increase in vegetation amount could be mistaken for a decrease in soil moisture in the phase time series. Before final soil moisture estimations may be made, the SNR phase time series at the sites with relatively significant vegetation change must be cleaned, or filtered, for vegetation effects. I will now describe the method used in the PBO H<sub>2</sub>O database for filtering phase time series for vegetation.

The filter described here is a compromise between the need for accuracy, computational efficiency, and generality for the variety of vegetation conditions found at the PBO sites. The filter relies on the soil-vegetation model, described and validated in [62], to provide simulations of how SNR metrics change with canopy height and permittivity changes (Figure 21), in the

absence of soil moisture change. Relationships between SNR metrics themselves, which result from the vegetation changes, are used to clean the SNR phase time series. In other words, changes in  $A_{norm}$ ,  $A_{LSPnorm}$ , and  $\Delta H_{eff}$  are used to predict changes in  $\Delta\phi$  from vegetation.

### 5.2.1 SNR model simulations

The SNR model simulations used in the vegetation filter are the result of pseudo-random combinations of vegetation parameters. Parameter sets representing different vegetation canopies needed to be realistic, but they also needed to be varied enough to encompass a wide range of canopy possibilities. The final filter includes 16000 vegetation parameter sets meant to represent both semi-dry natural environments as well as wetter agricultural fields, though a larger proportion of simulations represent natural environments. Parameter sets that resulted in vegetation canopies with an effective (real) permittivity of greater than 1.2 were excluded from the filter. Figure 29 shows distributions of vegetation parameters used in the model simulations.

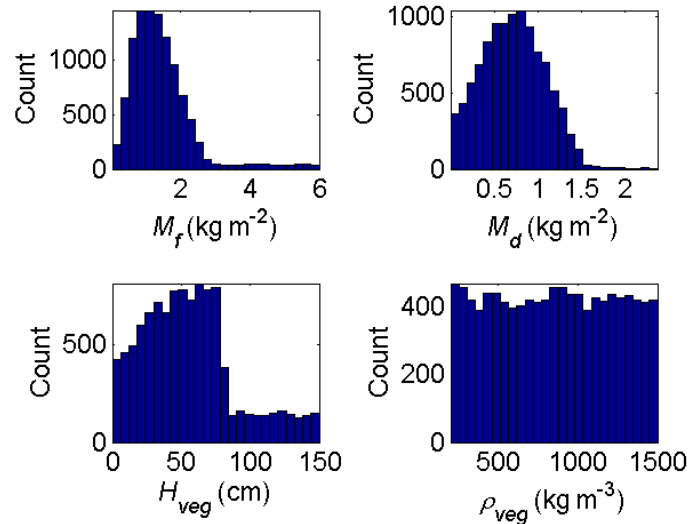


Figure 29: Distributions and ranges of vegetation parameters used in vegetation filter model simulations. Fresh biomass or the wet weight of vegetation is denoted by  $M_f$ , dry biomass is denoted by  $M_d$ , canopy height by  $H_{veg}$ , and true density by  $\rho_{veg}$ . Vegetation salinity was kept at its default value.

The model was run for these parameter sets assuming an underlying bare soil moisture content of  $0.15 \text{ cm}^3 \text{ cm}^{-3}$ . I chose to use  $0.15 \text{ cm}^3 \text{ cm}^{-3}$  because it was a compromise between the drier average SMC for desert or arid environments and the wetter average SMC for other sites, like Oklahoma (Figure 6). Assuming different underlying moisture contents does in fact change the filter—this is discussed below.

### 5.2.2 Relationships between SNR metrics

After the model simulations were created, SNR metrics were calculated. Once metrics were calculated, it was necessary to then understand how  $A_{norm}$ ,  $A_{LSPnorm}$ , and  $\Delta H_{eff}$  could be used to predict changes in  $\Delta\phi$ . Keep in mind that we are not actually trying to first estimate changes in vegetation with the filter—we only want to discover how the relationships between metrics themselves change due to changes in vegetation only.

Depending on the vegetation parameters, relationships between metrics themselves will change. Examples are shown in Figure 30 which depicts how the relationship between different metrics and phase will change depending on the vegetation canopy. It is apparent from Figure 30 that no one SNR metric, in the absence of abundant vegetation field data, can accurately predict the change in phase. However, using the combination of SNR metrics can provide more accurate predictions (Figure 31). Figure 31a shows how  $A_{norm}$  and  $A_{LSPnorm}$  can be used together to predict changes in phase due to vegetation. Once  $A_{norm}$  decreases to about 0.4, phase is not well-predicted by changes in the two amplitude metrics. However, as Figure 31b shows, using information contained in reflector height variations can help predict changes in phase past an amplitude decrease beyond 0.4. It should be noted that the relationships between SNR metrics and phase are not smoothly-varying when amplitudes are below 0.4 and reflector height has not

changed by more than 10 cm (Figure 31b). One would thus expect more error in phase predictions in these situations.

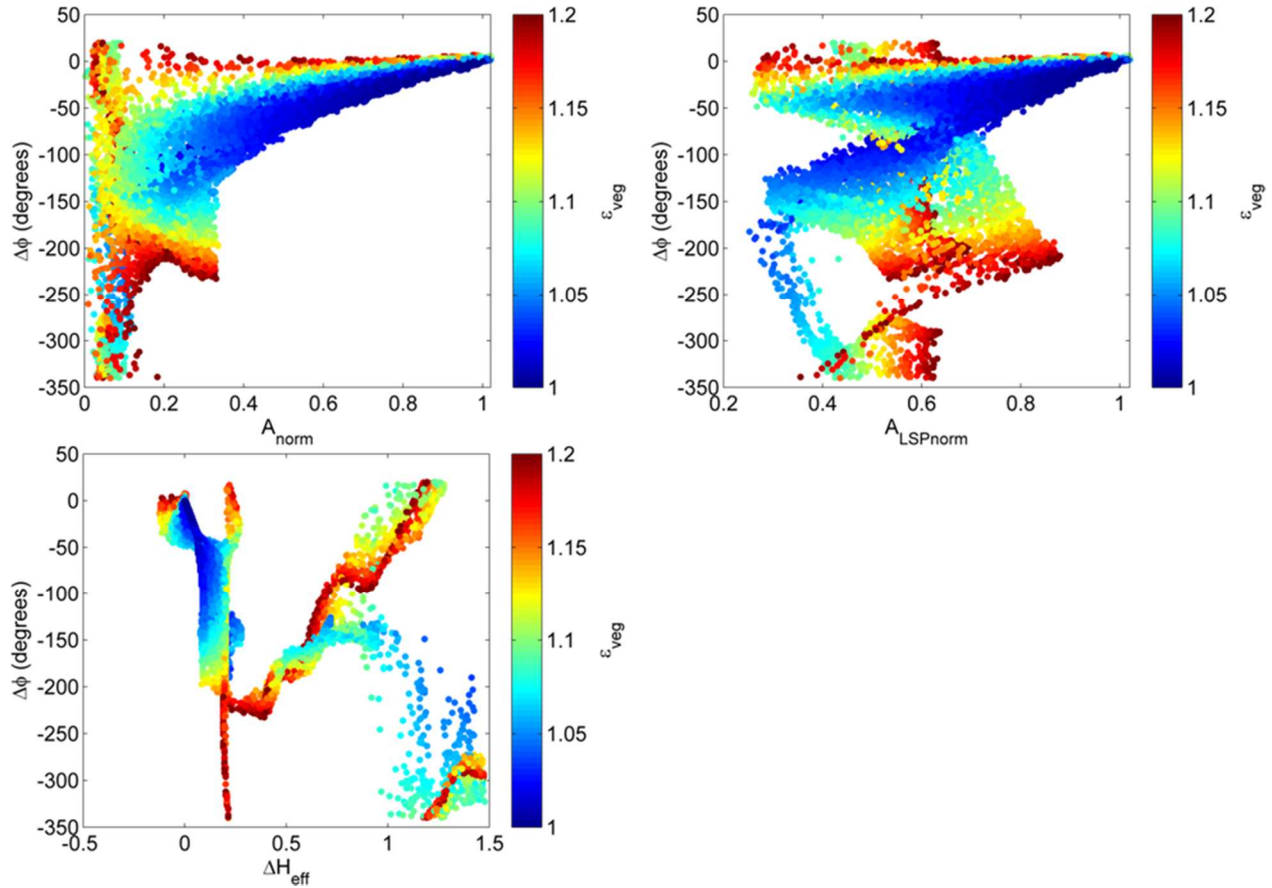


Figure 30: The relationships between SNR metrics and  $\Delta\phi$ , which vary depending on vegetation parameters. Here, points are colored by canopy permittivity (real part).

### 5.3 Processing observed SNR metrics

Because soil moisture changes will affect all SNR metrics to different degrees, the observed LSP amplitude, amplitude, and reflector height time series are first smoothed before being used in the filter (examples shown in Figure 32). Smoothing the time series means that we are assuming that long-term changes in the SNR metrics are only due to vegetation change and not due to long-term (i.e., seasonal) changes in surface soil moisture. Despite this, I have found

that the filter does a sufficient job at preserving the longer term soil moisture signals, at least at our validation sites in Oklahoma.

The choice of a smoothing method is relatively important due to the fact that changes in vegetation may occur rapidly at a site. Moving mean and median filters are sometimes successful, though occasionally they can over-smooth rapid vegetation growth and senescence. For very small vegetation changes, a moving mean or median is probably sufficient, though in these cases the necessity of the vegetation filter itself is questionable.

Using a Savitzky-Golay filter has shown to be more successful at preserving the timing and magnitude of vegetation growth and senescence while still being relatively insensitive to noise. A Savitzky-Golay filter fits subsets of adjacent data points with low-order polynomials using least-squares. The parameters needed for the filter have been found to be important in smoothing the SNR metric time series. In the current version of the vegetation filter, a polynomial order of 4 and data span of 63 days is used to smooth each time series. The filter is least successful in smoothing reflector height time series due to the relatively high proportion of noise to long-term change.

#### **5.4 Estimating phase change due to vegetation**

As it was shown in Figure 30 and Figure 31, the effect of vegetation on the relationship between SNR metrics is complicated without obvious functional relationships. For this reason, the SNR metrics derived from the model simulations are saved in a data cube or lookup table. An observed triplet of  $A_{norm}$ ,  $A_{LSPnorm}$ , and  $H_{eff}$  (after smoothing) is compared to the triplets contained in the metric lookup table. A linear nearest neighbor search algorithm is used to find the best-matching modeled triplet and its associated phase change. Although generally computationally

inefficient for large data sets, the search algorithm does not take significantly long for the modeled data set used in the vegetation filter.

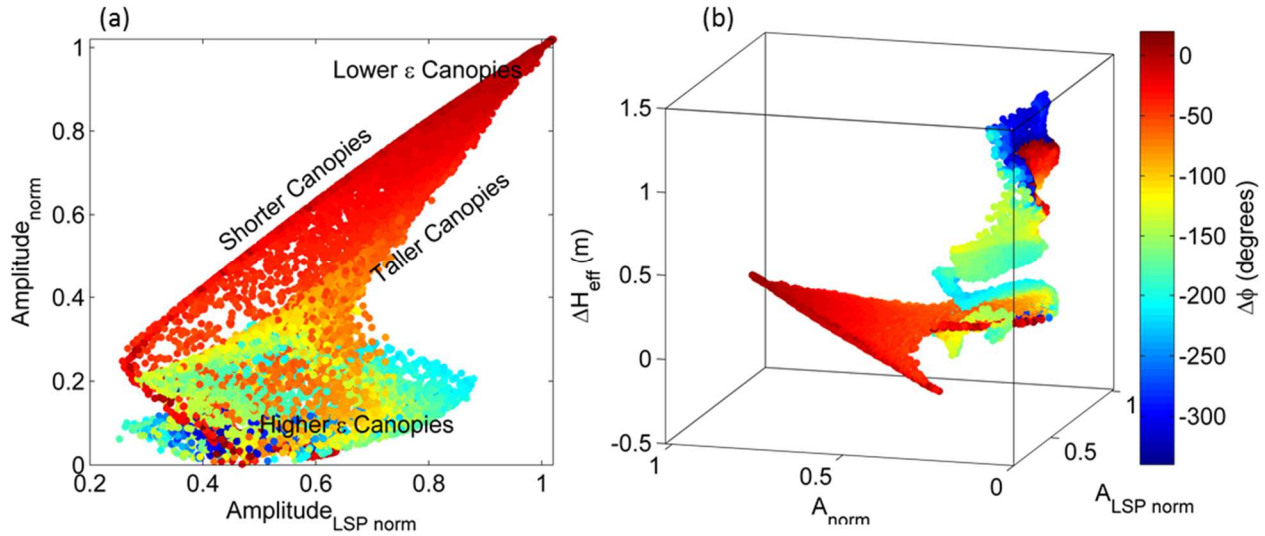


Figure 31: (a) Relationship between  $A_{norm}$ ,  $A_{LSP\ norm}$ , and  $\Delta\phi$ , for the simulations used in the vegetation filter. (b) Same relationships as in (a) except also with  $\Delta H_{eff}$ .

Predicted phase changes due to vegetation are also smoothed to mitigate noise introduced by the linear nearest neighbor search algorithm. The predicted phase change due to vegetation,  $\Delta\phi_{veg}$ , is subtracted from the observed phase time series, to retain only the phase change due to soil moisture,  $\Delta\phi_{SMC}$  (35) (example shown in Figure 32). Note that this is just a modified version of (34), which means the vegetation filter assumes that the total phase change is a linear combination of the phase change from vegetation and soil moisture.

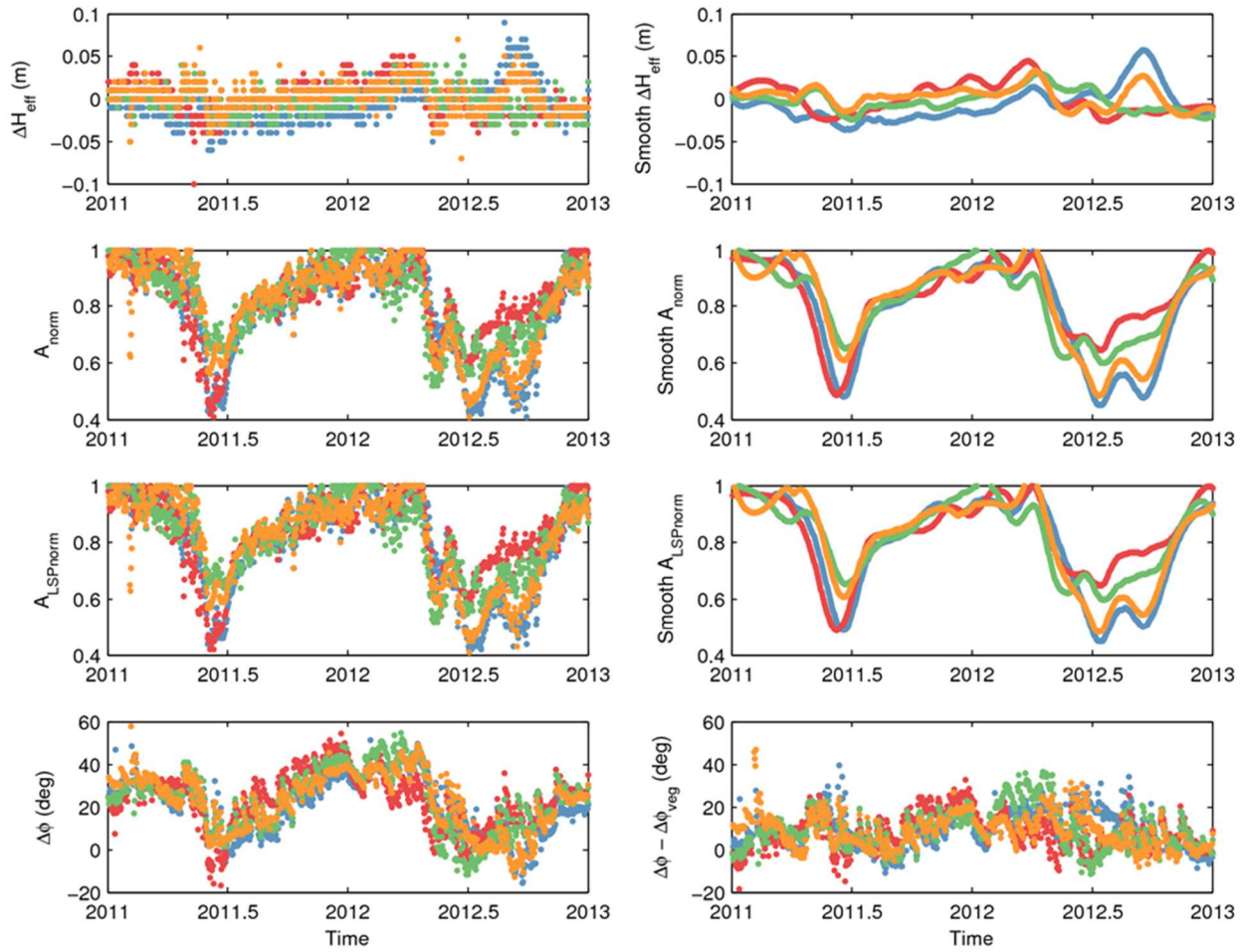


Figure 32: SNR metrics for four satellite tracks at the Oklahoma site. The left column contains SNR metrics for the four tracks, except they have been either normalized (in the case of amplitude), subtracted from the estimated *a priori* antenna height, or zeroed with respect to the baseline phase values. The right column contains smoothed  $\Delta H_{eff}$  and amplitudes used in the vegetation filter. The panel at the bottom of the right hand column shows the phase time series after the vegetation effect has been removed.

$$\Delta\phi_{SMC} = \Delta\phi - \Delta\phi_{veg} \quad (35)$$

The same vegetation parameter sets used in the vegetation filter are also used to predict the sensitivity change of phase to soil moisture. These sensitivity changes are similar to those shown in Figure 26d. To compute the sensitivity changes, I ran the model simulations used in the filter twice again—once assigning the underlying soil moisture to be  $0.05 \text{ cm}^3 \text{ cm}^{-3}$  and once assigning it to be  $0.45 \text{ cm}^3 \text{ cm}^{-3}$ . Assuming a linear relationship between phase and soil moisture

regardless of vegetation extent, I calculate a new slope based on the phase changes from the two different model simulation sets. The set of slopes (or relationships between phase and changes in soil moisture) for each vegetation parameter set is matched with the vegetation parameter set used to create the data cube described above. Thus, when the linear nearest-neighbor search is conducted, it will not only choose a predicated phase change due to vegetation, but also the predicted relationship between phase and a change in soil moisture for that point in time.

## **5.5 Justification for the current filter**

There are numerous ways a vegetation filter could have been developed. This section briefly describes why this design was chosen over others.

### **5.5.1 Concurrent inverse estimation of soil moisture and vegetation**

The obvious question has always been: why not concurrently solve for both soil moisture and vegetation changes using the modeled SNR data? It was shown in [62] that the soil-vegetation model is able to recreate the overall shape of SNR data, given appropriate vegetation and soil moisture inputs. Unfortunately, the modeled shape is not able to be used to estimate soil and vegetation parameters in an inverse procedure for the following reasons (though it has been tried):

1. Frequency of SNR oscillations: In order to match observed SNR interferograms to modeled, the modeled interferograms must have the correct frequency. Each satellite track at each GPS site has its own *a priori* reflector height, which means any library of modeled interferograms would require many duplicates of simulations with varying *a priori* heights. The *a priori* reflector height would need to be known perfectly.

2. Surface roughness and tilting in observed data: Since real environments are not flat, slight surface roughness or surface tilting will result in smaller amplitudes of SNR oscillations at higher elevation angles. This seemingly-small effect causes both vegetation and soil moisture to be overestimated at a site.
3. Noise in observed oscillations: Interferograms recorded from some satellite tracks at some sites have what should be called ‘trademarks.’ One satellite track could have a persistent amplitude or other anomaly at certain elevation angles, which could be caused by receiver, gain pattern, or topographic issues. Even small ‘trademarks’ cause a mis-estimation of vegetation.
4. Magnitude of amplitude oscillations: As discussed previously, the magnitude of the amplitude of oscillations is determined by factors such as the transmit power of the satellite. Modeled SNR interferograms would all need to be scaled to match this amplitude for each satellite track, negating some of the initial advantages of shape-matching.
5. Phase of bare soil interferograms: As also discussed previously, the baseline phase value for each satellite track is different. Modeled interferograms would need to be shifted to match the satellite track’s bare soil phase value. This also negates some of the initial advantages of shape-matching.

If comparing modeled and observed interferograms directly to one another is not feasible, could one compare modeled and observed SNR metrics to inversely estimate soil and vegetation parameters concurrently? The answer to this question is: sometimes, but not without at least as much effort as is put into the current vegetation filter, and soil moisture estimation is still unfeasible. Inverse estimation of both soil and vegetation parameters using the simplified SNR

metrics is difficult due to the combination of (basically) non-unique solutions and the presence of noise in observed SNR metrics.

For example, the variance of the observed  $A_{norm}$  and  $A_{LSPnorm}$  time series for one satellite track at a PBO site is on the order of 0.03. If one were to look at, say, model simulations that could produce  $A_{norm}$  and  $A_{LSPnorm}$  between 0.75 and 0.78, one would see that very dissimilar vegetation canopies could result in this range of amplitude values. For this particular example, simulations that could produce such SNR metrics range from a 20 cm tall canopy with a permittivity of 1.004, to an 80 cm tall canopy with a permittivity of 1.0178. And this is assuming the underlying soil moisture content is perfectly known. It is thus difficult to inversely estimate vegetation parameters, due to variance in observed data, which is why the vegetation filter skips this step.

However, it is important to point out that there has been some success in implementing this procedure at a GPS site located next to an alfalfa field near Boulder, Colorado. Figure 33 shows inversely-estimated vegetation height using observed SNR metrics and assuming that underlying soil moisture remained a constant  $0.15 \text{ cm}^3 \text{ cm}^{-3}$ . Each estimated height is the median estimated height from all available satellite tracks in the southern quadrants. Observed heights show the mean and standard deviation from field sampling surveys. Part of the errors in estimated heights are attributed to the smoothing of the SNR amplitude time series—smoothing does not allow for abrupt changes such as harvests. I have not had as much success at estimating canopy height in natural environments, possibly due to the complicating effects of soil moisture.

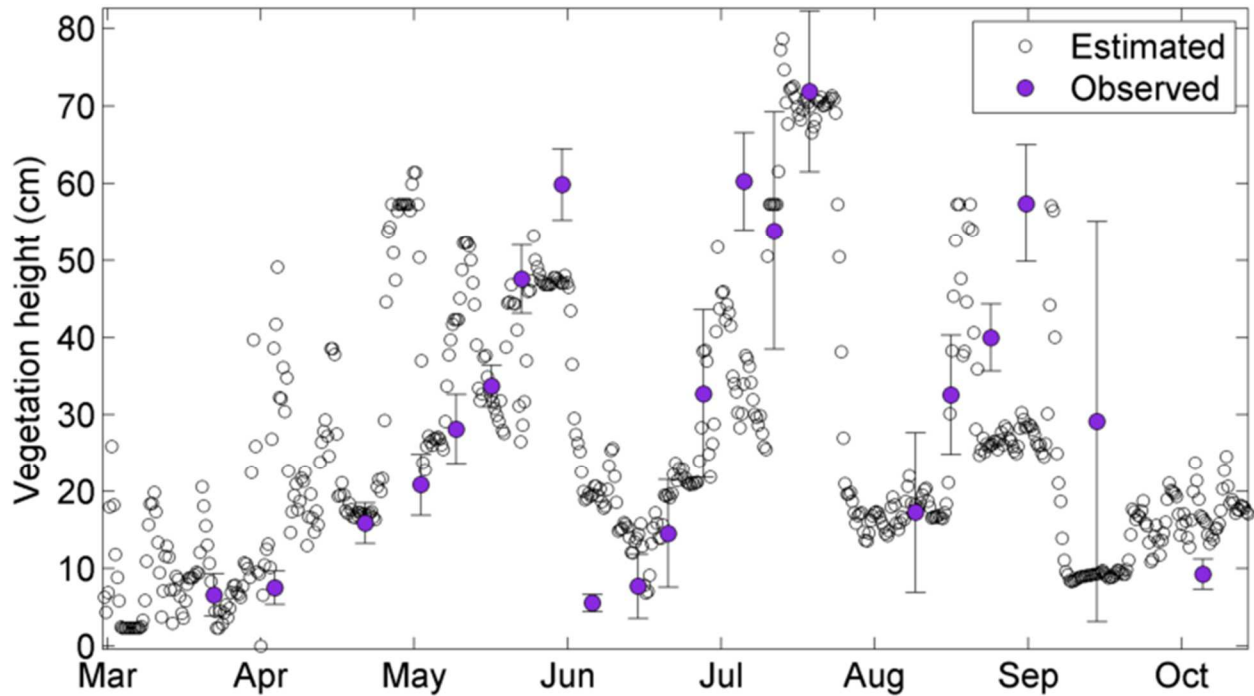


Figure 33: Estimated (open circles) versus observed (purple dots) values of vegetation height at a GPS site located next to an alfalfa field. Standard deviations of observations are also shown.

How could the current vegetation filter be successful then, if the non-uniqueness problem and noise in observations make the inverse estimation of environmental parameters unfeasible? The current vegetation filter does not try to estimate soil or vegetation parameters using the model simulations. It instead estimates changes in phase expected, based on model simulations, from changes in other SNR metrics (which, in the model simulations, change only due to vegetation changes).

This aspect to the vegetation filter may not appear to be too important. However, when one considers that errors in observed SNR amplitude and effective reflector height time series are likely similar to errors in observed phase time series, predicting phase changes using other SNR metrics makes sense. The filter by design mitigates the detrimental effect of observed noise since the phase time series will likely contain the effects of this noise as well.

### 5.5.2 The use of a more complex characteristic SNR equation

It was discussed in Chapters 4 and 5 that oftentimes the presence of vegetation introduces complexities into SNR interferograms that are not adequately characterized using the metrics derived from (2). The presence of multiple frequencies in the interferogram or no clear distinct frequency introduces errors into our estimation of phase and amplitude. The vegetation filter's success hinges on the assumption that the errors in phase and amplitude estimation of both observed and simulated interferograms are the same.

This then, begs the question: Why use Eq. 2 to characterize the interferograms at all? Why not come up with an alternative characterization of SNR data, one that allows for multiple frequencies or the variation of amplitude with elevation angle?

Here enter the problems that arise when applying a model to a large network of antennas and receivers that were not designed to do remote sensing. It has been a struggle to balance investigating the science behind what drives changes in SNR interferograms, and actually putting the conclusions of these investigations into practice. Observed SNR data are, for a lack of a better word, quirky.

To illustrate potential complications that would arise from introducing a more complex version of (2), let's assume for a moment that it was possible to introduce variations of amplitude with elevation into the soil-vegetation model, such that  $A$  in (2) was replaced with  $A_{\sin(E)}$ , which is the variation of amplitude with elevation angle. This collection of terms that comprise  $A_{\sin(E)}$  all vary to different degrees with changes in soil moisture, vegetation, surface roughness, topography, tilting of the ground surface and the gain pattern of the antenna, not to mention the

phase of the interferogram (which determines ‘where’ in elevation angle the peaks and troughs of the interferogram begin).

Soil moisture and vegetation changes would be included in  $A_{\sin(E)}$  as some sort of function of the reflection coefficients at that elevation angle, which cannot be determined analytically due to the nature of variable vegetation canopy heights, among other factors. Figure 34 shows the complicated relationships between elevation angle, the reflection coefficients, and soil and vegetation parameters. In Figure 34a,b reflection coefficients are presented as a function of elevation angle for a bare soil, for the case when soil moisture is  $0.04 \text{ cm}^3 \text{ cm}^{-3}$  and also when soil moisture is  $0.4 \text{ cm}^3 \text{ cm}^{-3}$ . One could see that perhaps an analytical relationship could be derived for the relationship between the uniform soil moisture profile and reflection coefficients at every elevation angle for the bare soil case. But now, when we introduce a vegetation layer on top of the soil layer, as in Figure 34c,d, we see that deriving such relationships are not going to be so simple. (For reference, the vegetation layer added in Figure 34c,d was a 30 cm tall canopy, with a wet weight of  $1 \text{ kg m}^{-2}$ , dry weight of  $0.5 \text{ kg m}^{-2}$ , and true density of  $500 \text{ kg m}^{-3}$ .)

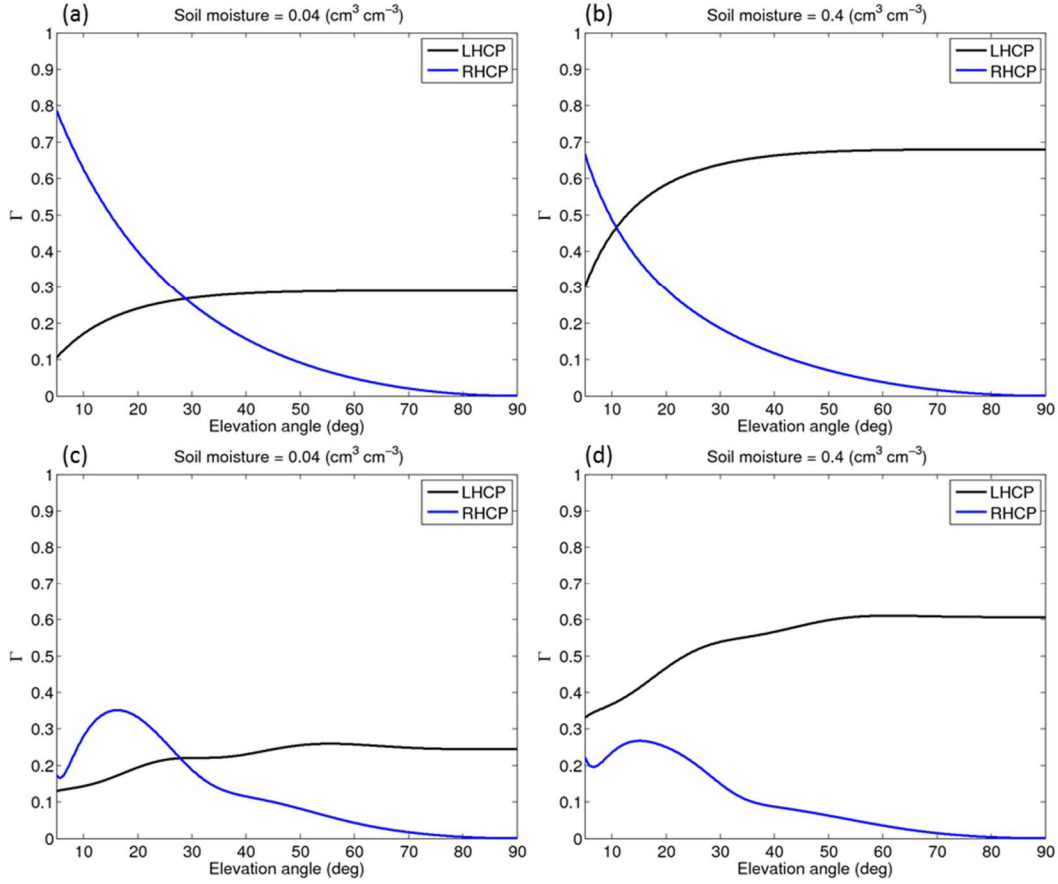


Figure 34: (a) Left- (black) and right-handed (blue) reflection coefficients at circular polarization for a bare soil with moisture content  $0.04 \text{ cm}^3 \text{ cm}^{-3}$ . (b) Same as (a), except moisture content is  $0.4 \text{ cm}^3 \text{ cm}^{-3}$ . (c) Same as (a), except now a vegetation layer of 30 cm and permittivity (real part) of 1.05. (d) Same as (c), except with a soil moisture content of  $0.40 \text{ cm}^3 \text{ cm}^{-3}$ .

### 5.6 Limitations of the vegetation filter

There are several limitations of the vegetation filter that are important to mention. One of the most obvious limitations is the fact that the filter was designed assuming the base soil moisture content is  $0.15 \text{ cm}^3 \text{ cm}^{-3}$ . Figure 35 shows how the assumed relationships between  $A_{norm}$ ,  $A_{LSPnorm}$ , and  $\Delta\phi$  change when the assumed underlying soil moisture content is changed from  $0.05 \text{ cm}^3 \text{ cm}^{-3}$  to  $0.45 \text{ cm}^3 \text{ cm}^{-3}$ . Even though short term variations in observed SNR metrics are smoothed out before the vegetation filter is used, if the mean observed soil moisture content is not  $0.15 \text{ cm}^3 \text{ cm}^{-3}$ , there will be error introduced in the estimated phase change due to vegetation. These errors appear to increase as the SNR amplitude metrics decrease. In order to

mitigate these errors, for sites with minimal changes in vegetation, soil moisture content is allowed to vary randomly in the model simulations. Otherwise, I have found that the vegetation filter consistently will over-correct for vegetation.

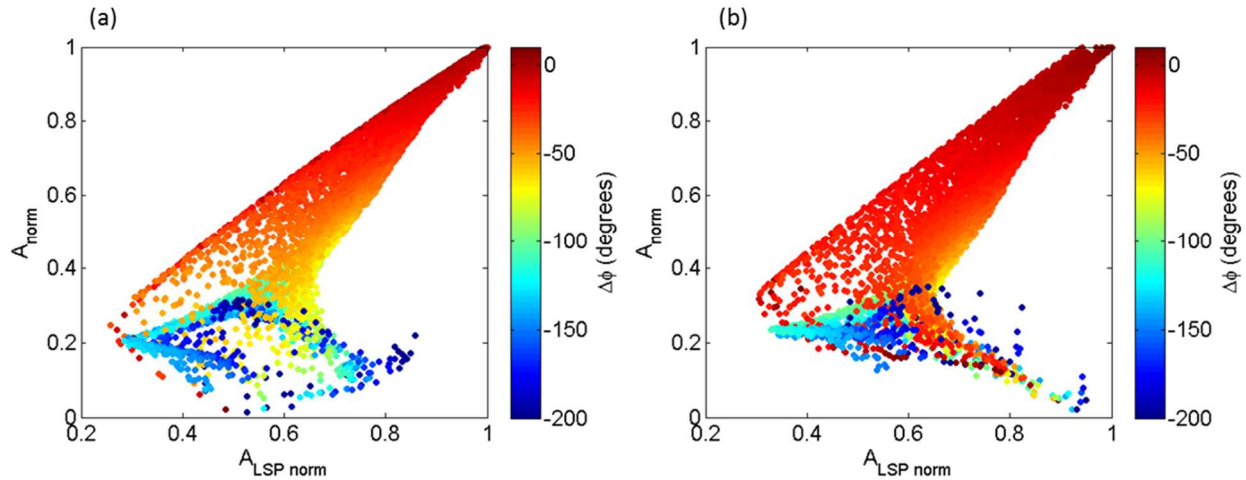


Figure 35: (a) Variation of SNR amplitude metrics with phase for the simulations used in vegetation filter, assuming an underlying SMC of  $0.05 \text{ cm}^3 \text{ cm}^{-3}$ . (b) Variation of SNR amplitude metrics with phase for the simulations used in vegetation filter, assuming an underlying SMC of  $0.45 \text{ cm}^3 \text{ cm}^{-3}$ .

A second important limitation of the filter is that it currently assumes that the *a priori* reflector height is known perfectly, and that at some point during the year the site is completely bare.

The success of the vegetation filter hinges on the assumption that the mischaracterization of the SNR interferogram using the constant frequency equation is exactly the same in model simulations and observations. It was mentioned in both [62] and [43] that shifting the dominant frequency of the interferogram too far away from the bare soil frequency will lead to an overall mischaracterization of the SNR interferogram and essentially make the phase and amplitude estimates ‘meaningless’ in that they are no longer representative of the interferogram. The vegetation filter assumes that modeled SNR metrics and observed metrics are meaningless in the

same way and that the meaningless metrics are related to one another in the same way. The filter thus, to some extent, is matching modeled and observed errors to one another. If and when this assumption breaks down, the vegetation filter will not work.

In addition, it cannot be stressed enough how important the gain and phase patterns of the antenna are in determining the characteristics of the SNR interferogram. The relationships described in this document are very specific to the choke ring antenna. The procedure for determining the relationships would be the same for other antennas, however, and the soil-vegetation model still works for other antenna power patterns. It just produces different SNR interferograms, and hence different SNR metrics.

For example, let us pretend that we have a GPS antenna that is isotropic in both right- and left-handed circular polarizations. An isotropic antenna allows radiation in from all elevation angles indiscriminately. This means that the antenna does not suppress ground-reflections from higher elevation angles. Changes in the amplitude of the SNR interferogram with elevation angle are now only the result of soil and vegetation parameters. For this experiment, the gain pattern of the antenna at all elevation angles, for both right- and left-handed polarizations, was set to be the mean value of the right-handed gain pattern. Other values were tested, and while the absolute magnitude of the SNR interferogram changed, its variation with elevation angle was the same no matter the value of gain used.

SNR interferograms for a bare soil and varying moisture content were simulated for the isotropic antenna. Some examples are shown in Figure 36a. Ignoring the absolute magnitude of power on the y-axis, Figure 36a shows that there are still oscillations with elevation angle, as expected, since this is mostly a geometric effect. It also shows that drier soils have a larger

amplitude at lower elevation angles than wetter soil. This is due to the partitioning of the reflected signal into left- and right-handed polarizations are the reflection coefficients of these polarizations for the specified permittivity. In addition, each interferogram begins at grazing angles with a relatively large amplitude, then this amplitude decreases to nearly 0 at some elevation angle, after which point it begins to increase again. The point at which it decreases to 0 appears to be a function of its moisture content and is also the point at which both left- and right-handed reflection coefficients are equal (Figure 36).

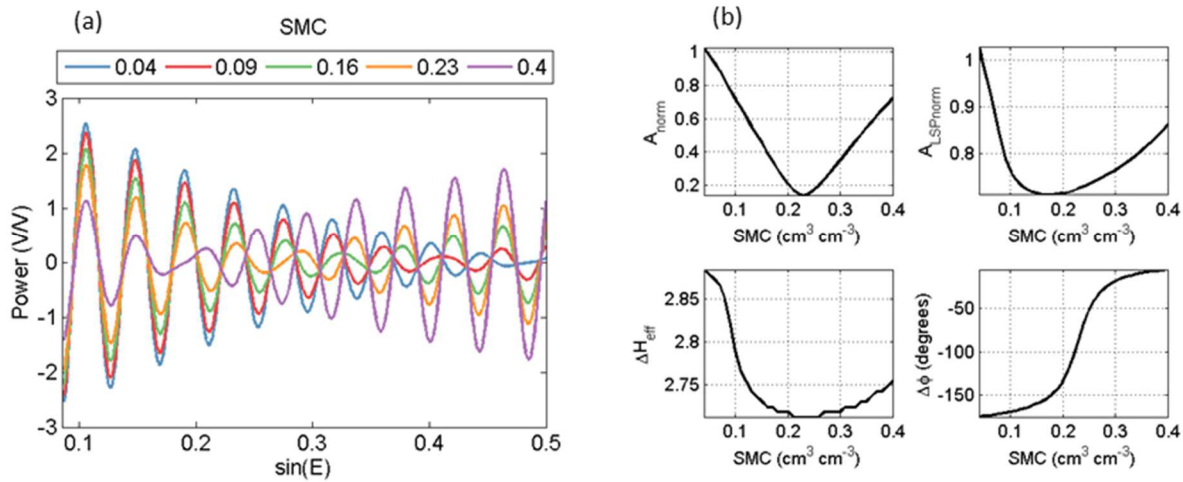


Figure 36: (a) Modeled interferograms for a theoretical, isotropic antenna. Interferograms are representative of a bare soil with the indicated moisture contents. (b) SNR metrics calculated from the interferograms (and other interferograms at different moisture contents) in (a).

It is apparent that these interferograms, like the interferograms resulting from the choke ring antenna's gain pattern, also are not well-characterized by the SNR equation (2). However, their corresponding SNR metrics are presented in Figure 36. The point of this exercise is to only point out what a difference in the antenna gain and phase pattern makes. It would be unwise to apply the specific relationships in this document to other varieties of GPS antennas.

## **Chapter 6: Soil Moisture Estimations using GPS-IR**

This chapter is a departure from the model simulations presented in Chapter 4, though it does make use of the vegetation filter presented in Chapter 5. This chapter describes how SNR data are transformed into soil moisture estimations. First, examples of issues that may be present in empirical data are shown, after which the algorithm currently used for soil moisture estimation is described.

### **6.1 Empirical data issues**

The vegetation filter cannot resolve all data issues that arise in every observed SNR time series. Other complications may arise, either due to permanent changes in the environment (trenching, etc.) or problems within the antenna or receiver that can cause data from one or more satellite tracks to be of poor quality. These long-term or permanent changes in data quality are different from the occasional random noise in the interferogram that may cause the data to be of bad quality for a day or two. Systemic, long-term, or permanent changes to the SNR data quality for a satellite track have the potential to introduce large errors in soil moisture estimations, especially for sites with few good satellite tracks to begin with. Here, I will provide examples of some of these problems and my attempts to mitigate them. However, the problems described here are by no means the only problems that may be present in the data, though they are some of the biggest complicating factors in using the vegetation filter on empirical data.

#### **6.1.1 Persistent amplitude anomalies**

One example of a persistent amplitude anomaly comes from the GPS sites in Oklahoma (okl3). PRN 7 Q 4 at okl3 began to exhibit an SNR anomaly on DOY 300 in 2012 (Figure 37). From 7-12 degrees, amplitude remains depressed throughout the winter, while the amplitude of surrounding angles increases, as expected. This anomaly persists in the interferograms for this

satellite track until at least mid-2013 (Figure 37). The anomaly is not present in nearby satellite tracks and could be due to any one of a number of factors, such as the DoD changing the orbit of the satellite such that its ground track changes. Or, perhaps a cow stood right in that spot for nearly a year. Regardless of the source, the anomaly results in the  $A_{LSPnorm}$  and  $A_{norm}$  time series remaining far below 1.0 in the winter (Figure 38). In other words, it causes an apparent persistent vegetation signal in the time series when there should not be one. The vegetation filter fails to appropriately correct phase values from mid-2012 forward. Because there are a relatively large number of other satellite tracks at this GPS site, the overall soil moisture time series is not greatly affected. However, GPS sites with fewer usable tracks would be significantly affected by such an anomaly.

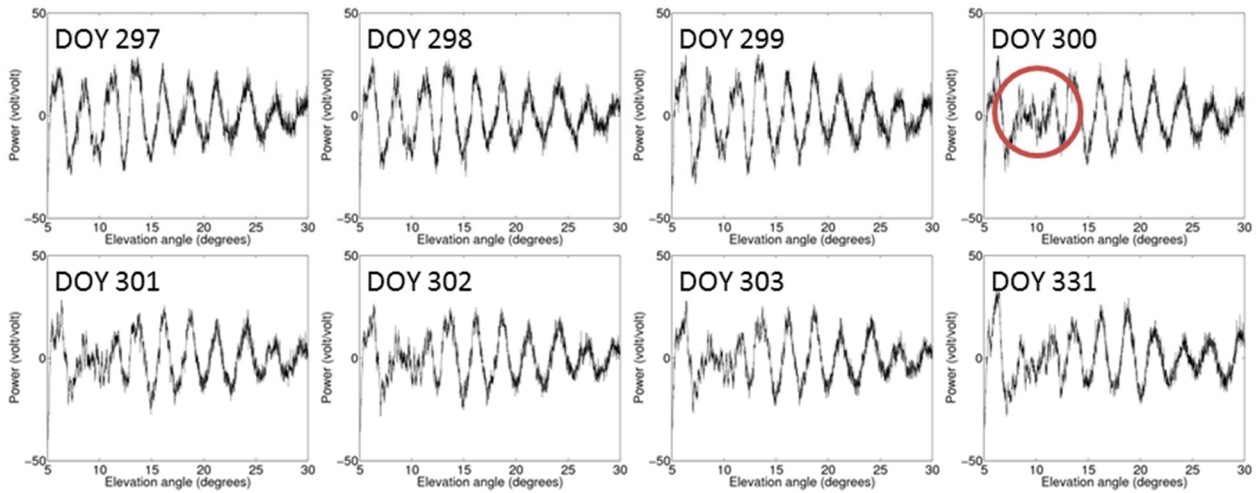


Figure 37: SNR interferograms for PRN 7, quadrant 4, OKL3. Something happens on DOY 300 (red circle) that persists for the remainder of the available data.

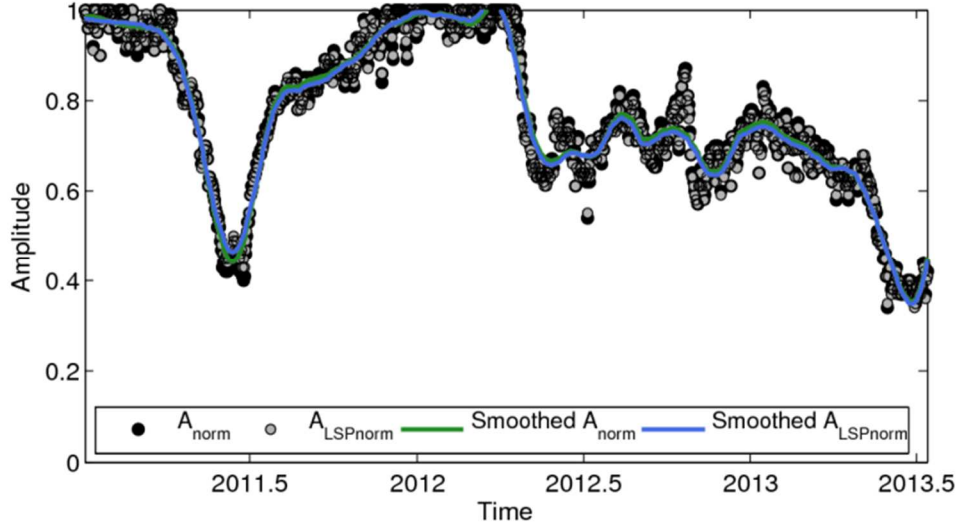


Figure 38: Amplitude time series for PRN 7, quadrant 4, at the GPS site OKL3. 2011 shows the expected seasonal cycle of amplitude decreasing during vegetation growth and increasing once vegetation dies. This cycle is no longer apparent after mid-2012.

In order to mitigate this issue and other similar issues with amplitude anomalies, an empirical method to flag these anomalies and remove them from consideration has been implemented. In order to implement the method, the mean and standard deviation of  $A_{LSPnorm}$  time series for all supposedly ‘good’ satellite tracks for a GPS station is calculated.  $A_{LSPnorm}$  data for a satellite track that is too far from the mean is excluded from further processing and soil moisture estimations. To quantify how far is ‘too far’ from the mean, the standard deviation is used. However,  $A_{LSPnorm}$  data from different satellite tracks naturally diverge from one another during times of vegetation growth, due to spatial heterogeneities in vegetation cover. Therefore, the rule of thumb for excluding  $A_{LSPnorm}$  data that is too far away from the mean is relaxed during times of vegetation growth, or when the mean of  $A_{LSPnorm}$  is relatively low. Figure 39 and (36) summarizes the empirical rule for excluding SNR data:

$$\tau = \begin{cases} 2.5\sigma^2 - \overline{A_{LSPnorm}} \sigma^2 / 0.78, & \overline{A_{LSPnorm}} < 0.78 \\ \sigma^2, & \overline{A_{LSPnorm}} \geq 0.78 \end{cases} \quad (36)$$

Where:  $\sigma^2$  is the standard deviation of the  $A_{LSPnorm}$  time series for all good satellite tracks,  $\overline{A_{LSPnorm}}$  is the mean of the  $A_{LSPnorm}$  time series for all good satellite tracks, and  $\tau$  is the upper and lower allowance for the deviation of one satellite track's  $A_{LSPnorm}$  time series away from the mean. Data are excluded when  $A_{LSPnorm}$  for a satellite track exceed this limit.

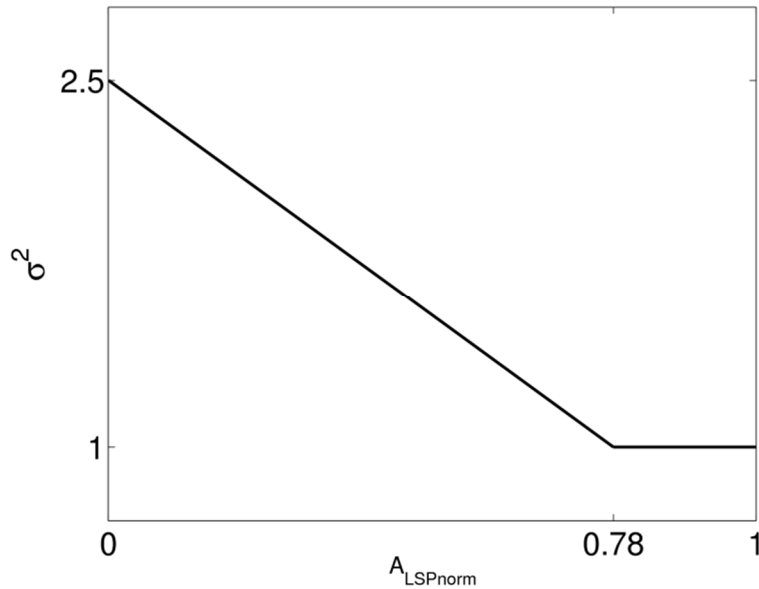


Figure 39: The relationship between  $A_{LSPnorm}$  for a single satellite track and the standard deviation of the mean  $A_{LSPnorm}$  time series used to determine how much a particular  $A_{LSPnorm}$  time series is allowed to deviate from the mean.

An example of these bounds for the GPS station in Oklahoma (OKL3) is shown in Figure 40. The empirical filter would not consider much of the aberrant data for PRN 7 quadrant 4 in 2012, indicated by the data (green dots) falling outside the bounds (black lines). It also excludes data for other satellite tracks at different points in the time series.

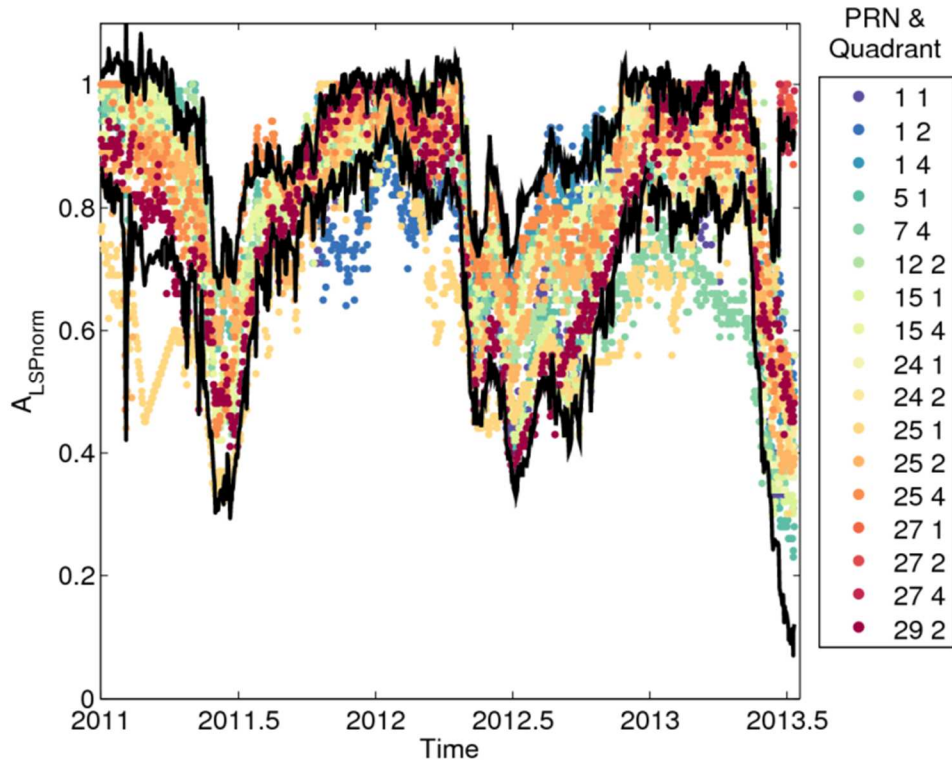


Figure 40: Time series of  $A_{LSPnorm}$  for all supposedly good satellite tracks at OKL3 (colored dots). Black lines indicate the range of values allowed to be considered for further processing in the vegetation filter and in soil moisture estimations. Colored points outside this range would be removed from final soil moisture estimations.

## 6.1.2 Reflector height considerations

### 6.1.2.1 Anomalous reflector height shifts

We have at least one example of a potential long-term reflector height change unrelated to soil moisture or vegetation. At p041 in late 2013, we observe an apparent step change in reflector height that appears thus far to be permanent. We believe the step change was caused by the large flooding event in September of that year, with enough sediment being redistributed to cause changes in the reflector height that should be used as the *a priori* height.

Figure 41 shows a time series of  $\Delta H_{eff}$  for PRN 1, quadrant 1. Positive values indicate that the reflector height is lower than the prescribed *a priori* height, and vice versa. After the

flood, reflector height showed a step change of approximately 3 cm, which would indicate sedimentation of no more than 3 cm in the footprint of that satellite track (this is the upper bound because an increase in soil moisture will also cause a decrease in apparent reflector height).

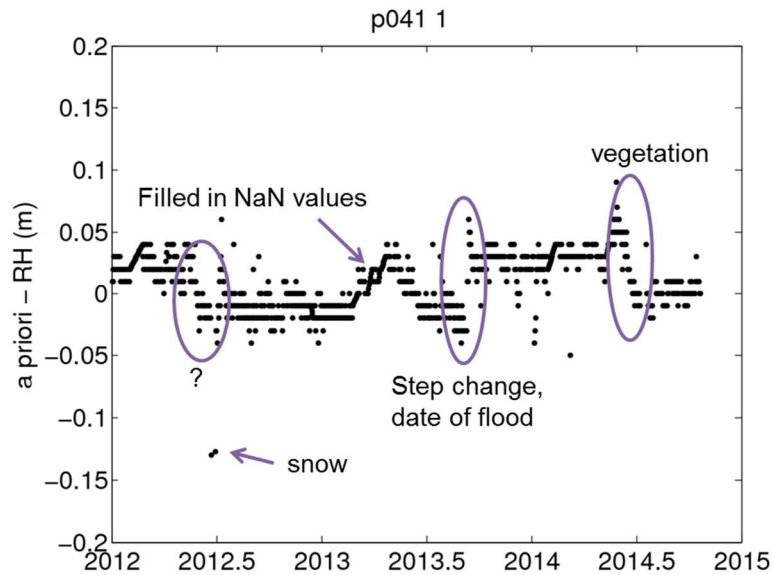


Figure 41: Time series of  $\Delta H_{eff}$  for PRN 1, quadrant 1 at p041. Circled are time periods of significant reflector height change. Note the step change in reflector height in late 2013, coincident with the date of a significant flooding event.

*In situ* probe data does show that 5 cm average soil moisture did remain quite high post-flood and into the winter (Figure 42). However, using the same *a priori* reflector height after the flood results in soil moisture estimates that are too high. The cyan points in Figure 42 are GPS estimated soil moisture (with no vegetation filter), and the blue line shows data from TDR probes. GPS soil moisture tracks nicely with TDR estimates until the flood, after which time they are too high. If these problems are not detected, errors can obviously be significant.

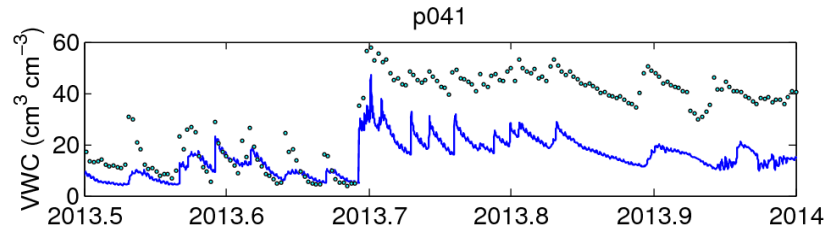


Figure 42: Time series of satellite-track averaged soil moisture estimated (grey points) and *in situ* probe data (blue line) for p041 near Marshall, Colorado.

The reflector height problem could manifest itself in ways other than step changes. In the reflector height time series above, note the time period circled in 2012 with a question mark. Here, reflector height increases with respect to the *a priori* height, in other words making the ground surface appear lower than it actually is. This could be due to changes in the vegetation canopy, though the reflector height anomaly does not appear to be seasonal in nature, as it persists into the spring of the following year, which might be an indicator that this wouldn't be due to 'normal' vegetation effects.

The effect of this anomaly of the phase and subsequently estimated soil moisture time series is not small. Figure 43 shows the estimated time series along with TDR estimates (here, theta probe surveys are shown in yellow). The second half of 2012 shows great agreement with TDR estimates. However, the first half of 2012 shows that GPS estimates are much too high. This is not due to errors in the relationship between phase and soil moisture, since we see that the rest of 2012 is fine. Instead, I believe these errors are due to the unexplained reflector height anomalies described and shown above, as they are well-correlated in time.

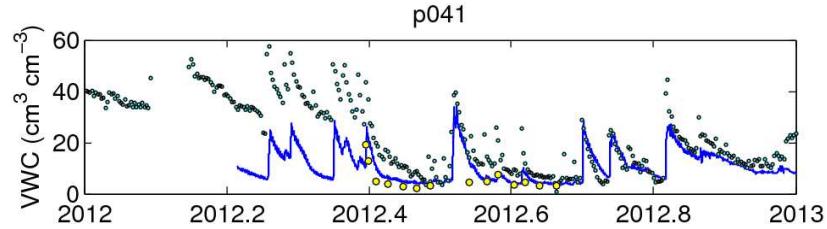


Figure 43: Data from p041 in Marshall, Colorado. *In situ* probe data are shown by the blue line. Yellow points are theta probe data. Grey points are the track-averaged soil moisture estimates from GPS.

### 6.1.2.2 Correcting reflector height issues

I have attempted to quantify effects in the phase time series and subsequent soil moisture estimations due to anomalous variations in reflector height that the vegetation filter might not account for. Let us create a cosine wave with a known frequency, amplitude, and phase, which are constant with elevation angle. Frequency is determined using the equation for SNR frequency as a function of antenna height ( $\frac{4\pi H}{\lambda}$ ). For now, let us say that  $H = 2.4$  m, amplitude = 20 volt/volt, and phase = 0 degrees. What if we were to estimate phase and amplitude for this sine wave, except we are mistaken in the frequency that we use in least-squares? There will be some amount of error in phase and amplitude estimation. These errors would be similar to expected errors introduced when the frequency of an observed SNR interferogram change anomalously. In Figure 44 I show errors in phase and amplitude estimation as a function of the error in frequency used for least-squares (black line).

This correction is not exactly the same as it would be for re-calculating phase and amplitude using the raw SNR data. If one were to re-calculate phase using the raw SNR data, the relationships change. They change because SNR data are not constant frequency, constant amplitude, or constant phase sine waves. One would expect for these relationships to also depend on the permittivity of the reflecting surface. Figure 44 (colored points) shows these relationships

for bare soil with a uniform moisture profile. Figure 44a shows that, when one uses an *a priori* height that is greater than the actual antenna height, the calculated phase will be greater than it would be if one used the actual antenna height for phase calculation (points to the right of (0,0) in Figure 44a). The theoretical relationship for these variables, if the SNR data were constant frequency, amplitude, and phase is shown by the black line. The fact that the black line is quite close to the SNR data points indicates that phase is relatively constant with elevation angle.

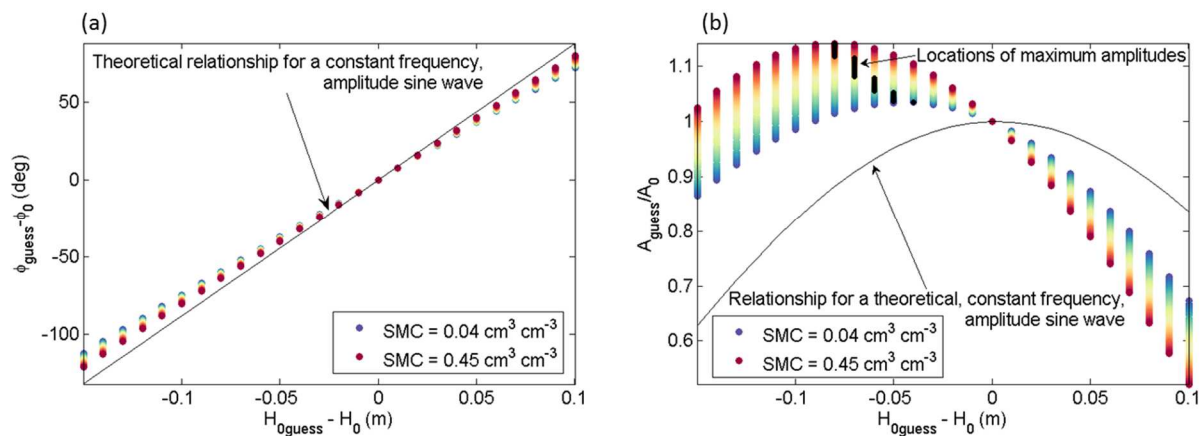


Figure 44: (a) The relationship between mistakes in the *a priori* reflector height ( $H_{0\text{guess}}$ ) and the actual antenna height ( $H_0$ ) and corresponding differences in phase. Points are colored by soil moisture content. The relationship using a constant frequency, amplitude, and phase sine wave is shown by the black line. (b) The relationship between mistakes in the *a priori* reflector height ( $H_{0\text{guess}}$ ) and the actual antenna height ( $H_0$ ) and corresponding differences in amplitude. Points are colored by soil moisture content. The relationship using a constant frequency, amplitude, and phase sine wave is shown by the black line. Black points are locations of the maximum values of amplitude. These locations correspond to peak frequencies in the LSP.

Figure 44b shows the same relationships for amplitude. Phase error does not depend on the starting value of phase, though amplitude error does, which is why the y-axis in the amplitude figure above is normalized. Here, amplitude is being normalized with respect to its ‘correct’ value. In this figure, the black, theoretical relationship is no longer close to the relationship using SNR data. This makes sense, since the SNR data are not constant amplitude. The locations of maximum amplitudes are indicated by the black points. These locations

correspond to the peak frequencies of the LSPs, which also makes sense, as the best estimate of amplitude will occur when a best-matching frequency is used in its estimation.

I have applied a correction to the phase and amplitude data, using the modeled SNR relationships in Figure 44. This involves a few assumptions. These relationships vary with soil moisture, so a median soil moisture content of  $0.15 \text{ cm}^3 \text{ cm}^{-3}$  is assumed. It is also assumed that the overall correction needed is:

$$H_{correction} = H_{0guess} - H_0$$

$$H_0 \cong \widetilde{H_{eff}}$$

Where  $H_{correction}$  is the bias needed to be introduced to the SNR metric time series,  $H_{0guess}$  is the current approximation of the *a priori* reflector height, and  $H_0$  is the actual *a priori* reflector height.  $H_0$  is approximated by the median reflector height in the time series ( $\widetilde{H_{eff}}$ ).

The equations for the correction, assuming a median SMC of  $0.15 \text{ cm}^3 \text{ cm}^{-3}$  are:

$$A_{corrected} = \frac{A_{guess}}{-18H_{correction}^2 - 2.1H_{correction} + 1} \quad (37)$$

$$\phi_{corrected} = \phi_{guess} - 759H_{correction} \quad (38)$$

$$H_{eff} = H_{eff} - H_{correction} \quad (39)$$

Where  $\phi_{guess}$  and  $A_{guess}$  are the phase and amplitude time series currently calculated using  $H_{0guess}$ , respectively, and  $\phi_{corrected}$  and  $A_{corrected}$  are the corrected time series.

Note that in Eq. (38), a 1 cm reflector height drift would equate to a 7.59 degree phase change. Since the total expected response of phase due to maximum changes in soil moisture is less than 30 degrees, a 1 cm reflector height drift is actually quite significant.

Let's revisit our reflector height and phase time series from p041 that were shown in Figure 41 and Figure 43. In the winter of 2012, reflector height was lower than the *a priori* height, which in that plot are positive values on the y-axis (i.e. the reflector height might have been 1.9 m, and the *a priori* height was 1.95 m or similar). During the summer of 2012, reflector height then increases and remains slightly above the *a priori* height until 2013 (i.e. reflector height might have been 1.96 m, if the *a priori* height was 1.95 m). So, in the winter of 2012 at p041, reflector height variations would be associated with positive values on the x-axis in the phase error plot in Figure 44. This means that we would expect to see higher than normal phase estimates during the winter of 2012 at p041. Indeed, in the phase time series (Figure 43), we see exactly this. Note that this example does not preclude vegetation being the source of this anomaly, though since it is either not seasonal in nature or just not obviously-seasonal, it could be from another source.

What happens if the phase and amplitude error relationships (Eq. (37) and (38)) for constant frequency sinewaves are used on observed SNR data? Let's examine p041 2012 data again. Figure 45a shows a reflector height time series for satellite 7, quadrant 3, and the best fit linear slope to the data. Nearly all satellite tracks in 2012 at p041 have a negative slope, similar to the one shown below. The reflector height trend can be converted to expected phase changes, using Eq. (38). These expected changes can be removed from the phase time series, which is what is shown in Figure 45b. In this figure, black points are the raw phase data, and the red points are the remainder after the reflector height trend has been removed. Note that there is still

a decrease in phase around 2012.4, which does correspond to the expected decrease due to vegetation growth. There is also an increase in phase at the end of summer, which would be expected once the vegetation water content decreases.

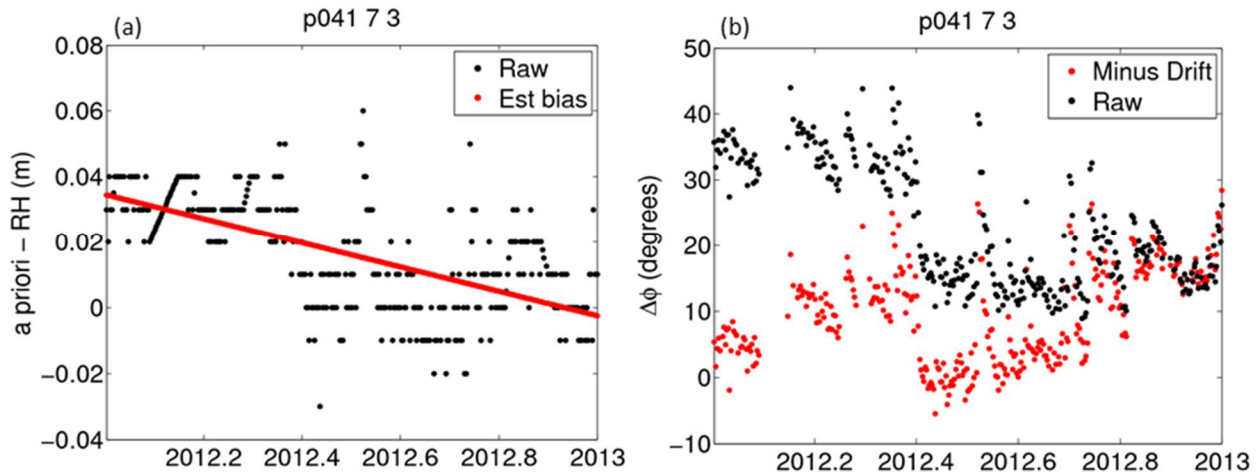


Figure 45: (a)  $\Delta H_{eff}$  time series for PRN 7 Q 3 at p041 (black dots) along with the best fit linear trend to the data (red line). (b) Phase time series for the same satellite track as in (a) (black dots). Red dots are the phase time series after the linear trend in reflector height has been removed, using the relationship in Eq. (38).

What is the final effect on the soil moisture time series, if these linear trends are removed on a track by track basis, and then vegetation filtered as normal? The results are shown in Figure 46. Figure 46a shows the track-averaged time series if there is no linear trend removed, and Figure 46b shows the time series if these trends are removed. If there is no trend removed, estimated soil moisture in the winter of 2012 is much too high. Estimated SMC is too low around 2012.7-2012.8. If a linear trend is removed, estimated SMC agrees quite well with *in situ* probe SMC in early 2012 and the SMC from 2012.7-2012.8 is also improved, though SMC at the end of the year is a little too high.

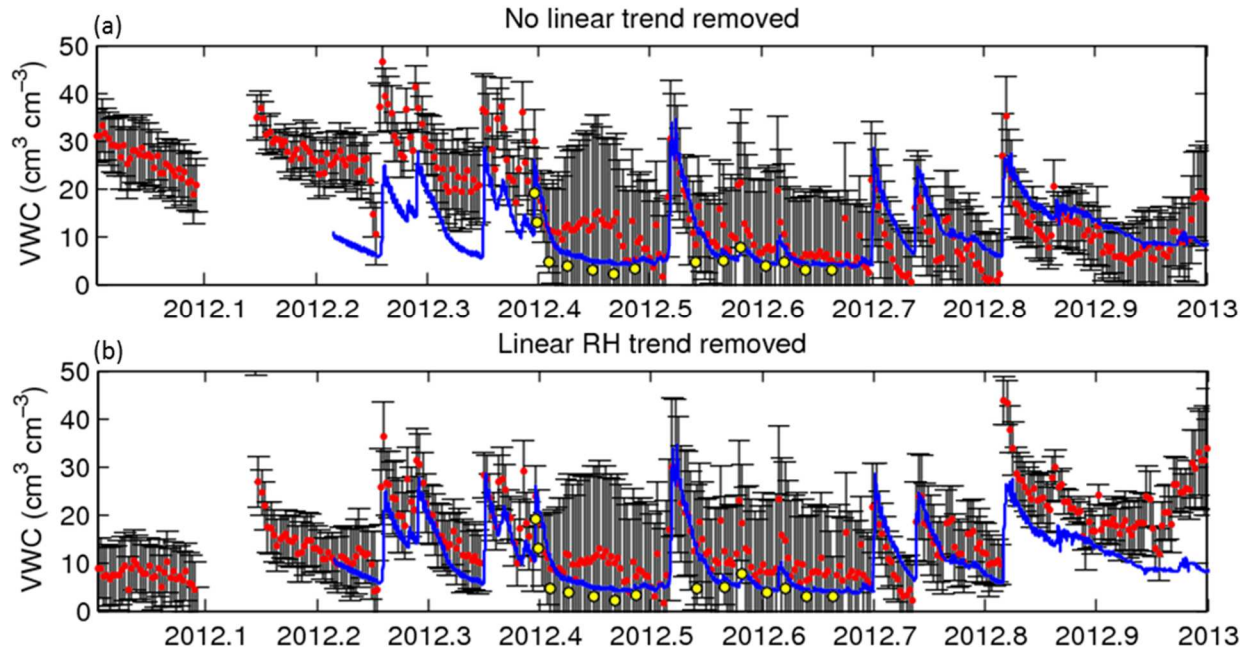


Figure 46: *In situ* probe SMC data (blue line), average SMC data from theta probe surveys (yellow points), and SMC estimated from GPS (red points). Error bars are the standard deviation of estimates from all available satellite tracks. (a) Time series if no linear trend in reflector height is removed. (b) Time series if a linear trend is removed from reflector height time series from each track, and if phase data are transformed using Eq. (38).

Unfortunately, removing a linear trend from other sites is not always so successful. Also, the linear trend, when taking multiple years into account, tends to decrease, so the effect of its removal is also decreased. Removing a seasonal trend would also be unwise, as this could have deleterious effects on the subsequent vegetation filter. Thus, this technique is more of a thought experiment and is not systematically implemented at PBO H<sub>2</sub>O sites. But, should there be notable anomalous reflector height drifts in a time series, one could use Eq. (37) and (38) to mitigate these effects.

### 6.1.2.3 Quick fixes for a priori reflector height changes

It was shown in Figure 15b that the difference between the distance between the ground and the antenna's phase center and  $H_{eff}$  for a bare soil could be anywhere between 4.5 and 7 cm, depending on the soil moisture ( $H_{eff}$  is underestimated). For observed  $H_{eff}$  time series, if the site

was entirely bare and had a median SMC value of  $0.35 \text{ cm}^3 \text{ cm}^{-3}$  or greater, the estimate of the *a priori* height would be 7 cm too low. Similarly, if the site were bare with a median SMC value of  $0.05 \text{ cm}^3 \text{ cm}^{-3}$ , the estimate would be 4.5 cm too low. In these cases, in order to estimate  $H_0$ , one would want to add between 4-7 cm to the median  $H_{eff}$  value, depending on the site's climatology.

However, it should be noted that the presence of persistent vegetation even in winter complicates the assumptions made to calculate the correction needed in the *a priori* height estimation. Figure 47a shows modeled relationships between vegetation height and  $\Delta H_{eff}$ , when underlying soil moisture is  $0.15 \text{ cm}^3 \text{ cm}^{-3}$ . As expected, the relationship is complex and only really correlates strongly with vegetation height for relatively high values of canopy permittivity. Figure 47b shows a close-up view of these relationships, for when canopy height is less than 30 cm. Notice that when the vegetation canopy is shorter than 14 cm, for most canopy permittivities the antenna actually appears taller than it would if there were no vegetation, which is the opposite of what we would expect.

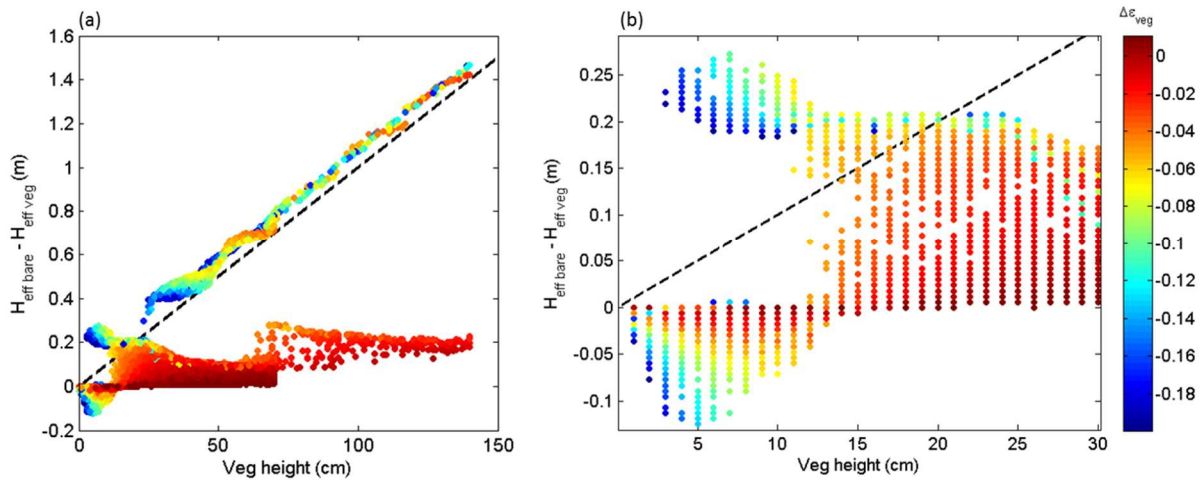


Figure 47: (a) Modeled relationships between canopy height and  $\Delta H_{eff}$ , assuming an overlying soil moisture content of  $0.15 \text{ cm}^3 \text{ cm}^{-3}$ . Points are colored by changes in canopy permittivity from air. (b) Same as (a), but zoomed in.

Residual vegetation could, then, negate the need for the adjustment of the estimated *a priori* reflector height. However, in the absence of detailed site information, it's difficult to determine what the residual vegetation state is. After all, if the minimal vegetation canopy is greater than 14 cm tall, then the adjustment of the *a priori* reflector height would need to be even larger than for just bare soil. Corrections are generalizations and may not work everywhere.

One could apply a correction to all time series, such that the *a priori* reflector height value is 'essentially' the median of the complete  $H_{eff}$  time series. I write 'essentially' because recalculating phase and amplitude for nearly all satellite tracks at every site would be too time-consuming. Most satellite tracks have been assigned  $H_0$  values quite close to the median value, though in some cases, values are a few centimeters off (Figure 48). This is because the *a priori* height is set once, but over time, the median value of the reflector height time series may change. Instead of recalculating phase and amplitude using the raw SNR data and the median value of  $H_0$ , one could use Eq. (37) and (38) as a sort of 'quick fix.' I do not necessarily advocate for this approach, but it can give a first look at what happens when the value of  $H_0$  is changed.

#### **6.1.2.4 Effect of changing the *a priori* reflector height**

The theoretical relationship between phase and soil moisture is based on the assumption that phase is calculated using the true value of  $H_0$ , though observed phase data are calculated using the median value of  $H_{eff}$ , or close to it (Figure 48). Therefore, it would be natural to think that if the 'true value' of  $H_0$  were somehow found, the RMSE between GPS-derived soil moisture and *in situ* data would decrease. Here, I show a few examples to see whether or not this is the case. I compare the RMSE between GPS soil moisture and *in situ* data on a track-by-track basis, first using the phase time series calculated using the current *a priori* reflector height, and

then re-calculating phase after introducing a reflector height bias. Phase is recalculated using Eq. (38).

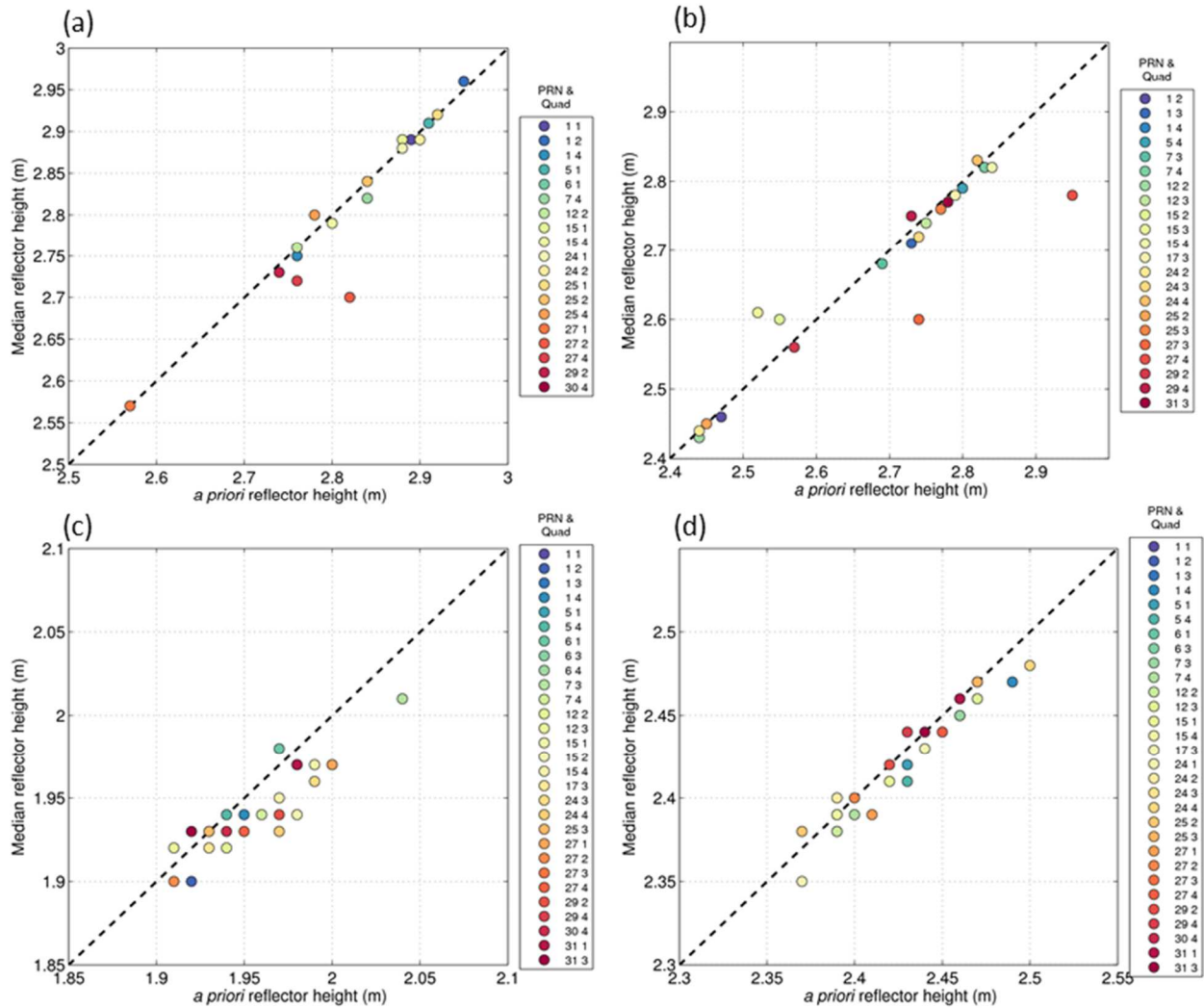


Figure 48: Examples of the set *a priori* reflector height ( $H_0$ ) versus the median reflector height, colored by PRN number and quadrant. (a) OKL3 (b) BCGR (c) p041 (d) grs2.

Results are shown in Figure 49. The left column of Figure 49 indicates that there can be a wide range of RMSE values for each satellite track at a specific site, either exhibiting the failure of the vegetation filter to remove vegetation for these tracks or perhaps indicating that some tracks are just not usable. The right column shows the difference in RMSE that one would get when introducing a bias versus no bias (0 cm). Results from these three sites indicate that

introducing additional biases into the *a priori* reflector height will cause inconsistent increases and decreases in RMSE across satellite tracks. Some satellite tracks are not sensitive to changes in the bias, whereas others show large effects. At this point, it appears that the addition of further reflector height biases will not significantly affect the RMSE of a site as a whole, without introducing track-specific biases for each track.

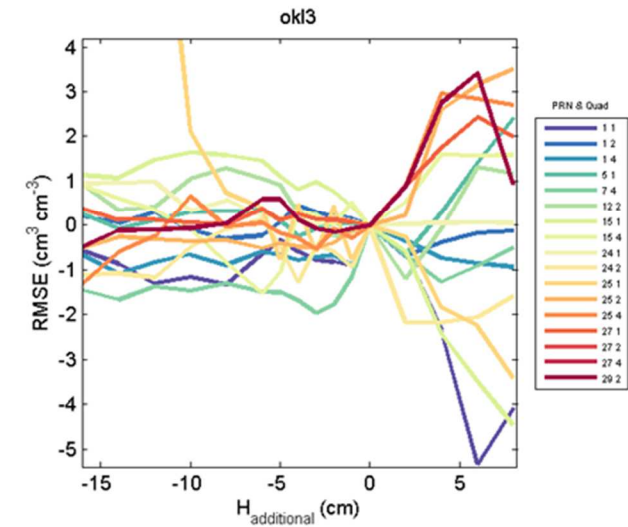
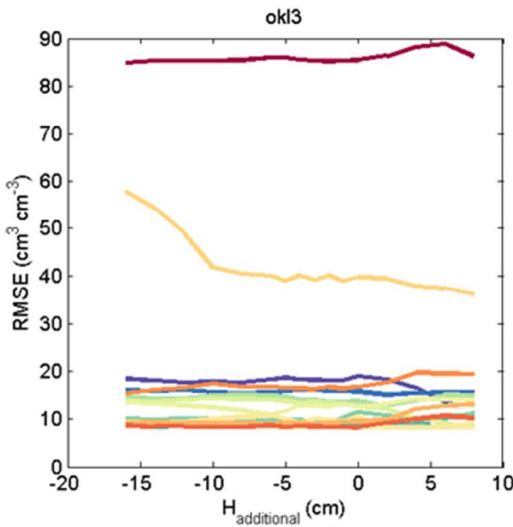
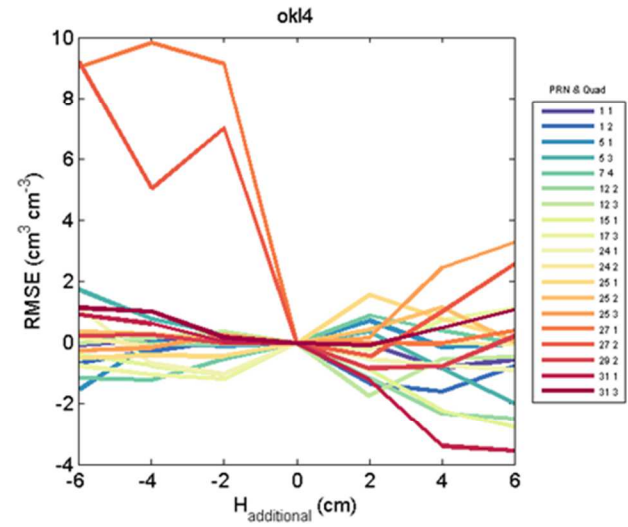
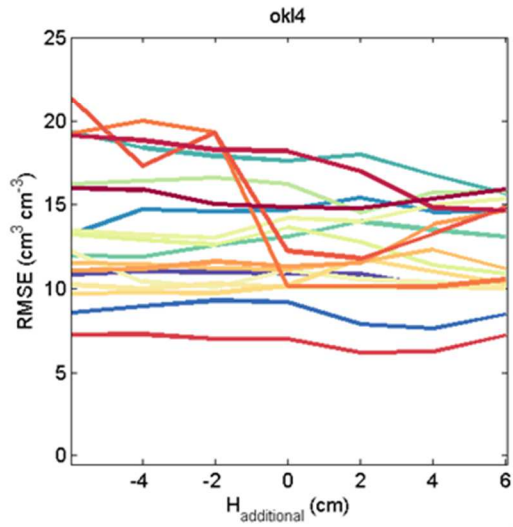
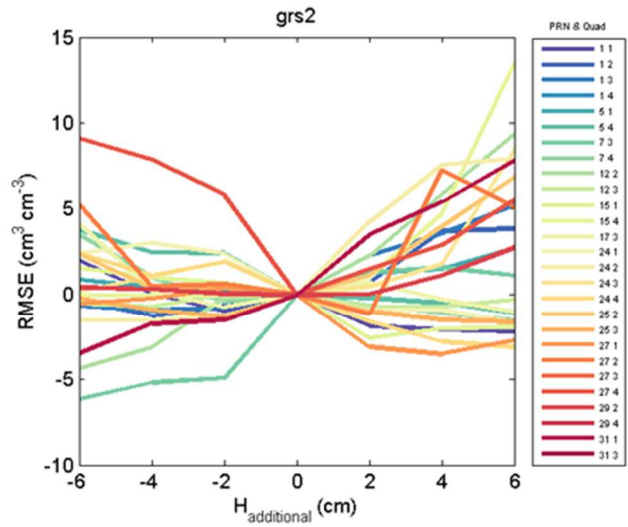
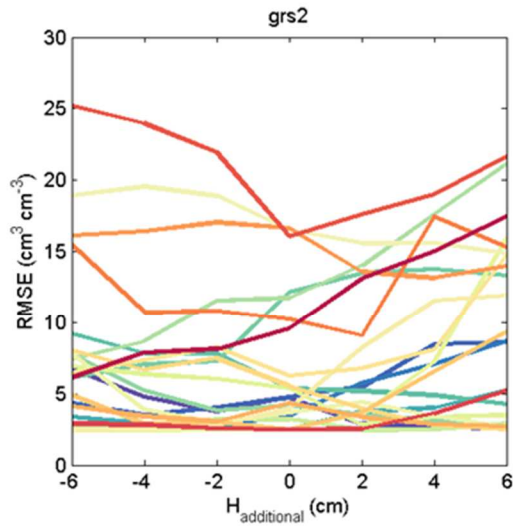


Figure 49: (*left column*) The RMSE between GPS soil moisture for individual satellite tracks and *in situ* probes at three sites, with additional reflector height biases added in. (*right column*) Same data as in the left column, but with the RMSE at 0 cm additional bias subtracted out.

## 6.2 Soil moisture retrieval algorithm

Here is described the algorithm that is currently used to produce the soil moisture estimations for the PBO H<sub>2</sub>O network. The vegetation filter from Chapter 5 is included in the algorithm. Parts of the algorithm are also described more completely in other chapters, though to make the steps of the algorithm coherent, I have chosen to repeat them in this section so that jumping around to other chapters isn't necessary.

### 1. Selection of useful satellite tracks

Not all satellite tracks at a particular site are useful for GPS-IR. Tracks should have consistent reflections between satellite elevation angles of 5-25 or 5-30 degrees; oscillations in the interferogram for higher angles are obscured by the antenna's gain pattern. Tracks should also not be obstructed by trees or buildings or reflect from manmade surfaces like roads. A track should have a relatively stable singular dominant frequency for periods of the year when vegetation water content or height is nearly constant. In general, the power ( $A_{LSP}$ ) of the dominant frequency ( $H_{eff}$ ) should be at least twice as high as the power of the noise or second most powerful frequency in the periodogram.

Examples of SNR data from two useful satellite tracks (red and green) and two tracks with significant noise corruption (blue and orange) are shown in Figure 4c. The noise-corrupted satellite tracks lack any dominant frequency, which could introduce significant errors in subsequent phase and amplitude estimation (Figure 4d). Part of the reason for these two tracks lacking a dominant frequency is due to the fact that the two satellites ground tracks pass over a region of sloped topography (see Figure 50 for a digital elevation model and ground paths of the satellite tracks). Satellite tracks that encompass areas with large topographic changes (on the

order of several meters) within 50 meters of the antenna should be avoided, though there is no standard for determining when topographic changes are too extreme.

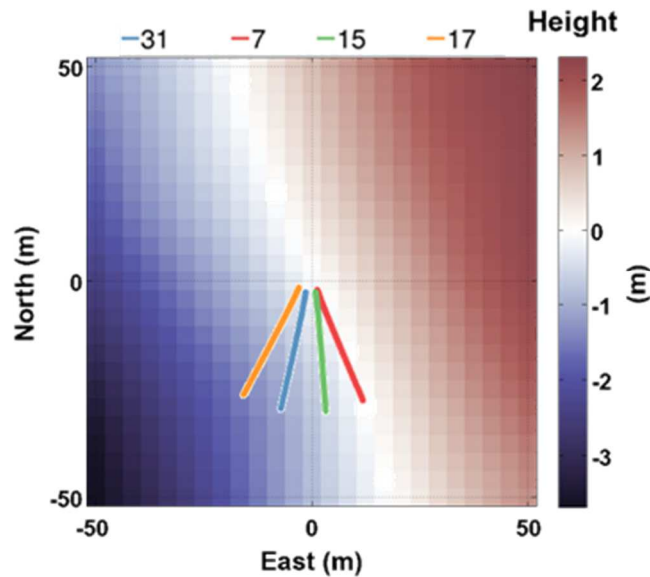


Figure 50: Digital elevation model (DEM) and the approximate specular point paths for four satellite tracks at the GPS station ok13 in Oklahoma. The DEM is referenced with respect to (0,0), which is the location of the antenna. The path traces represent specular reflection points for satellite elevation angles between 5 and 40 degrees. The two western tracks are the “bad” tracks in Figure 4c; the two eastern tracks are the “good” tracks in Figure 4c.

In general, the more useful satellite tracks at a site, the more reliable the final soil moisture time series tend to be. PBO H<sub>2</sub>O requires at least five useful satellite tracks at each site. Figure 51a shows a histogram of the number of tracks used at all PBO H<sub>2</sub>O stations in the fall of 2014. Figure 51b shows, for one example station, how the number of useful tracks has increased over the years as more satellites have been launched. Temporary decreases in the number of tracks occur due to abnormal noise that might be present in one or more interferograms. There are many possible sources of this noise, but a common culprit is a satellite rising during or immediately after a rainstorm, or when there is significant dew present on vegetation.

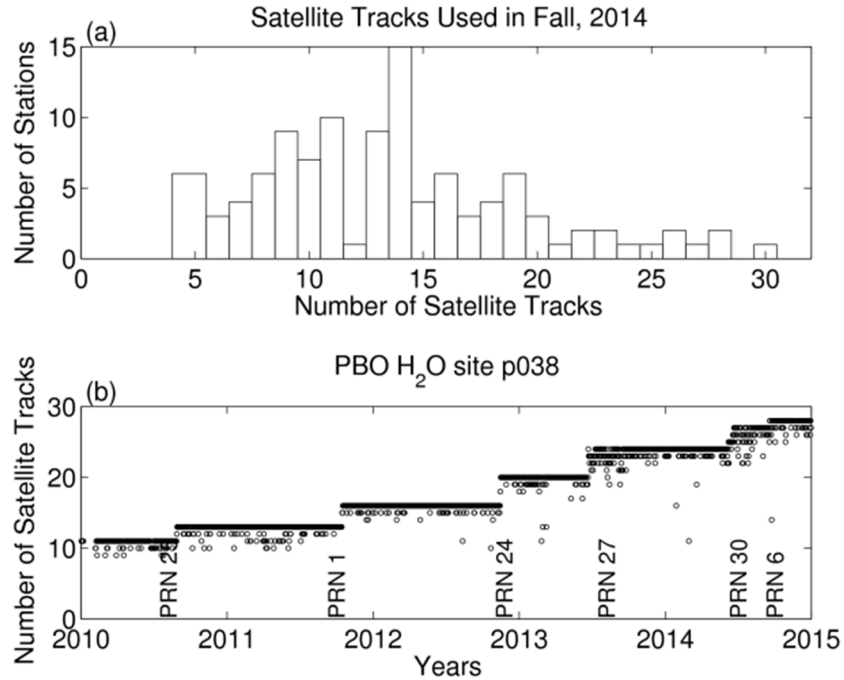


Figure 51: (a) Histogram of the number of satellite tracks used at PBO H<sub>2</sub>O stations during the fall of 2014. (b) Time series of the number of tracks used at site p038. Step increases occur when additional satellites were launched.

2. Estimation of each track's a priori reflector height,  $H_0$

Due to microtopography surrounding the antenna, the a priori reflector height ( $H_0$ ) is not known perfectly and has to be estimated from the SNR data. PBO H<sub>2</sub>O uses the median of  $H_{eff}$  data that are free of snow events and significant vegetation for the value of  $H_0$  for each satellite track.

3. Calculate SNR metrics:  $\phi$ ,  $A$ ,  $H_{eff}$ , and  $ALSP$

SNR metrics for each day and each satellite track are calculated using the procedure described in section 2.6.1 and 2.6.2.

4. Quantify vegetation effects

As described in section 5.1, if a satellite track's  $A_{norm}$  time series stays below 0.78 for an extended period of time is likely to be affected by something other than soil moisture variations

(i.e. vegetation changes). A track whose time series remains above 0.78 may have small vegetation effects, though for these cases it is difficult to determine whether decreases in  $A_{norm}$  are from vegetation or from soil moisture changes. In these cases, one may skip to Step 6 in the algorithm below and not use the vegetation filter.

If the GPS site does have a significant vegetation effect as determined by the  $A_{norm}$  time series, then one should proceed to the section “Algorithm for removing vegetation effects” before estimating soil moisture in Step 6. If there is a significant vegetation effect but the effect is of a short-enough duration, then the phase data when  $A_{norm}$  is below 0.78 may be removed, without using the vegetation filter. However, simply removing the phase data without implementing a vegetation correction will result in error for periods surrounding the affected interval, which are still affected by vegetation growth. It is up to the user whether or not greater error is acceptable for the tradeoff in simplicity of data analysis.

#### 6. *Soil moisture estimation*

At GPS sites with limited seasonal change in vegetation, as indicated by the  $A_{norm}$  time series, soil moisture estimation is relatively straightforward. We use data from the site mflc as an example.

##### 6a. *Zero the phase time series*

For each year of data, the phase time series for each satellite track is zeroed, such that the lowest values are near zero. Sites in the PBO H<sub>2</sub>O network are zeroed by first calculating the mean of the lowest 15% of observed phase data for each year and each track. The mean is then subtracted from the phase time series. 15% is a parameter that may be decreased or increased, depending on the amount of noise present in the data.

Phase time series are zeroed yearly; this assumes that soil moisture at the site reaches its residual value at some point during the year. This assumption is generally valid, at least for the PBO H<sub>2</sub>O sites. Yearly zeroing is done so that any period of anomalously low phase data (due to non-removal of vegetation effects or random noise) will not affect the entire time series.

6b. *Determine the residual soil moisture content*

Because temporal phase changes are relative and the minimum moisture content of a soil is never zero, the baseline phase value needs to be associated with the soil's residual moisture content. Residual moisture content,  $SMC_{resid}$ , is correlated with soil texture, and this data can be found in publicly-available data sets such as the U.S. Geological Survey's STATSGO data set [63]. However, optimally the residual moisture content of the soil at the site would be measured through the use of gravimetry or time domain reflectometry probes.

6c. *Estimate the soil moisture time series for each satellite track*

Modeled relationships between phase and soil moisture are used to compute the estimated soil moisture time series.

$$SMC_t = S\Delta\phi_t + SMC_{resid} \quad (40)$$

Where  $S$  is the expected slope between phase and soil moisture. For time series with no significant vegetation affect,  $S = 1.48 \text{ cm}^3 \text{ cm}^{-3} \text{ deg}^{-1}$ .

7. *Estimate the soil moisture time series for the GPS site as a whole*

To estimate site-averaged soil moisture on the daily timescale, the median soil moisture value of all tracks for each day is used. Uncertainties are computed as the standard deviation of

the soil moisture estimates from all satellite tracks. For sites with a large number of satellite tracks, the mean soil moisture value of all tracks could be used.

Figure 52 shows *in situ* soil moisture data from Campbell Scientific 616 probes that have been buried at 2.5 cm depth within 250 m of the desert steppe site (mfle). Also shown are soil moisture estimates using GPS-IR, using data from the GPS antenna. There is a good agreement between *in situ* measurements and GPS soil moisture estimations at this site, without a need for a vegetation filtering algorithm, as expected given the  $A_{norm}$  time series.

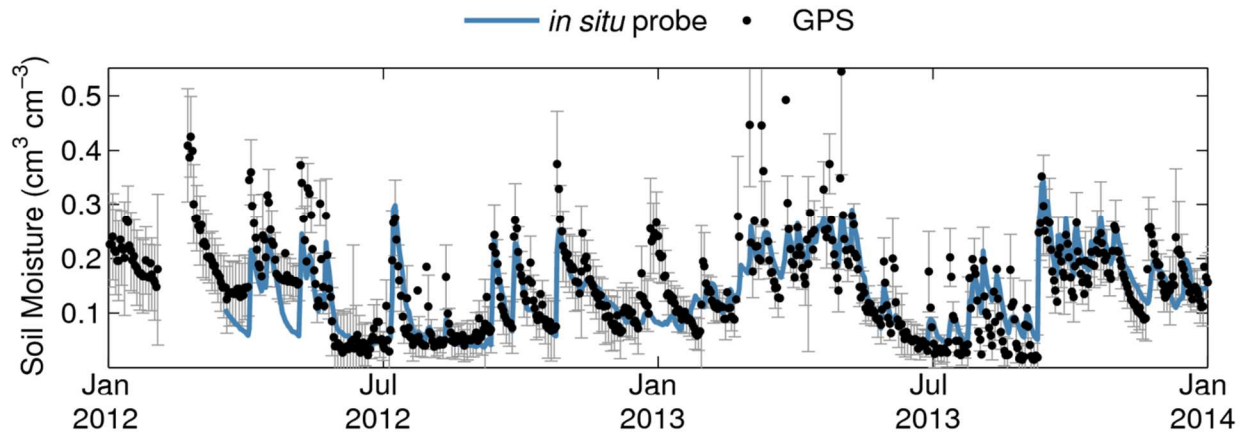


Figure 52: Soil moisture estimates from the desert steppe site (mfle) near Boulder, Colorado. The blue line is average data from five *in situ* sensors installed at 2.5 cm depth within 250 m of the antenna. Black points are the median soil moisture estimates resulting from SNR data from useful satellite tracks. Grey error bars represent the standard deviation of the estimates.

### Algorithm for removing vegetation effects

In this section, we describe how to correct the phase time series to remove the effects from variations in vegetation state around a GPS site. The vegetation adjustment algorithm corresponds to the box “5. Remove vegetation effects” in Figure 53.

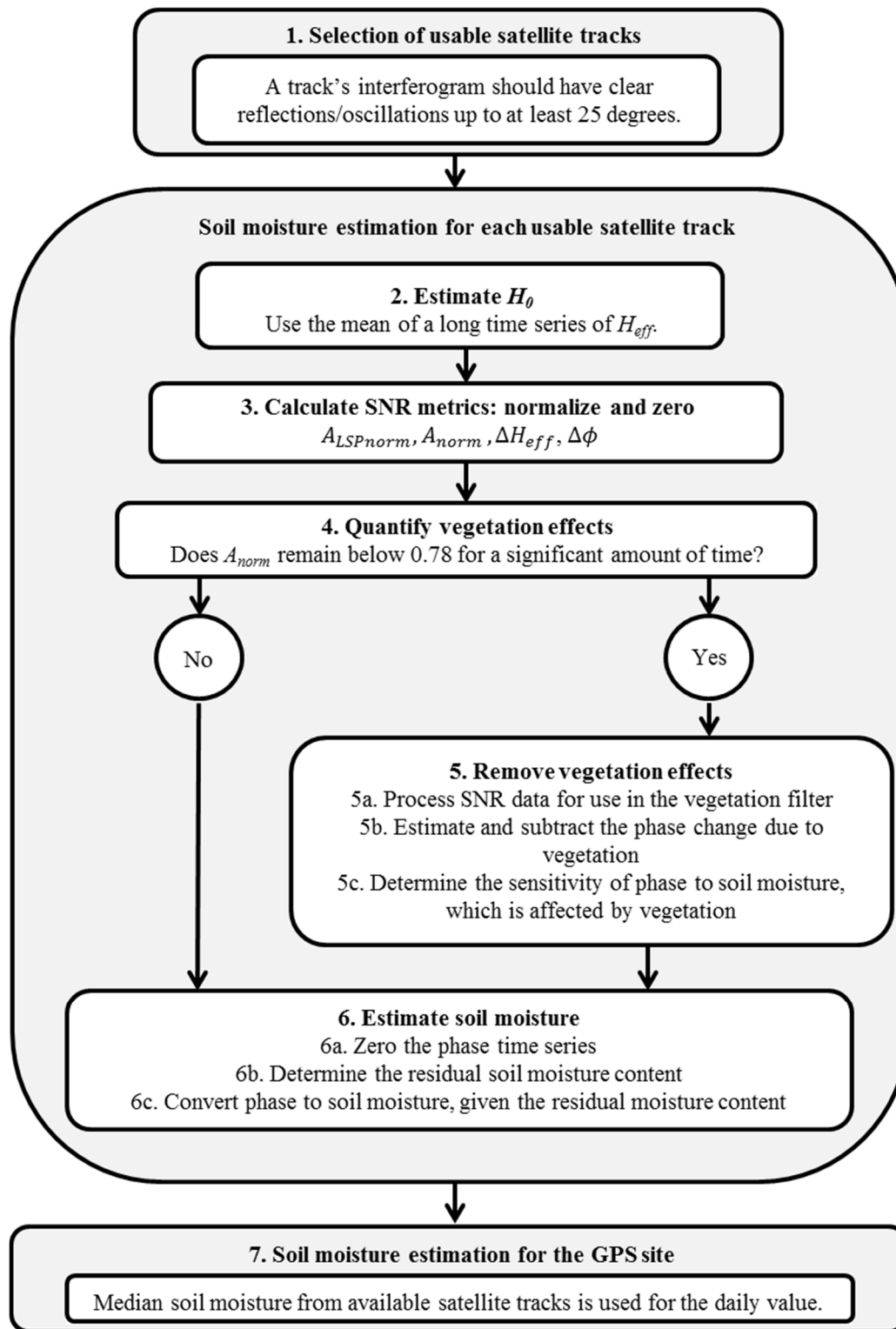


Figure 53: Flowchart depicting steps in the algorithm to estimate soil moisture for a GPS site.

We use data from the Oklahoma GPS site to demonstrate the importance of adjusting phase time series for vegetation. Fig. 6 (bottom) shows that the Oklahoma GPS station, ok13, is surrounded by vegetation that varies in water content and height, both seasonally and from year-to-year. Figure 54a shows how following the simple soil moisture estimation procedure described above would lead to poor agreement with *in situ* data. Because an increase in vegetation causes a decrease in phase, and the residual moisture content is set to the lowest observed phase value, vegetation growth causes the resulting soil moisture estimations to be over-estimated in winter. Clearly, an adjustment for vegetation is needed at this site. This could be determined solely from the  $A_{norm}$  time series, which shows values as low as 0.5 during the growing season.

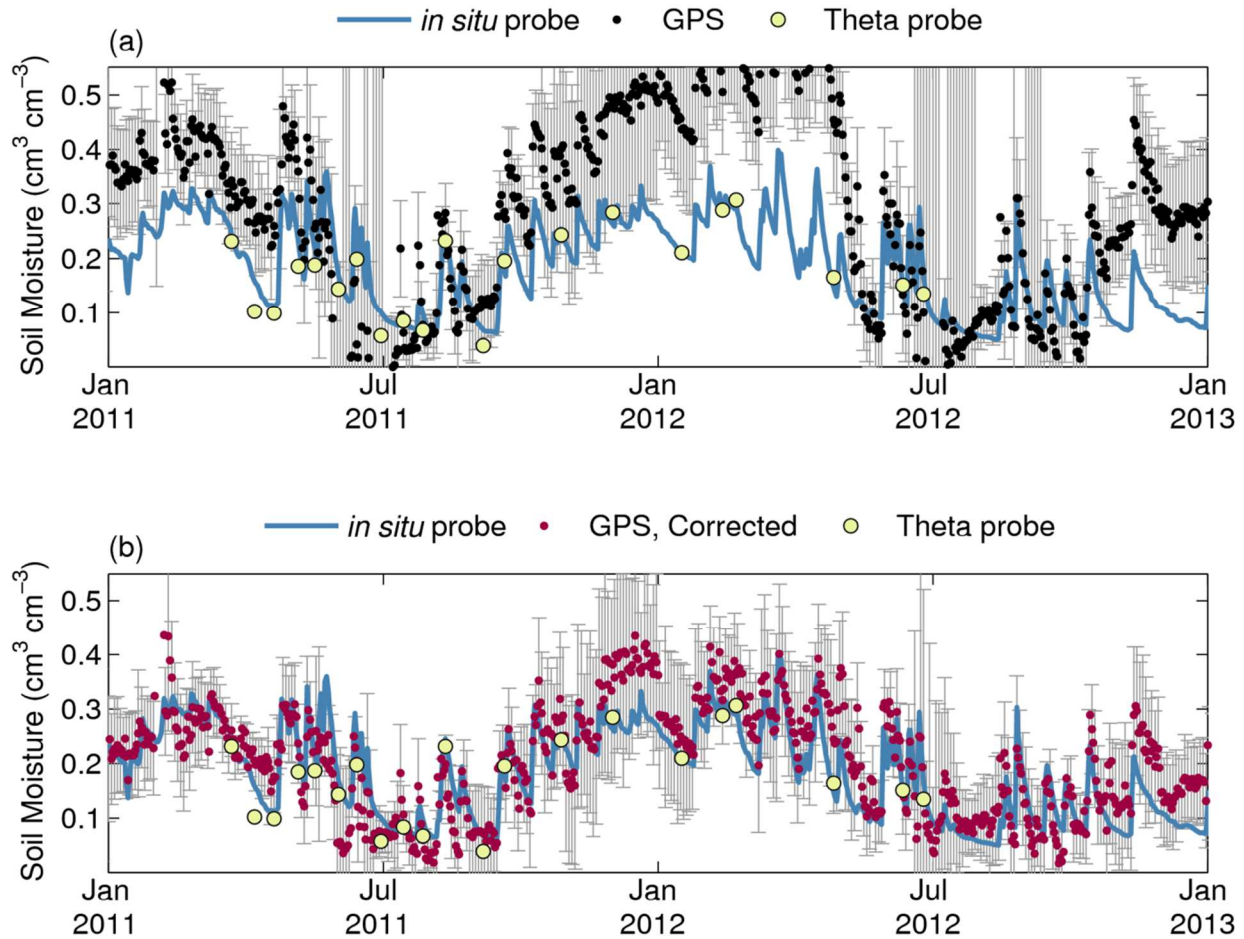


Figure 54: Blue lines are average soil moisture estimates from *in situ* probes installed at 2.5 cm depth within 50 feet of the GPS antenna ok13 in Oklahoma. Yellow points are the mean soil moisture estimates resulting from theta probe surveys. (a) Black points and grey error bars are the median and standard deviation of soil moisture estimates using GPS-IR, if no vegetation corrections are made. (b) Magenta points and grey error bars are the median and standard deviation of soil moisture estimates using GPS-IR, if the vegetation filtering algorithm is used to correct the phase data for vegetation effects.

At sites affected by vegetation, one can use the following vegetation filtering algorithm to mitigate the effect of vegetation. The filter is the one described in Chapter 5. Over 16,000 modeled SNR interferograms and associated metrics were simulated using random combinations of vegetation parameters (water content, biomass, and canopy height) and an underlying soil moisture content of  $0.15 \text{ cm}^3 \text{ cm}^{-3}$  as input to the soil-vegetation model. Changes in SNR metrics with respect to their bare soil values were calculated and saved in a database. The database can

be queried to estimate the change in phase corresponding to any observed combination of  $A_{norm}$ ,  $A_{LSPnorm}$ , and  $\Delta H_{eff}$  time series. The same random combinations of vegetation parameters were then used with underlying soil moisture contents of both  $0.05 \text{ cm}^3 \text{ cm}^{-3}$  and  $0.45 \text{ cm}^3 \text{ cm}^{-3}$  and the soil-vegetation model was run again. Another database was created from these simulations, which shows how SNR metrics are expected to respond to changes in underlying soil moisture given a particular vegetation state.

Now we describe how to use the model database to remove vegetation effects from observed SNR phase data. This is done on a track-by-track basis, as the input data (SNR metrics) are all track specific.

#### *5a. Process data for use in the vegetation filter*

The vegetation filter assumes that the phase time series has been zeroed such that data most affected by vegetation go below zero. In order to conform to this convention, the phase time series should be zeroed with respect to the median of the highest values in the time series. We have found the median of the highest 15% of observed phase data works well.

Use a low-pass filter to remove high frequency noise associated with soil moisture fluctuations from the  $A_{norm}$ ,  $A_{LSPnorm}$ , and  $\Delta H_{eff}$  time series. The ends of the  $A_{norm}$ ,  $A_{LSPnorm}$ , and  $\Delta H_{eff}$  time series are first padded to decrease edge effects. Thirty repetitions of the mean of the first and last 15 days of  $A_{norm}$ ,  $A_{LSPnorm}$ , and  $\Delta H_{eff}$  values are appended to the beginning and end of each time series.

$A_{norm}$ ,  $A_{LSPnorm}$ , and  $\Delta H_{eff}$  are smoothed using a Savitzky-Golay filter, a least-squares smoothing method. The S-G filter tends to be more successful than a moving

average or moving median filter, since with the right parameters it does not introduce time lags into smoothed time series and will not smooth out the maximum or minimum extents of the time series. Most of the time, a moving average filter is sufficient, though one must be careful to not over-smooth time series that may have significant, though short-lived, vegetation effects.

*5b. Estimate and subtract the phase change from vegetation from the observed time series*

A linear nearest neighbor search algorithm is used to find the estimated phase caused by vegetation fluctuations, given observed  $A_{norm}$ ,  $A_{LSPnorm}$ , and  $\Delta H_{eff}$  and the modeled database described in Chapter 5. Thus, one can estimate the effects of vegetation on phase using time series of the other three SNR metrics. No field observations of vegetation amount are needed. Estimated phase changes from the database are smoothed through time using the same Savitzky-Golay filter, and the padded ends are removed.

The expected phase changes due to vegetation are subtracted from the observed, unsmoothed phase time series, resulting in phase time series that indicate soil moisture variations only.

$$\phi_{SMC,t} = \Delta\phi_t - \phi_{veg,t} \quad (41)$$

Where  $\phi_{SMC,t}$  is the expected phase change due to soil moisture at time  $t$ ,  $\Delta\phi_t$  is the original observed time series at time  $t$ , and  $\phi_{veg}$  is the predicted phase change due to vegetation at time  $t$ . This relationship is a simplification, as it is based on the assumption that the total phase change is a linear combination of the phase change due to soil moisture and the phase change due to vegetation.

*5c. Determine the sensitivity change between phase and soil moisture due to vegetation*

Expected sensitivity changes between phase and soil moisture are estimated, using the same procedure and linear search algorithm described above. The sensitivity of phase to soil moisture will change depending on the extent of overlying vegetation, and thus the slope of the relationship between phase and soil moisture,  $S$ , will change throughout the year. Equation 40 used in Step 6 thus does not have a constant value of  $S$  for data processed with the vegetation filter, but rather a value that varies depending upon the vegetation state.

Once the phase data are processed with the vegetation filter, one can calculate a soil moisture time series for each track (Step 6, Figure 53). Residual moisture content is selected in the same way as for a bare soil case (Step 6b). When converting phase to soil moisture,  $S$  is a function of time, as described in Step 5c. The soil moisture time series for a phase time series filtered for vegetation will thus be a variant of Eq. (40):

$$SMC_t = S_t \Delta \phi_{SMC,t} + SMC_{resid} \quad (42)$$

As described above, the median of the track soil moisture time series is taken to be representative of the soil moisture of the site as a whole. There are additional uncertainties due to assumptions made in the vegetation filtering algorithm, which are not yet incorporated into final soil moisture estimates.

The vegetation-corrected soil moisture time series for the GPS station in Oklahoma is shown in Figure 54b, using the median soil moisture value for all tracks. Agreement between the GPS-derived soil moisture estimations and those from *in situ* data has been much improved over the non-vegetation-filtered estimations (Figure 54a). In particular, the large wintertime deviations described in the previous section have been significantly reduced.

### 6.3 Validation of soil moisture retrievals

This section describes the validation results from using the soil moisture retrieval algorithm described in 6.2 with observed data. Before results are presented, however, it is important to note that the choice of *in situ* data against which to compare GPS soil moisture time series is not a trivial one. All of the GPS soil moisture estimations presented here are either compared against the average from Theta probe surveys, or against Campbell Scientific 616 probe data. It is easy to assume that these *in situ* data represent the ‘true’ value of soil moisture. However, differences in spatial sensitivities of the probes versus GPS estimates (see Chapter 2.2) will lead to inherent differences in the data.

In addition, the probes themselves will not yield data that are perfectly comparable to even other probe data. Figure 55a shows a soil pit dug as part of the SMAP *in situ* test bed experiment in Oklahoma. Several different types of soil moisture probes were buried at the same depths and close to one another, to allow for the comparison of soil moisture time series. Figure 55b shows time series from three different types of probes from one of these pits; each probe was buried at 5 cm depth. There are clear differences between the probes, and the RMS error between each kind of probe is on the order of  $0.03 \text{ cm}^3 \text{ cm}^{-3}$ . One might question the practicality of producing GPS soil moisture time series, or satellite soil moisture estimations, with an RMS error below  $0.04 \text{ cm}^3 \text{ cm}^{-3}$  when the probes themselves show such disagreement. Even so, since we conducted several soil moisture surveys with a theta probe, I will present validation results plotted against data from the theta probe.

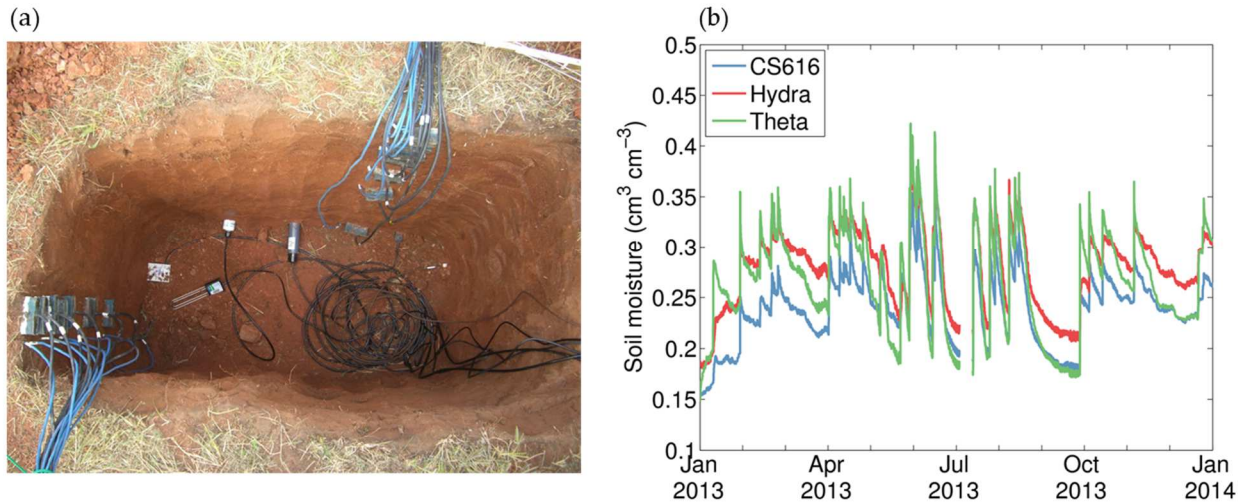


Figure 55: (a) A 1 m deep pit in Oklahoma with several types of soil moisture probes. (b) Probe data from three different brands of probes buried at the same depth, next to one another.

Figure 56a is a scatterplot of soil moisture estimated using GPS-IR and the algorithm presented in 6.2 and *in situ* data from theta probe surveys. No bias has been removed from the data. Not all sites with theta probe surveys are shown; these are just a subset of the data.

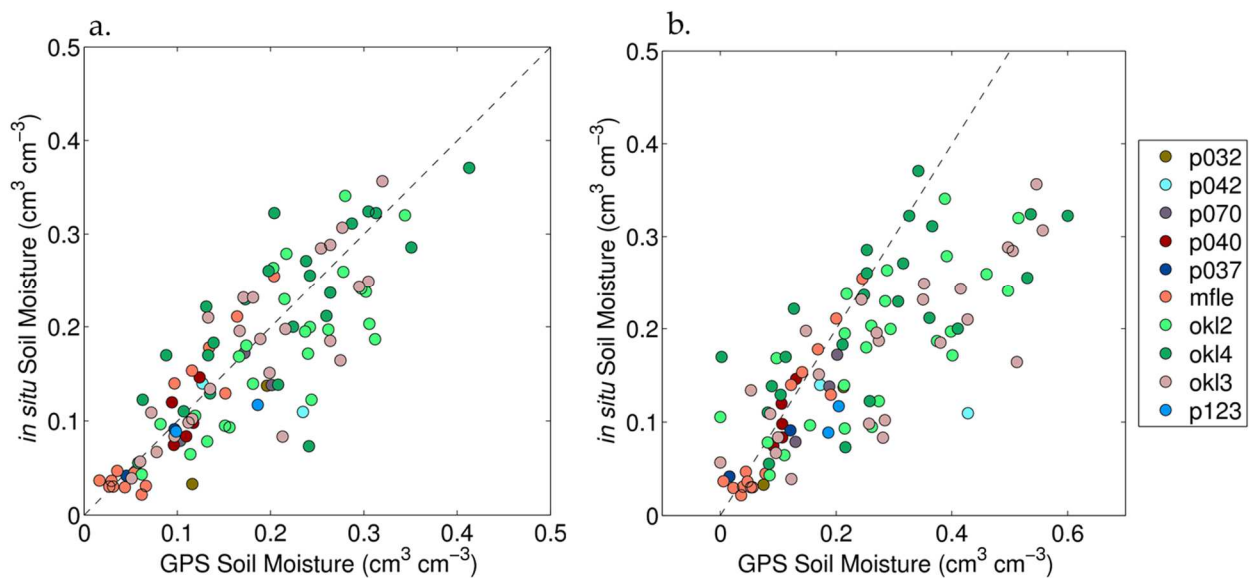


Figure 56: GPS soil moisture estimates versus *in situ* soil moisture data taken with a theta probe. GPS soil moisture values represent the mean of the soil moisture estimates from available useful tracks. Theta probe estimates are the mean of at least 25 points measurements taken within 50 m

of the GPS antenna during each survey. (a) Estimates using the vegetation filter. (b) Estimates without using the vegetation filter.

There is good correspondence between the two methods of soil moisture estimation; the RMS error is  $0.053 \text{ cm}^3 \text{ cm}^{-3}$ . This is a bit higher than the  $0.04 \text{ cm}^3 \text{ cm}^{-3}$  required by the SMAP mission, though some of these estimations were produced during times when vegetation extent was relatively high ( $>1 \text{ kg m}^{-2}$ ). For comparison, the GPS-IR soil moisture estimates without using the vegetation filter are shown in Figure 56b (note the scale difference of the x-axis). The RMS error for these estimates is  $0.12 \text{ cm}^3 \text{ cm}^{-3}$ . Thus, the addition of the vegetation has decreased the RMS error by almost  $0.07 \text{ cm}^3 \text{ cm}^{-3}$ .

One improvement that has not yet been made to the data is taking into account the fact that the residual moisture content has been set for each satellite track. Therefore, the lowest of the mean moisture content of the tracks is going to always be somewhat higher than the residual. This could lower the RMS error for some sites like p032, for example. I also believe that if I were actually to develop an outlier detection algorithm beyond the bare bones one currently in place, the RMS error could decrease further.

#### **6.4 Effect of changing model parameters**

The soil moisture algorithm outlined in 6.2 has several parameters that are important in the final soil moisture estimations. Here, I describe the parameters in more detail and the potential effects of changing some of the key parameters.

Table 7 contains a summary of the parameters that are used in the algorithm. Some of these parameters, though not all, were mentioned in 6.2. Many of the parameters, such as the parameters relating to amplitude normalization or phase zeroing, only need to be set ‘reasonably,’ i.e. a small change in the parameter will not visibly affect soil moisture time series.

Other parameters, such as the *a priori* reflector height offset (for some sites) and choice of smoothing method and associated parameters, are extremely important for the algorithm to work.

I will now show the effects of changing these parameters.

Table 7: Description of parameters used in the soil moisture algorithm.

<b>Parameter Description</b>	<b>Abbreviation</b>	<b>Range of values</b>	<b>Default value</b>
$H_0$ offset*	hbias	0-9 cm	0 cm
Outlier removal	remoutli	0 (no) or 1 (yes)	1
Correct for $H_{eff}$ anomalies	Acc_rhdrift	0 (no) or 1 (yes)	0
Amplitude veg flag	Smm	0-1	0.8
Use all tracks, or the list of good ones	Which_sats	0 (all) or 1 (good tracks)	1**
Fraction of $\phi$ to zero to	zphival	0.05-0.25	0.15
Method to fill in NaN values	nanopt	0-5	5
# of days to calculate amplitude variance for outliers	Ampvarday	3-7	3
Amplitude variance limit (V/V) for outliers	ampvarlimit	0-3	1
Remove phase outliers	remoutliP	0 (no) or 1 (yes)	1
Zero the entire phase time series (or yearly)	zallts	0 (yearly) or 1 (full time series)	0
2 <sup>nd</sup> $\phi$ zeroing parameter	zphivalP	0.05-0.25	0.15
For veg filter, zeroing w.r.t. max $\phi$ values	Mzphival	0.05-0.25	0.15
Smoothing method	Sm_method	1 (Savitzky-Golay) or 2	1

(moving average)			
# of days to smooth, if using moving average	smnum	33-365	181
Savitzky-Golay day length	sgolnum	33-163	99
Savitzky-Golay polynomial	sgolply	2-5	2
# of days for padding	padlen	0-1000	200
# of days to average before padding	men	0-50	20
Method for combining track SMC estimates	Combine_method	'mean', 'median', 'weighted'	'mean'

\*Only able to be used in the test code, not with the metrics obtained from the results directory

\*\*Oklahoma sites:

#### 6.4.1 Sensitivity to changing the *a priori* reflector height

Some sites, the soybean field 'ames' in particular, are significantly affected by the choice of  $H_0$ . Figure 57a,b both show phase time series from two different satellite tracks at ames. The phase values were calculated using the median value of  $H_{eff}$  for  $H_0$ . The black lines indicate the predicted phase change due to vegetation, using the vegetation filter. There is a problem here—the predicted phase change due to vegetation is too small, and subsequent soil moisture estimations still show a large vegetation signal.

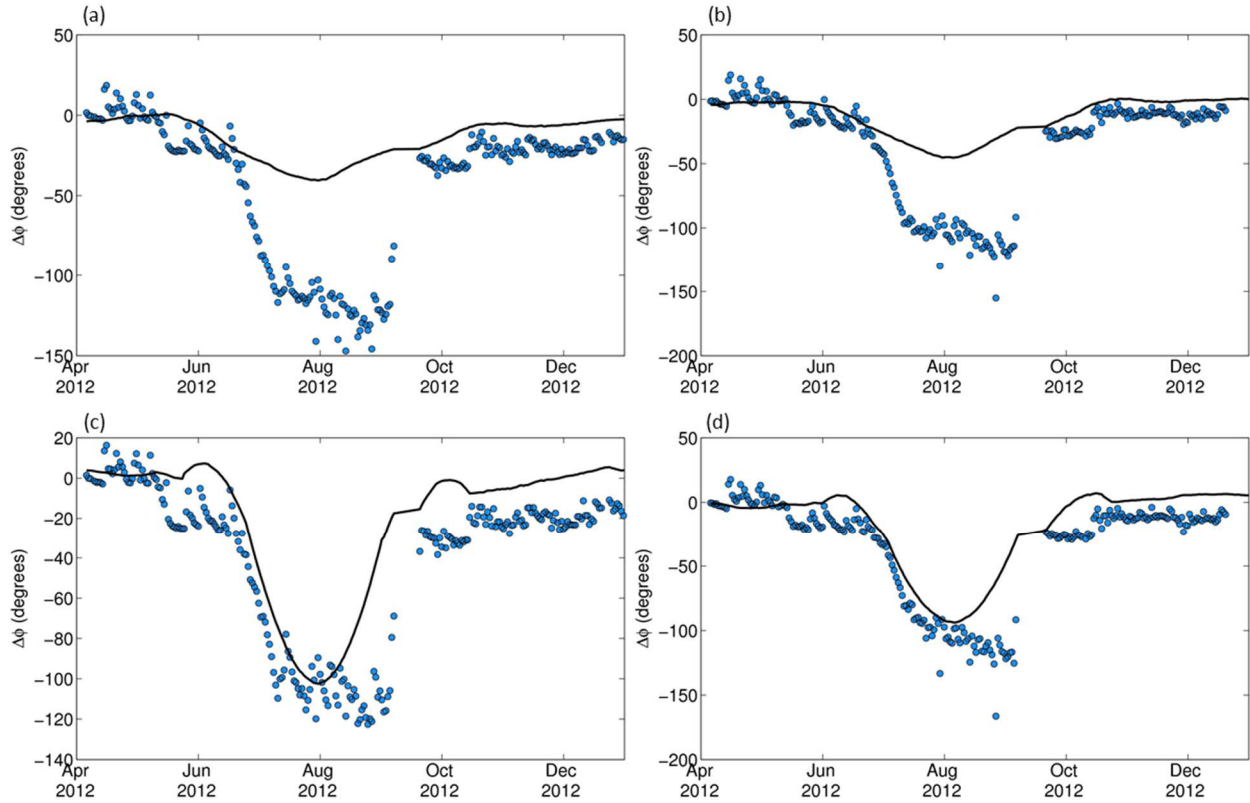


Figure 57: (a) Phase data from PRN 1 Quadrant 1 at GPS sites ames (blue dots). Black line is the predicted phase change due to vegetation. (b) Same as (a), except for PRN 17 Quadrant 3. (c) Same as (a), except metrics were calculated using an *a priori* height that was 9 cm taller than those calculated in (a). (d) Same as (b), except metrics were calculated using an *a priori* height that was 9 cm taller than those calculated in (b).

If, however, metrics are recalculated for both tracks using a value for  $H_0$  that is 9 cm taller than  $H_{eff}$ , the vegetation filter does a better job at predicting the phase change due to vegetation (Figure 57c,d). Obviously, there are still some problems at the end of the growth season in September, but I attribute at least part of this problem to the multi-week data gap post-harvest and smoothing problems surrounding the gap.

The solution to this problem is not to just recalculate SNR metrics for all satellite tracks at this site and others, using a value of  $H_0$  that is 9 cm taller than its current value. Unfortunately, some tracks are hardly at all affected by such a change, and others are negatively affected,

meaning that adding 9 cm to  $H_0$  actually causes an over-prediction of phase change due to vegetation.

#### **6.4.2 Sensitivity to changes in the smoothing method**

This section might be unnecessary if a better alternative for the linear nearest-neighbor search could be found. Predicted phase changes due to vegetation can be noisy, due to the search algorithm, the number of simulations used in the search algorithm, and mismatches between simulations and observations. Because of this noise, it is necessary to smooth the phase change predictions before removing them from the observed phase time series. And, because of the noise, the changing the smoothing method or the method's parameters can change the phase predictions significantly. Although I will only describe the differences between moving average and Savitzky-Golay filters, I have also tried other filtering techniques (Fourier filters and wavelets, for example) and have found similar results to the ones described below.

An example of the different phase predictions for different smoothing methods is shown in Figure 58. In this figure, the different panels represent either predictions made with the Savitzky-Golay filter (Figure 58a,c) or the moving average filter (Figure 58b,d). The filters span either 15 days (Figure 58a,b) or 63 days (Figure 58c,d). It is apparent that the 15-day filters are characterized by too much high frequency noise. The 63-day filters are less influenced by noise, though the moving average filter is starting to be over-smoothed, whereas the Savitzky-Golay filter better preserves the timing and magnitude of phase change due to increases in vegetation.

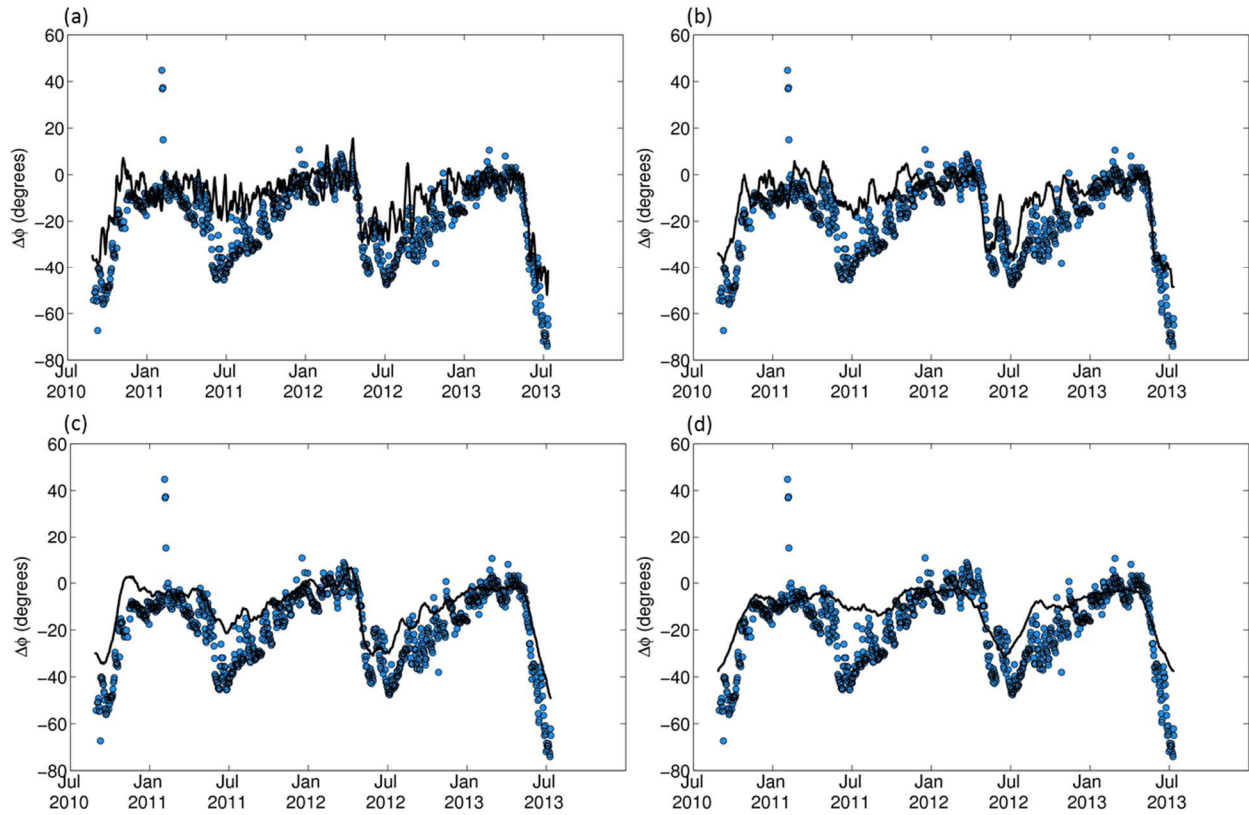


Figure 58: All data in this figure are from PRN 25 Quadrant 2 at GPS station okl3. Blue dots in each panel are the raw phase observations—data end in July 2013 due to power issues at the site. Black lines are the predicted phase changes due to vegetation using different smoothing methods: (a) Savitzky-Golay filter, 15 day span (b) moving average filter, 15 day span (c) Savitzky-Golay filter, 63 day span (d) moving average filter, 63 day span.

## Chapter 7: Error Quantification

This chapter focuses on potential sources of error in soil moisture estimates. The errors mentioned here are only errors that can be quantified using the electrodynamic model. Errors due to issues like noise in SNR observations, the DoD changing the orbit of a satellite, etc. are not included.

### 7.1 Errors for bare soil

#### 7.1.1 Imperfect knowledge of *a priori* reflector height

The electrodynamic model assumes that the distance from the ground to the phase center of the antenna, is known perfectly. This is what is deemed the *a priori* reflector height. However, even for a bare, flat soil in model simulations, the calculated reflector heights never match the input  $H_0$ . Model simulations instead show that, if one were to estimate antenna height using calculated reflector height, one would underestimate the height of the antenna by 3-7 cm, depending on the soil moisture. This is due to the fact that the permittivity of the ground is not high enough to act as a perfect reflector. Changes in microtopography surrounding a real antenna will add additional uncertainty to this estimate.

The errors introduced from this uncertainty are illustrated in the following example. The model was run for a bare soil, using a set of soil moisture observations as input. Phase is then calculated using three different *a priori* reflector heights: the 'known' antenna height, a height that is 3 cm shorter than the known height, and a height that is 7 cm shorter than the known height. Phase is then converted into its corresponding soil moisture time series, using the equation derived from the bare soil model, which assumes  $H_0$  is known perfectly. The resulting

soil moisture time series along with the synthetic soil moisture input data (*in situ*) are shown in Figure 59.

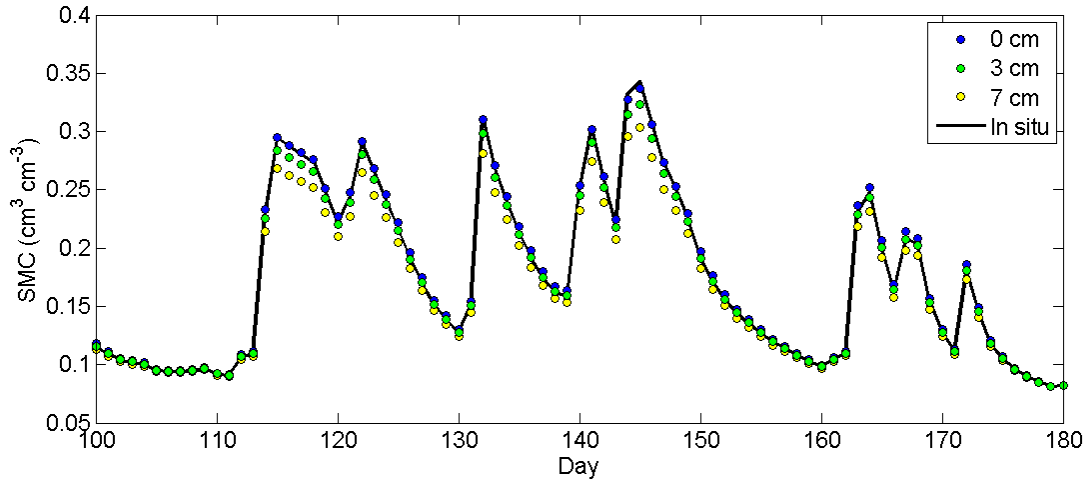


Figure 59: Synthetic soil moisture observations (*in situ*) and corresponding soil moisture estimates, assuming different under-estimations of the *a priori* reflector height (colored points).

We see that, as antenna height is underestimated, there is an underestimation of soil moisture, particularly for high soil moisture. Although the RMS error for the 7 cm case is only  $0.013 \text{ cm}^3 \text{ cm}^{-3}$ , when the target RMS error is below 0.04, errors in antenna height estimation (for a bare, flat soil with no other sources of errors) will account for 25% of the target RMS error, which is certainly not insignificant. Conversely, if one were to over-estimate antenna height, soil moisture would thus be overestimated as well.

In theory, if one had a long enough ‘perfect’ reflector height time series (i.e. perfectly flat, satellite tracks not moving spatially, no noise in estimations, no vegetation, etc.) one could probably estimate the correct *a priori* height perfectly by adding  $\sim 3\text{-}5$  cm (depending on the soil’s residual SMC value) to the highest reflector height observation.

### 7.1.2 Vertical gradients in SMC profiles

The current retrieval algorithm assumes that soil moisture profiles do not vary with depth, though in reality gradients will occur—immediately after a rainstorm the surface will be wetter than at depth and otherwise the surface will nearly always be drier. This was briefly mentioned in Section 4.3.3.5.

Shows results from model simulations generated from 1500 soil moisture profiles for a loam soil with an *a priori* height of 2.4 m. Soil moisture was specified at 2.5, 7.5, and 20 cm depth, which were random values between 0.05 and 0.40. The model interpolates between depths to get the full soil moisture profile, the number of layers being 1001, which means each interpolated layer was 0.2 mm thick. Because of the cubic extrapolation method to find soil moisture at the surface, some surficial soil moisture values were nearly 0, which is unrealistic, so these simulations were removed. This resulted in about 1000 total simulations from which the

Each soil moisture profile has an associated phase value from the SNR data. Figure 60a shows phase versus the surface soil moisture value and phase versus the average soil moisture value for the top 5 cm of soil.

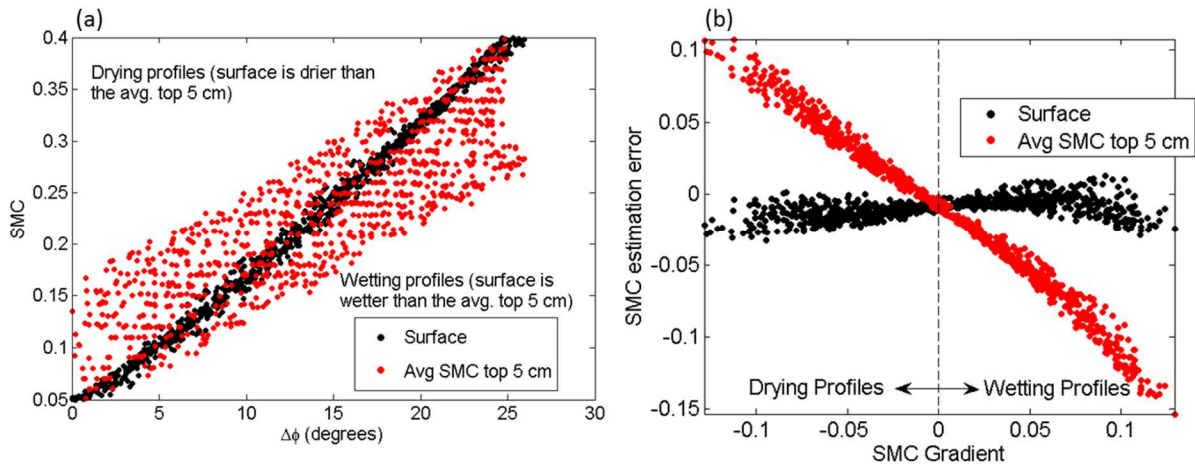


Figure 60: (a) Phase versus soil moisture for  $\sim 1000$  randomly-generated soil moisture profiles. Points are plotted by either the value of the soil moisture at the surface (black), or by the value of the average soil moisture of the top 5 cm of soil (red). (b) The same model simulations used in (a) are plotted by the difference between the surface soil moisture and the average top 5 cm soil moisture (red points). Points to the right of zero are wetter on the surface than at depth, and vice versa.

We see that soil moisture at depths beneath the surface do not change the retrieval algorithm between surface soil moisture and phase (black points all cluster closely around the constant soil moisture profile relationship). It is also apparent that if there is a strong soil moisture gradient in the near-surface profile (i.e. surface SMC is not close the average SMC for the top 5 cm of soil), the correlations between probe estimates and GPS estimates could disagree significantly.

In the example below we will consider the soil moisture gradient to just be the difference between the soil moisture at the surface and the average value over the top 5 cm. A negative value indicates that the soil is wetter at depth, and vice versa. I will use the quadratic retrieval algorithm (fit a quadratic to modeled, non-varying SMC profiles, i.e. Figure 12b) to see errors in surface soil moisture estimation for the above simulations, as a function of the soil moisture gradient. We will also see what the perceived errors could be if we compare the soil moisture estimates to the actual average soil moisture in the top 5 cm. In this case, we are quantifying the

disagreement we could see when we compare our soil moisture estimations to probe data. Of course this experiment assumes that both wetting and drying profiles are nearly equally present in real field data, even though drying profiles will likely occur more frequently for the vast majority of sites.

The results are in Figure 60b. If one uses the retrieval algorithm derived from Figure 12b on the phase data from the simulated soil moisture profiles, and compares the estimated soil moisture to the actual surface soil moisture, then one would get errors similar to the black dots in Figure 60b. Errors are not large, except for the case of extreme soil moisture gradients. However, if you compare the estimated soil moisture to the actual average soil moisture over the top 5 cm of soil, errors are much larger (red dots). Thus, extreme wetting or drying profiles could result in large disagreement between *in situ* probes and GPS estimations.

### **7.1.3 Differences in antenna height**

The relationship between soil moisture and phase does not significantly change if you have a short (1 m) vs. tall (3 m) antenna Figure 61. The ‘baseline’ phase value does change, however, but since the phase time series is always zeroed, this does not affect soil moisture estimations.

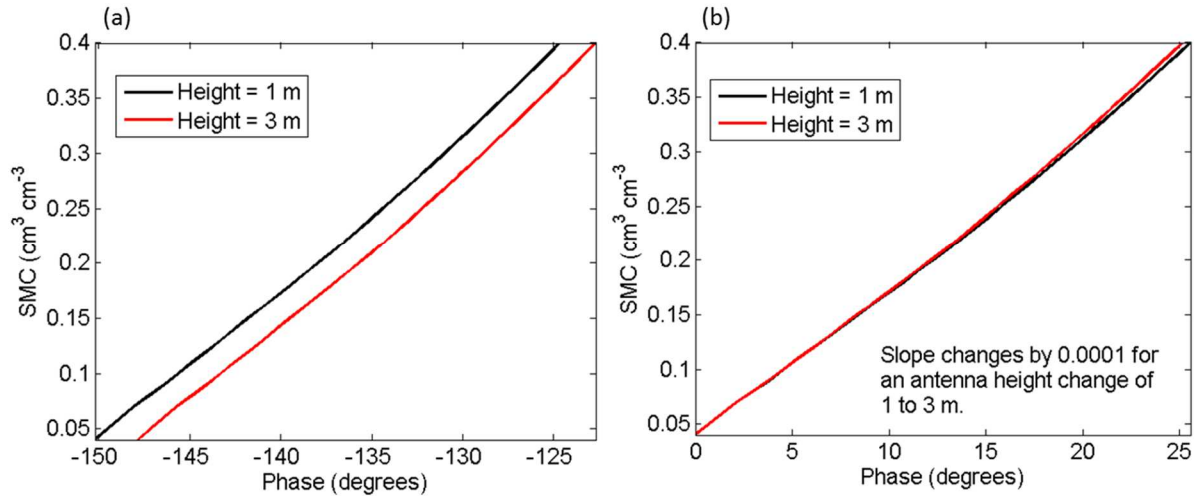


Figure 61: (a) Model simulations for a bare soil and soil moisture profiles that are uniform with depth. Simulations were run using an *a priori* height of 1 m (black line) and 3 m (red line). (b) Same as (a), except the baseline phase value has been removed from the simulations.

#### 7.1.4 Differences in soil texture

The relationship between soil moisture and phase will change only slightly when soil texture is changed. For example, if the soil texture is changed from a sand to a silty clay, the slope of the relationship between soil moisture and phase will change by  $0.0003 \text{ cm}^3 \text{ cm}^{-3}$ . The baseline phase values changes, but again, due to zeroing this will not matter (Figure 62a). The slopes in Figure 62b are very similar—the lines look different because of the kink in the silty clay curve for very low soil moisture contents. Also, recalling Table 5, the calculated slopes for the relationships between phase and soil moisture for the five soil types available in the model are very similar to one another.

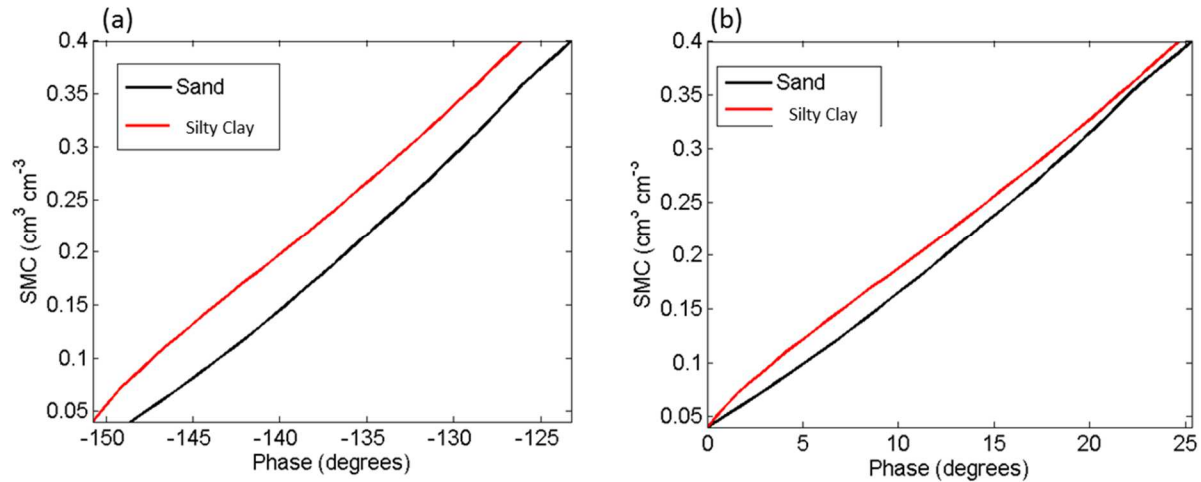


Figure 62: (a) The relationship between phase and soil moisture for uniform moisture profiles, specifying the soil texture as either a sand (black line) or silty clay (red line). (b) Same as (a), except with the baseline phase values removed.

### 7.1.5 Changes in soil temperature

A few of the PBO H<sub>2</sub>O sites are located in areas with large diurnal or seasonal temperature swings, such as those in Alaska or in deserts like the Sevilleta. Therefore, it is important to know how changes in ground temperature will affect SNR metrics. In order to investigate this, I used published relationships between soil temperature, soil texture, and permittivity found in [64]. One shortcoming of these data was that soil moisture was kept at 0.30 cm<sup>3</sup> cm<sup>-3</sup>, so different moisture contents could respond differently to changes in temperature.

Data from [64] were used in the electrodynamic model, assuming a bare soil, constant temperature profile with depth, and constant soil moisture with depth of 0.30 cm<sup>3</sup> cm<sup>-3</sup>. The ground temperature was varied, SNR data were simulated, and both phase and amplitude were computed. As always, the elevation angle range for the SNR data was the standard 5-30 degrees. Results from this experiment are shown in Figure 63. It appears that changes in soil temperature only minimally affect SNR metrics, except during periods of thawing or freezing, during which effects will be significant.

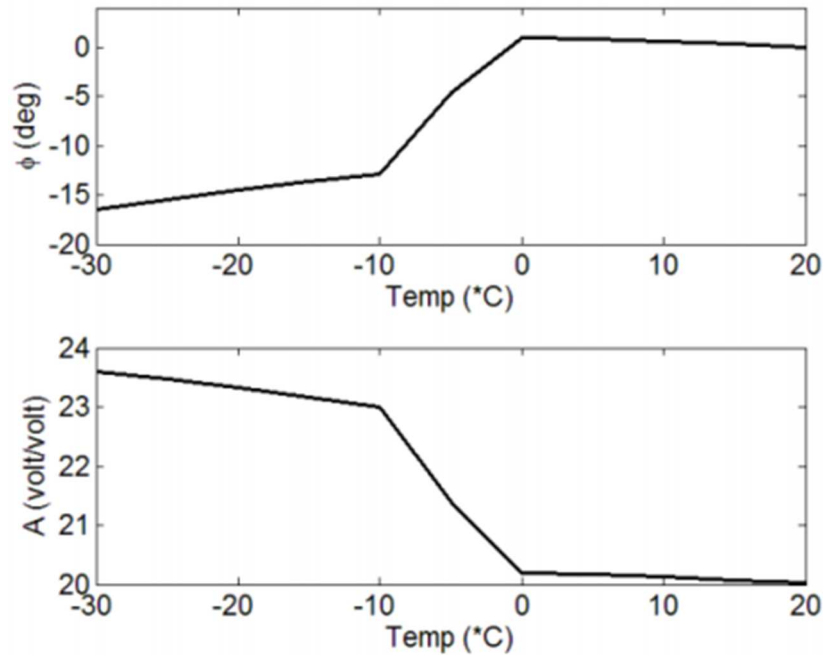


Figure 63: (*top*) Effect of ground temperature changes on phase, when  $SMC = 0.3 \text{ cm}^3 \text{ cm}^{-3}$ . (*bottom*) Effect of ground temperature changes on amplitude, when  $SMC = 0.3 \text{ cm}^3 \text{ cm}^{-3}$ .

### 7.1.6 Changes in receiver temperature

I do not have a way to model receiver temperature. Though, there does appear to be a correlation between average surface temperature and amplitude at grs2 in New Mexico (Figure 64a), but not as much of a correlation between surface temperature and phase (Figure 64b). Amplitude and temperature appear to perhaps be inversely correlated, which I believe would be expected. Since there isn't a corresponding effect in phase, I think the amplitude effect is indeed due to temperature and not to temperature/soil moisture or temperature/vegetation correlations. If the temperature effect is real, this could affect how successful the vegetation filter is (an increase in temperature could be mistaken for an increase in vegetation).

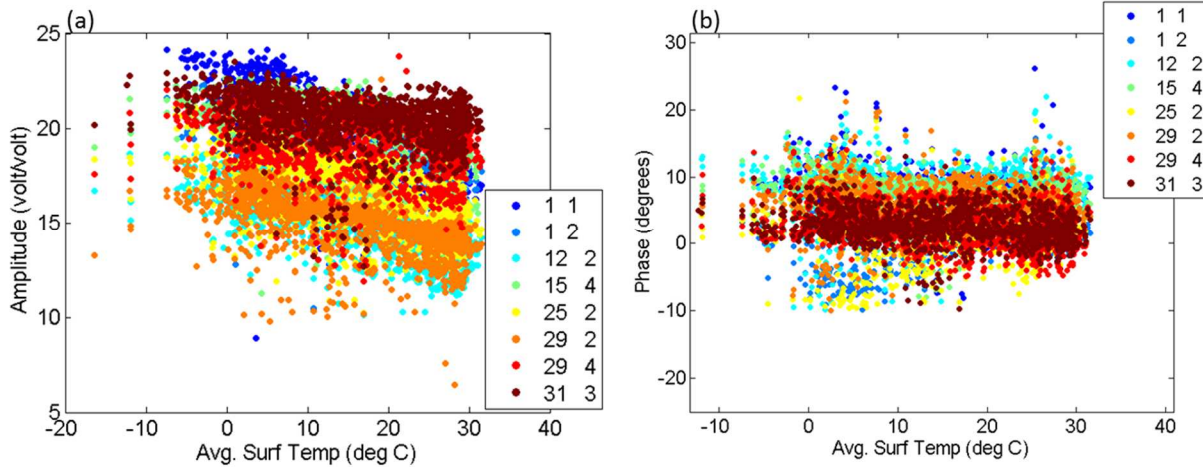


Figure 64: (a) Observed relationship between the daily-average surface temperature and amplitude for several satellite tracks (colored points) at site grs2 in New Mexico. (b) Same as (a), except for phase.

### 7.1.7 Surface roughness

The soil moisture retrieval algorithm is based on the assumption that the surface surrounding the antenna is perfectly flat—of course, this is never really the case. It is expected that increasing surface roughness will increase the amount of signal scattering and decrease the reflection coefficient. The rough surface reflection coefficient is given by [65]:

$$S_r = \exp\left(-2\left(\frac{2\pi h_{rms} \sin E}{\lambda}\right)^2\right) \quad (43)$$

Where  $h_{rms}$  is the root mean square surface height irregularity.  $S_r$  may be multiplied by the horizontal or vertical reflection coefficients to obtain the total reflection coefficient at either horizontal or vertical polarizations. These reflection coefficients may then be transformed into reflection coefficients for circular polarization via the equations in 4.1.1.

I have not included any divergence factor, which takes into account a curved earth, into the reflection coefficient calculations. However, I expect the divergence factor to be negligible,

since it is related to the ratio of (basically) the specular reflection point distance to the antenna and the radius of the Earth, and this value is nearly zero [65].

I added surface roughness into the bare soil model and simulated SNR interferograms for varying soil moisture (uniform with depth) and surface roughness. Figure 65 shows how the relationships between SNR metrics and soil moisture are expected to change with increasing surface roughness. As surface roughness increases, the range of the response of metrics to soil moisture decreases (i.e. sensitivity decreases). Effective reflector height does not change significantly for roughness increases up to 10 cm. Surface roughness affects the absolute maximum value of amplitude, though when normalized, the effect of surface roughness is greatly diminished. Surface roughness perhaps most significantly affects phase, though only after the roughness value is larger than about 4 cm.

Since surface roughness changes the slope between phase and soil moisture, using the modeled slope for a flat surface will introduce errors into soil moisture estimations. The theoretical error in soil moisture estimations that would be introduced from the presence of surface roughness is shown in Figure 66. If one wants the error to be less than  $0.04 \text{ cm}^3 \text{ cm}^{-3}$ , then the surface roughness must not exceed  $\sim 6$  cm.

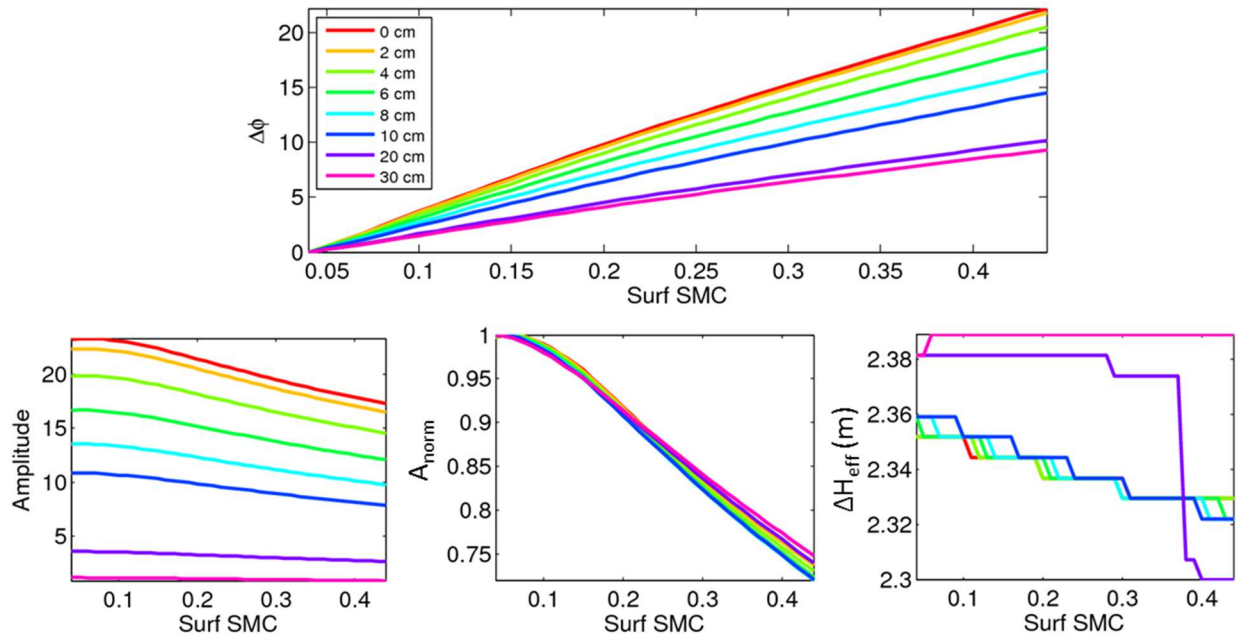


Figure 65: The effect of surface roughness on phase, amplitude, and effective reflector height. Lines are colored by the surface roughness height. Soil moisture profiles were uniform with depth.

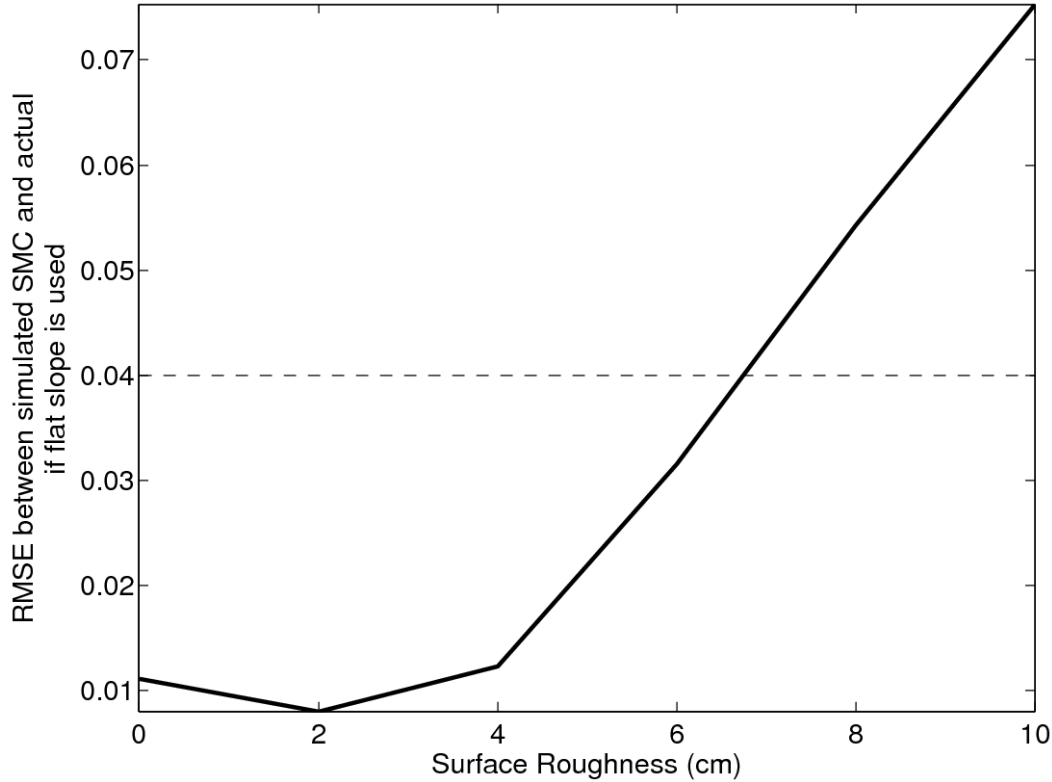


Figure 66: The RMS error (in  $\text{cm}^3 \text{cm}^{-3}$ ) between simulated soil moisture and ‘truth’ if no correction for surface roughness is made in the slope between phase and soil moisture. The dashed line denotes the  $0.04 \text{ cm}^3 \text{cm}^{-3}$  target for this project.

## 7.2 Errors for vegetated environments

Here, I address errors or uncertainties in the vegetation filter described in Chapter 5, which takes into account changes in amplitude, LSP amplitude, and reflector height in order to estimate changes in phase from vegetation.

### 7.2.1 Imperfect knowledge of antenna height

Just like in the bare soil case, we still do not have a perfect knowledge of antenna height for areas with soil and vegetation. Unfortunately vegetation in natural environments causes additional uncertainty in knowing what the *a priori* reflector height should be. Natural environments are almost never completely devoid of vegetation; even in the winter there will be some amount of standing vegetation. Thus, the *a priori* reflector height that is estimated for these

environments is the height for bare soil plus some amount of residual vegetation. Figure 47 showed how the estimated *a priori* height could be higher or lower than the actual antenna height, depending on vegetation amount.

This is important because the modeled relationships between SNR metrics to correct for vegetation are not linear. In Section 4.4.2 and Figure 25, it was determined that vegetation water content affects both phase and amplitude linearly until water content exceeds 1-1.5 kg m<sup>-2</sup>. (This is true for vegetation types that have a 1:1 relationship with true density and water content; it's not quite as linear for those that do not.) However, the relationship between metrics and other metrics is not as straightforward, given the wide scatter in relationships in Figure 31. Therefore, if we attempt to use any vegetation filter that assumes relationships between  $A_{LSPnorm}$  and  $A_{norm}$  for example, there will be errors due to this residual vegetation amount. Vegetation filters, without extensive knowledge of vegetation at the site, assume that at some point during the year, vegetation extent was zero and that the *a priori* height was determined from this time period. This could be the case for agricultural environments, but not for natural areas.

We can quantify theoretical errors in the vegetation filter from using an incorrect *a priori* reflector height to estimate phase and amplitude. Let us take a random set of 365 of the model simulations used in the vegetation filter (out of ~16000 possible simulations) and recalculate phase and amplitude, using an *a priori* height that is X cm away from the actual antenna height. This subset becomes our one year dataset of synthetic observations. Here, we still assume that we know the 'bare soil' amplitude and phase values, though in reality these are also unknown. We can implement the vegetation filter on our synthetic observations and see how uncertainties vary with errors in the *a priori* height. Figure 67 shows how errors in phase change estimation

are dependent on the magnitude and direction of *a priori* reflector height errors, as well as the height of the canopy.

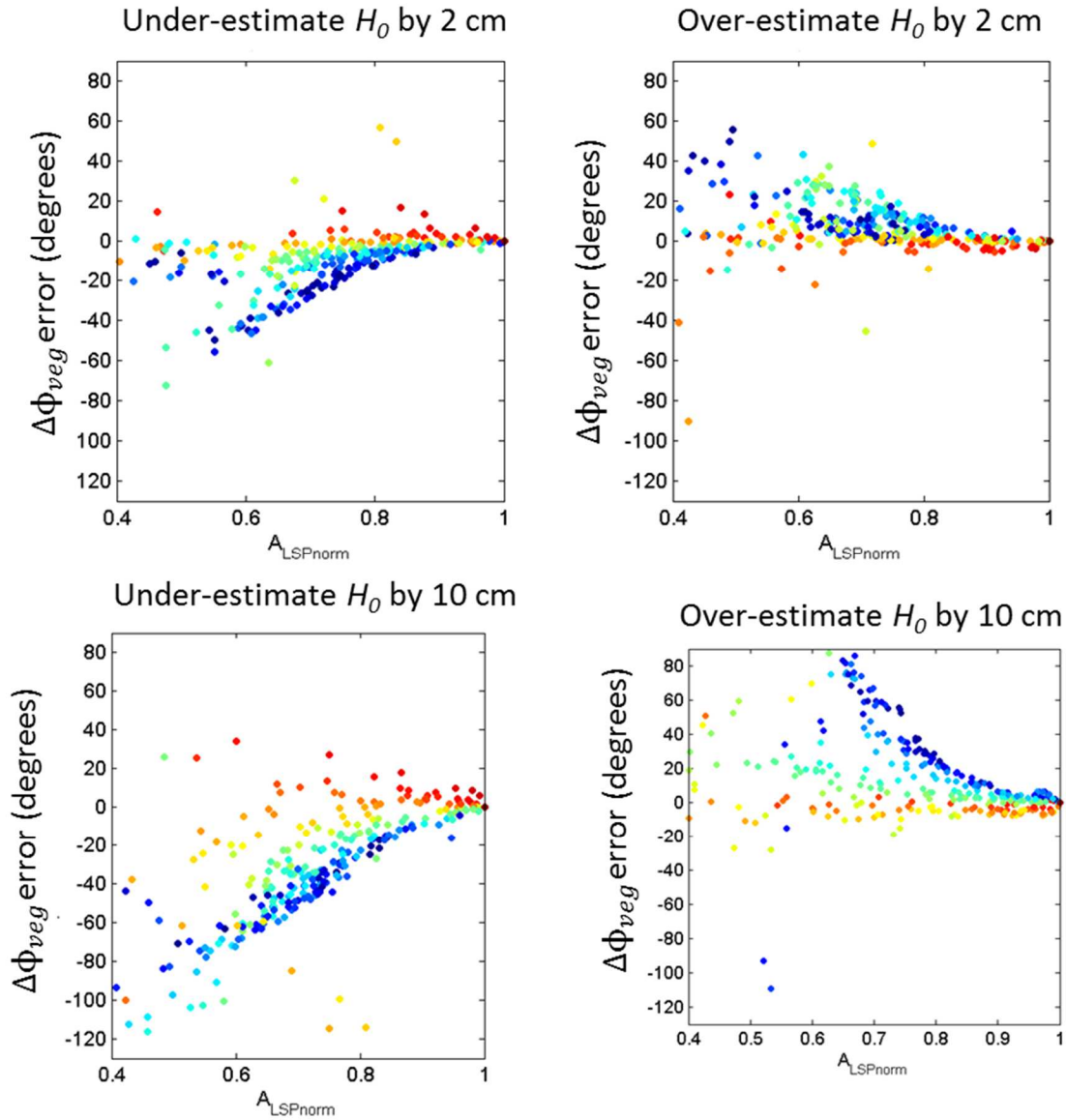


Figure 67: Errors in the estimation of phase change due to vegetation, if the *a priori* reflector height is over- or under-estimated. Although points are plotted against  $A_{LSPnorm}$ , they could have been plotted against other SNR metrics. Points are colored by vegetation height, with warmer colors indicating shorter vegetation canopies.

What we see is that phase estimation errors increase as the reflector height error increases. We also see that errors may increase with greater vegetation extent/lower amplitude.

An over-estimation of antenna height would subsequently lead to an ‘overfixing’ of phase, and vice versa. Recall that normally, the *a priori* height will be under-estimated, leading to an ‘underfixing’ of phase with the vegetation filter. This could potentially be the cause of the significant differences in predicted phase at ames when the *a priori* height is changed, as in Figure 57.

The relationships in Figure 67 may change with the presence of residual vegetation, as shown in the reflector height plot in the beginning of this section. General rules of thumb for estimating these errors, however, is difficult, since we do not know what our reflector height error is, or any information as to canopy height or permittivity.

## Chapter 8: Future Work

There are many ways that the soil moisture retrieval algorithm could be improved in the future to make the addition of new sites easier and to refine retrievals at existing sites.

### 8.1 Improvements in model simulations for the vegetation filter

As was stated previously, the current plane-stratified model does not take into account the effects of plant geometry on the reflected signal, nor does it consider volume scattering. I have found that the vegetation filter does not work well for agricultural environments such as bcgr (alfalfa field) or ames (soybean field). I believe part of the problem lies in the plane stratified approach to modeling the vegetation canopy. It is possible that including these effects could provide insight into why relationships between SNR metrics are not well simulated at these sites. In addition, modeling sites with topography or a significant slope and the effects of the slope on SNR metric relationships would probably improve retrievals, though doing so could reduce the algorithm's efficiency.

The vegetation filter could also be refined to improve retrievals. The filter is currently comprised of thousands of random combinations of vegetation parameters, which is useful when there is no *a priori* vegetation information for a site. However, in reality, we do know at least a little bit about most of the sites in the PBO network. For example, we know that nearly all of the sites in Montana are natural grasslands, and we have dozens of *in situ* vegetation measurements from some of these stations. It could be advantageous, for the sites in Montana, to restrict the vegetation parameter sets in the filter to only those representing typical grasslands. Similarly, one could restrict the filter for desert environments, and so on.

In addition, the assumption in the simulations that soil moisture does not change seasonally, concurrently with vegetation, is a limitation that needs further work. The current simulations used in the filter assume the bare soil moisture content is  $0.15 \text{ cm}^3 \text{ cm}^{-3}$  and allows soil moisture and vegetation amount to change concurrently. If the simulations instead assume the bare soil moisture content is  $0.25 \text{ cm}^3 \text{ cm}^{-3}$  and that soil moisture when vegetation is present decreases to  $0.15 \text{ cm}^3 \text{ cm}^{-3}$ , then the filter predicts different changes in vegetation.

Figure 68a shows, for one satellite track at site p042, the phase observations and the predicted phase change due to vegetation. We see that phase is under-predicted around 2013.75. Figure 68b shows how the predictions change if the simulations are changed to those described above ( $0.25 \text{ cm}^3 \text{ cm}^{-3}$  decreasing to  $0.15 \text{ cm}^3 \text{ cm}^{-3}$ ). Phase is no longer under-predicted.

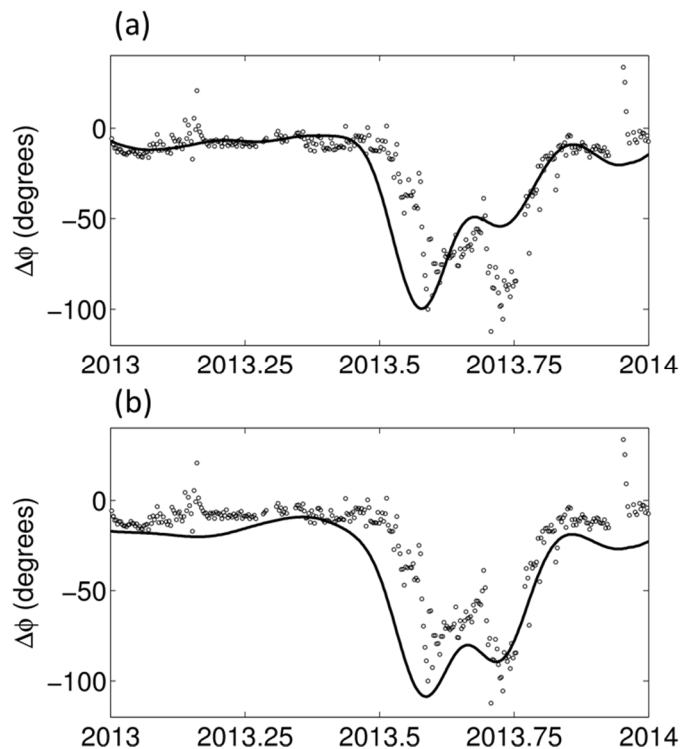


Figure 68: (a) Observed phase data from PRN 25 Quadrant 4 at site p042 in Wyoming (open circles) and predicted phase change due to vegetation (black line), using the model simulations assuming an underlying soil moisture of  $0.15 \text{ cm}^3 \text{ cm}^{-3}$ . (b) Same as (a) except the model

simulations assumed a bare soil moisture content of  $0.25 \text{ cm}^3 \text{ cm}^{-3}$  that decreases to  $0.15 \text{ cm}^3 \text{ cm}^{-3}$  when vegetation is present.

Similarly, Figure 69a shows soil moisture retrievals for site masw in California, using the standard vegetation filter. Soil moisture is unrealistically high in the winters of 2012 and 2013. However, if the alternate simulations are used in the vegetation filter, soil moisture retrievals are more realistic (Figure 69b). More work needs to be done to determine whether imposing different soil moisture restrictions in the model simulations would improve retrievals across sites, and if so, what the optimum restrictions are.

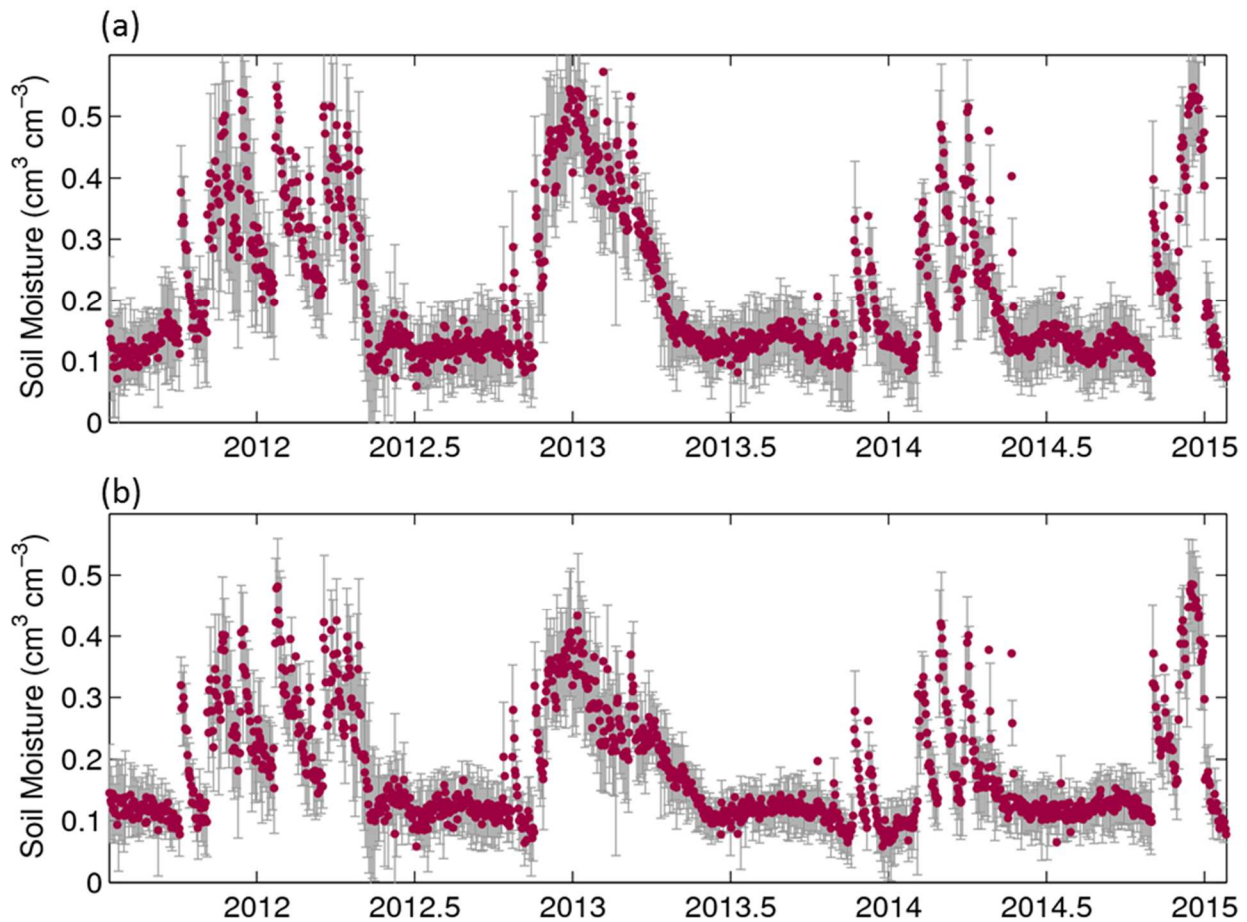


Figure 69: GPS-estimated soil moisture for site masw in California. (a) The vegetation filter used model simulations that assumed an underlying soil moisture content of  $0.15 \text{ cm}^3 \text{ cm}^{-3}$ . (b) The vegetation filter used model simulations that assumed the bare soil moisture content was  $0.25 \text{ cm}^3 \text{ cm}^{-3}$  and decreased to  $0.15 \text{ cm}^3 \text{ cm}^{-3}$  when vegetation was present.

An effort should also be made to better incorporate the uncertainties described in Chapter 8 into the soil moisture retrievals. Currently, the error bars represent the variability in retrievals from different satellite tracks. If this variability could be decreased, either by better outlier identification or by improving the algorithm, then the errors described in Chapter 8 could be more reasonably incorporated.

## **8.2 Improvements in quality control of observations**

Even if the vegetation filter were refined, a big challenge that still remains is better identifying when and where data from tracks are reliable. Although one method of identifying bad data based on amplitude was described in Section 6.1.1, there are other issues that must be mitigated, such as satellite maneuvers that change the ground track (and *a priori* reflector height). One could recognize that the DoD changed the satellite's orbit slightly and adjust the track's *a priori* height accordingly, though automating this and other quality controls is desirable.

The saying, "One bad apple can spoil the bunch," definitely applies to final soil moisture estimations, especially if and when the mean of the track-by-track soil moisture estimates is taken. It is expected that there is some variation in the track-by-track soil moisture estimations, though occasionally one track will perform much worse than the others. Reasons for worse performance can be related to the empirical issues described above, but there are also times when the vegetation filter does not do a good job. Here, I will describe what some of these outliers may look like, and how I have attempted to remove them.

Figure 70 shows what the track-by-track soil moisture estimates look like at site ok13, along with *in situ* data. The light orange points in this figure are data from PRN 25 Quadrant 1, and we see that right before mid-2011, the soil moisture estimates are unreasonably high for a

very short period. Similarly, the light blue points in this figure are data from PRN 1 Quadrant 2, which also show unreasonably high soil moisture retrievals in the first half of 2012.

Although retrievals from both satellite tracks are anomalously high, their reasons for being so are different. PRN 25 (orange points) are too high because for an unknown reason the amplitude time series began to decrease before the phase time series did, which caused phase to be ‘over-fixed’ during that brief interval. PRN 1 (blue dots), on the other hand was not corrected enough in 2012 for vegetation. This is possibly because the smoothing algorithm over-smoothed the reflector height time series, making the magnitude of vegetation change appear smaller than it actually was. The end result is anomalously high soil moisture during the spring months.

Improving the smoothing algorithm could mitigate this issue. However, there is not currently a way to automatically detect when there are outliers, since there are many causes for outliers, as was just described.

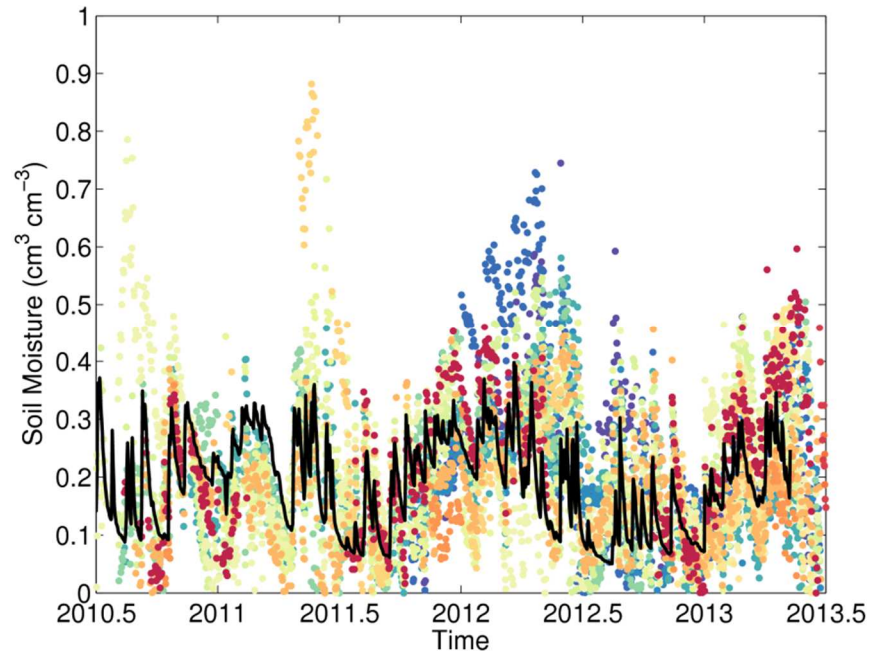


Figure 70: Time series of track-by-track estimated soil moisture (colored dots are retrievals from different PRNs), and *in situ* data (black line) from Oklahoma GPS site ok13.

## Chapter 9: Conclusions

Here I have described the development of an algorithm to retrieve soil moisture from GPS ground reflection data, which includes corrections for deleterious effects from vegetation growth. The algorithm was designed for use with the choke ring antennas frequently used in GPS networks, though similar algorithms with different parameters could be developed for use with different types of antennas.

Initial observations of SNR metrics from several GPS sites indicated a change in soil moisture induced changes in SNR metrics to different degrees. Observations also indicated that seasonal changes in SNR metrics were associated with vegetation growth and senescence. Due to spatial heterogeneities in soil moisture and vegetation and other unknowns (receiver influences on the ground-reflected signal, etc.) an electrodynamic model was used to elucidate the effects of soil moisture and vegetation changes alone on the ground-reflected signal.

The electrodynamic model was originally developed for a bare, planar surface. How changes in soil moisture affected each SNR metric was first investigated for this simple case. It was found that the SNR metric phase is the variable most indicative of changes in soil moisture, though all SNR metrics are affected by soil moisture change. Soil texture and antenna height were determined to not significantly impact the relationships between soil moisture and SNR metrics. Additionally, it was also determined that surface soil moisture change was the most important driver of SNR metric change, as opposed to changes in soil moisture at depth.

The allowance for a vegetation canopy was next included in the model, and this model was validated against observations from four different GPS sites. It was determined that the height of the canopy as well as its permittivity, which itself is a combination of other vegetation

parameters, are the two metrics that determine how SNR metrics respond to changes within in the canopy. Commonly measured vegetation parameters, such as vegetation water content, will only be well correlated with SNR metric change if it is also correlated with other vegetation canopy parameters, in particular the true density of vegetation. All SNR metrics were determined to be affected by vegetation growth. It is nearly impossible to untangle the influences of concurrent changes in soil moisture and vegetation, for short or low permittivity canopies. Vegetation growth mimics a decrease in soil moisture; a rise in soil moisture mimics a decrease in vegetation growth.

In order to remove the effect of vegetation on the phase time series, which is then used to estimate changes in soil moisture, a vegetation filter was designed. The vegetation filter used SNR metrics from model simulations that represented how theoretical vegetation canopies would affect SNR metrics. The filter does not estimate vegetation; rather, it compares three of the four observed SNR metrics to modeled metrics and predicts how much phase, the fourth metric, likely changed due to changes in the vegetation canopy.

The vegetation filter makes up part of the final soil moisture algorithm. Possible errors in final soil moisture estimates are caused by inaccurate values of the *a priori* reflector height, confounding influences of underlying soil moisture on total SNR metric change that is not well represented in the model simulations, and inadequate smoothing of the SNR metric time series.

Validation of the algorithm and vegetation filter at sites with *in situ* soil moisture data indicates that the addition of the vegetation filter improves retrieval accuracy. Data resulting from the algorithm are available for download at <http://xenon.colorado.edu/portal>.

## Bibliography

- [1] D. Entekhabi, I. Rodriguez-Iturbe, and F. Castelli, "Mutual interaction of soil moisture state and atmospheric processes," *J. Hydrol.*, vol. 184, pp. 3–17, 1996.
- [2] A. Robock, K. Y. Vinnikov, G. Srinivasan, J. K. Entin, S. E. Hollinger, N. A. Speranskaya, S. Liu, and A. Namkhai, "The Global Soil Moisture Data Bank," *Bull. Am. Meteorol. Soc.*, vol. 81, no. 6, pp. 1281–1299, 2000.
- [3] R. D. Koster, P. a Dirmeyer, Z. Guo, G. Bonan, E. Chan, P. Cox, C. T. Gordon, S. Kanae, E. Kowalczyk, D. Lawrence, P. Liu, C.-H. Lu, S. Malyshev, B. McAvaney, K. Mitchell, D. Mocko, T. Oki, K. Oleson, A. Pitman, Y. C. Sud, C. M. Taylor, D. Verseghy, R. Vasic, Y. Xue, and T. Yamada, "Regions of strong coupling between soil moisture and precipitation.," *Science (80-. )*, vol. 305, no. 5687, pp. 1138–40, Aug. 2004.
- [4] K. Rajkai and B. E. Ryden, "Measuring areal soil moisture distribution with the TDR method," *Geoderma*, vol. 52, pp. 73–85, 1992.
- [5] B. D. Entekhabi, E. G. Njoku, P. E. O. Neill, K. H. Kellogg, W. T. Crow, W. N. Edelstein, J. K. Entin, S. D. Goodman, T. J. Jackson, J. Johnson, J. Kimball, J. R. Piepmeier, R. D. Koster, N. Martin, K. C. McDonald, M. Moghaddam, S. Moran, R. Reichle, J. C. Shi, M. W. Spencer, S. W. Thurman, L. Tsang, and J. Van Zyl, "The soil moisture active passive (SMAP) mission," *Proc. IEEE*, vol. 98, no. 5, pp. 704–716, 2010.
- [6] J. R. Wang, E. T. Engman, J. C. Shiue, and M. Rusek, "Observations of Microwave Dependence on Soil Moisture , Surface Roughness , and Vegetation Covers," *IEEE Trans. Geosci. Remote Sens.*, vol. GE-24, no. 4, pp. 510–516, 1986.
- [7] F. T. Ulaby, R. K. Moore, and A. K. Fung, *Microwave Remote Sensing Active and Passive- Volume II: Radar Remote Sensing and Surface Scattering and Emission Theory*. Addison-Wesley Publishing Company, 1982.
- [8] L. Tsang, J. A. Kong, and R. T. Shin, *Theory of microwave remote sensing*, 1st ed. Wiley-Interscience, 1985.
- [9] M. T. Hallikainen, F. T. Ulaby, M. C. Dobson, M. A. El-Rayes, and L.-K. Wu, "Microwave Dielectric Behavior of Wet Soil-Part 1: Empirical Models and Experimental Observations," *IEEE Trans. Geosci. Remote Sens.*, vol. GE-23, no. 1, pp. 25–34, 1985.
- [10] I. M. Fuks and A. G. Voronovich, "Wave diffraction by rough interfaces in an arbitrary plane-layered medium," *Waves in Random Media*, vol. 10, pp. 37–41, 2000.
- [11] W. J. Rawls, D. L. Brakensiek, and K. E. Saxton, "Estimation of Soil Water Properties," *Trans. ASAE*, vol. 25, no. 5, pp. 1316–1320, 1982.

- [12] P. A. Ferre, D. L. Rudolph, and R. G. Kachanoski, "Spatial Averaging of Water Content by Time Domain Reflectometry: Implications for Twin Rod Probes with and without Dielectric Coatings," *Water*, vol. 32, no. 2, pp. 271–279, 1996.
- [13] F. T. Ulaby, P. P. Batlivala, and M. C. Dobson, "Microwave Backscatter Dependence on Surface Roughness, Soil Moisture, and Soil Texture: Part II-Bare Soil," *IEEE Trans. Geosci. Electron.*, vol. GE-16, no. 4, pp. 286–295, 1978.
- [14] E. G. Njoku and D. Entekhabi, "Passive microwave remote sensing of soil moisture," *J. Hydrol.*, vol. 184, no. 1–2, pp. 101–129, Oct. 1996.
- [15] M. Schwank, C. Mätzler, S. Member, M. Guglielmetti, and H. Flübler, "L-Band Radiometer Measurements of Soil Water Under Growing Clover Grass," *IEEE Trans. Geosci. Remote Sens.*, vol. 43, no. 10, pp. 2225–2237, 2005.
- [16] T. J. Jackson and D. E. Le Vine, "Mapping surface soil moisture using an aircraft-based passive microwave instrument: algorithm and example," *J. Hydrol.*, vol. 184, pp. 85–99, 1996.
- [17] I. Mladenova, V. Lakshmi, T. J. Jackson, J. P. Walker, O. Merlin, and R. A. M. de Jeu, "Validation of AMSR-E soil moisture using L-band airborne radiometer data from National Airborne Field Experiment 2006," *Remote Sens. Environ.*, vol. 115, no. 8, pp. 2096–2103, Aug. 2011.
- [18] T. J. Jackson, D. M. Le Vine, C. T. Swift, T. J. Schmugge, and F. R. Schiebe, "Large Area Mapping of Soil Moisture Using the ESTAR Passive Microwave Radiometer in Washita '92," *Remote Sens. Environ.*, vol. 53, pp. 27–37, 1995.
- [19] F. T. Ulaby, P. C. Dubois, and J. van Zyl, "Radar mapping of surface soil moisture," *J. Hydrol.*, vol. 184, pp. 57–84, 1996.
- [20] A. W. Western, G. Bloschl, and R. B. Grayson, "Geostatistical characterisation of soil moisture patterns in the Tarrawarra catchment," *J. Hydrol.*, vol. 205, pp. 20–37, 1998.
- [21] A. Gomez-Plaza, M. Martinez-Mena, J. Albaladejo, and V. M. Castillo, "Factors regulating spatial distribution of soil water content in small semiarid catchments," *J. Hydrol.*, vol. 253, pp. 211–226, 2001.
- [22] G. Baroni, B. Ortuani, a. Facchi, and C. Gandolfi, "The role of vegetation and soil properties on the spatio-temporal variability of the surface soil moisture in a maize-cropped field," *J. Hydrol.*, vol. 489, pp. 148–159, May 2013.
- [23] L. Brocca, R. Morbidelli, F. Melone, and T. Moramarco, "Soil moisture spatial variability in experimental areas of central Italy," *J. Hydrol.*, vol. 333, no. 2–4, pp. 356–373, Feb. 2007.
- [24] J. S. Famiglietti, J. W. Rudnicki, and M. Rodell, "Variability in surface moisture content along a hillslope transect: Rattlesnake Hill, Texas," *J. Hydrol.*, vol. 210, no. 1–4, pp. 259–281, Sep. 1998.

- [25] C. D. Hall and R. A. Cordey, "Multistatic Scatterometry," in *Proceedings of IGARSS '88 Symposium*, 1988, pp. 561–562.
- [26] V. U. Zavorotny and A. G. Voronovich, "Scattering of GPS Signals from the Ocean with Wind Remote Sensing Application," *IEEE Trans. Geosci. Remote Sens.*, vol. 38, no. 2, pp. 951–964, 2000.
- [27] A. Komjathy, V. U. Zavorotny, P. Axelrad, G. H. Born, and J. L. Garrison, "GPS Signal Scattering from Sea Surface : Wind Speed Retrieval Using Experimental Data and Theoretical Model," *Remote Sens. Environ.*, vol. 73, pp. 162–174, 2000.
- [28] E. Cardellach, G. Ruffini, D. Pino, A. Rius, A. Komjathy, and J. L. Garrison, "Mediterranean Balloon Experiment: ocean wind speed sensing from the stratosphere, using GPS reflections," *Remote Sens. Environ.*, vol. 88, no. 3, pp. 351–362, Dec. 2003.
- [29] S. T. Lowe, C. Zuffada, Y. Chao, P. Kroger, L. E. Young, and J. L. Labrecque, "5-cm-Precision aircraft ocean altimetry using GPS reflections," *Geophys. Res. Lett.*, vol. 29, no. 10, pp. 10–13, 2002.
- [30] M. Martin-Neira, "A passive reflectometry and interferometry system (PARIS): Application to ocean altimetry," *ESA J.*, vol. 17, pp. 331–355, 1993.
- [31] A. Komjathy, J. Maslanik, V. U. Zavorotny, P. Axelrad, and S. J. Katzberg, "Sea Ice Remote Sensing Using Surface Reflected GPS Signals," in *Geoscience and Remote Sensing Symposium, 2000.*, 2000, pp. 2855–2857.
- [32] M. D. Jacobson, "Inferring Snow Water Equivalent for a Snow-Covered Ground Reflector Using GPS Multipath Signals," *Remote Sens.*, vol. 2, no. 10, pp. 2426–2441, Oct. 2010.
- [33] E. Cardellach, F. Fabra, A. Rius, S. Pettinato, and S. D'Addio, "Characterization of dry-snow sub-structure using GNSS reflected signals," *Remote Sens. Environ.*, vol. 124, pp. 122–134, Sep. 2012.
- [34] N. Rodriguez-Alvarez, A. Aguasca, E. Valencia, X. Bosch-Lluis, I. Ramos-Perez, H. Park, A. Camps, and M. Vall-llossera, "Snow monitoring using GNSS-R techniques," *Geosci. Remote Sens. Symp.*, pp. 4375–4378, 2011.
- [35] D. S. Masters, "Surface Remote Sensing Applications of GNSS Bistatic Radar : Soil Moisture and Aircraft Altimetry," University of Colorado at Boulder, 2004.
- [36] N. Rodriguez-Alvarez, X. Bosch-lluis, A. Camps, I. Ramos-Perez, E. Valencia, H. Park, and M. Vall-llossera, "Vegetation Water Content Estimation Using GNSS Measurements," *IEEE Geosci. Remote Sens. Lett.*, vol. 9, no. 2, pp. 282–286, 2012.
- [37] N. Rodriguez-Alvarez, X. Bosch-Lluis, A. Camps, A. Aguasca, M. Vall-llossera, E. Valencia, I. Ramos-Perez, and H. Park, "Review of crop growth and soil moisture monitoring from a ground-based instrument implementing the Interference Pattern GNSS-R Technique," *Radio Sci.*, vol. 46, no. 6, p. n/a–n/a, Dec. 2011.

- [38] P. Ferrazzoli, L. Guerriero, N. Pierdicca, and R. Rahmoune, "Forest biomass monitoring with GNSS-R: Theoretical simulations," *Adv. Sp. Res.*, vol. 47, no. 10, pp. 1823–1832, May 2011.
- [39] K. M. Larson and F. G. Nievinski, "GPS snow sensing: results from the EarthScope Plate Boundary Observatory," *GPS Solut.*, vol. 17, no. 1, pp. 41–52, Mar. 2013.
- [40] F. G. Nievinski and K. M. Larson, "Forward modeling of GPS multipath for near-surface reflectometry and positioning applications," *GPS Solut.*, vol. 18, no. 2, pp. 309–322, Jun. 2014.
- [41] E. E. Small, K. M. Larson, and J. J. Braun, "Sensing vegetation growth with reflected GPS signals," *Geophys. Res. Lett.*, vol. 37, no. 12, pp. 1–5, Jun. 2010.
- [42] S. G. Evans, E. E. Small, and K. M. Larson, "Comparison of vegetation phenology in the western USA determined from reflected GPS microwave signals and NDVI," *Int. J. Remote Sens.*, vol. 35, no. 9, pp. 2996–3017, Apr. 2014.
- [43] W. Wan, K. M. Larson, E. E. Small, C. C. Chew, and J. J. Braun, "Using geodetic GPS receivers to measure vegetation water content," *GPS Solut.*, May 2014.
- [44] K. M. Larson, J. J. Braun, E. E. Small, V. U. Zavorotny, E. D. Gutmann, and A. L. Bilich, "GPS Multipath and Its Relation to Near-Surface Soil Moisture Content," *IEEE J. Sel. Top. Appl. Earth Obs. Remote Sens.*, vol. 3, no. 1, pp. 91–99, 2010.
- [45] K. M. Larson, E. E. Small, E. Gutmann, A. Bilich, P. Axelrad, and J. Braun, "Using GPS multipath to measure soil moisture fluctuations: initial results," *GPS Solut.*, vol. 12, no. 3, pp. 173–177, Aug. 2008.
- [46] F. G. Nievinski, "Forward and Inverse Modeling of GPS Multipath for Snow Monitoring," University of Colorado at Boulder, 2013.
- [47] K. M. Larson, E. E. Small, E. D. Gutmann, A. L. Bilich, J. J. Braun, and V. U. Zavorotny, "Use of GPS receivers as a soil moisture network for water cycle studies," *Geophys. Res. Lett.*, vol. 35, no. 24, pp. 1–5, Dec. 2008.
- [48] P. Axelrad, K. M. Larson, and B. Jones, "Use of the correct satellite repeat period to characterize and reduce site-specific multipath errors," *ION GNSS 18th Int. Tech. Meet. Satell. Div.*, no. September, pp. 2638–2648, 2005.
- [49] "CS616 and CS625 Water Content Reflectometers."
- [50] "User Manual for the ML3 ThetaProbe." pp. 1–47.
- [51] V. U. Zavorotny, K. M. Larson, J. J. Braun, E. E. Small, E. D. Gutmann, and A. L. Bilich, "A Physical Model for GPS Multipath Caused by Land Reflections : Toward Bare Soil Moisture Retrievals," *IEEE J. Sel. Top. Appl. Earth Obs. Remote Sens.*, vol. 3, no. 1, pp. 1–11, 2010.

- [52] M. C. Dobson, F. T. Ulaby, M. T. Hallikainen, and M. A. El-Rayes, "Microwave Dielectric Behavior of Wet Soil-Part Dielectric Mixing Models," *IEEE Trans. Geosci. Remote Sens.*, vol. GE-23, no. 1, pp. 35–46, 1985.
- [53] E. P. W. Attema and F. T. Ulaby, "Vegetation modeled as a water cloud," *Radio Sci.*, vol. 13, no. 2, pp. 357–364, Mar. 1978.
- [54] F. T. Ulaby and E. A. Wilson, "Microwave Attenuation Properties of Vegetation Canopies," *IEEE Trans. Geosci. Remote Sens.*, vol. GE-23, no. 5, pp. 746–753, 1985.
- [55] F. T. Ulaby and M. a El-Rayes, "Microwave Dielectric Spectrum of Vegetation - Part II: Dual-Dispersion Model," *IEEE Trans. Geosci. Remote Sens.*, vol. GE-25, no. 5, pp. 550–557, 1987.
- [56] E. J. Burke, R. C. Harlow, and T. P. A. Ferré, "Measuring the dielectric permittivity of a plant canopy and its response to changes in plant water status: An application of Impulse Time Domain Transmission," *Plant Soil*, vol. 268, no. 1, pp. 123–133, Jan. 2005.
- [57] E. Bäumlér, A. Cuniberti, S. M. Nolasco, and I. C. Riccobene, "Moisture dependent physical and compression properties of safflower seed," *J. Food Eng.*, vol. 72, no. 2, pp. 134–140, Jan. 2006.
- [58] S. O. Nelson, "Dielectric properties of agricultural products-measurements and applications," *IEEE Trans. Instrum. Meas.*, vol. 41, no. 1, pp. 385–387, 1991.
- [59] R. Bindlish and A. P. Barros, "Parameterization of vegetation backscatter in radar-based, soil moisture estimation," *Remote Sens. Environ.*, vol. 76, no. 1, pp. 130–137, Apr. 2001.
- [60] K. Lee, R. Chawn Harlow, E. J. Burke, and W. J. Shuttleworth, "Application of a plane-stratified emission model to predict the effects of vegetation in passive microwave radiometry," *Hydrol. Earth Syst. Sci.*, vol. 6, no. 2, pp. 139–152, 2002.
- [61] T. Mo, B. J. Choudhury, T. J. Schugge, J. R. Wang, and T. J. Jackson, "A Model for Microwave Emission from Vegetation-Covered Fields," *J. Geophys. Res.*, vol. 87, no. 1, pp. 11229–11237, 1982.
- [62] C. C. Chew, E. E. Small, K. M. Larson, and V. U. Zavorotny, "Vegetation sensing using GPS-Interferometric Reflectometry: Theoretical effects of canopy parameters on signal-to-noise ratio data," *IEEE Trans. Geosci. Remote Sens.*, vol. 53, no. 5, pp. 2755–2764, 2015.
- [63] G. E. Schwarz and R. B. Alexander, "Soils data for the Conterminous United States Derived from the NRCS State Soil Geographic (STATSGO) Data Base. [Original title: State Soil Geographic (STATSGO) Data Base for the Conterminous United States.]" U.S. Geological Survey, Reston, VA, 1995.
- [64] L. Zhang, J. Shi, Z. Zhang, and K. Zhao, "The estimation of dielectric constant of frozen soil-water mixture at microwave bands," *Geosci. Remote Sens. Symp. 2003. IGARSS '03. Proceedings. 2003 IEEE Int.*, vol. 4, pp. 2903–2905, 2003.

- [65] B. R. Mahafza, *Radar Systems Analysis and Design using MATLAB Second Edition*. Boca Raton: Chapman and Hall, 2005.